High harmonic generation from relativistic plasma

Inaugural-Dissertation

zur

Erlangung des Doktorgrades der

Mathematisch-Naturwissenschaftlichen Fakultät

der Heinrich-Heine-Universität Düsseldorf

vorgelegt von
Teodora Baeva
aus Sofia

Mai 2008

Aus dem Institut für theoretische Physik
der Heinrich-Heine Universität Düsseldorf

Gedruckt mir der Genehmigung der
Mathematisch-Naturwissenschaftlichen Fakultät der
Heinrich-Heine Universität Düsseldorf

Referent: Prof. Dr. A. Pukhov
Koreferent: Prof. Dr. K.-H. Spatschek
Koreferent: Prof. Dr. K. Taylor

Tag der mündlichen Prüfung: 30.06.2008

Contents

1 Introduction **5**
- 1.1 Advent of Non-Linear Optics 5
- 1.2 High-Order Harmonics from Gases 6
- 1.3 Coherent X-rays from Plasma 10
  - 1.3.1 First Theoretical Approaches to Relativistic Harmonics 11
  - 1.3.2 Theory of Relativistic Spikes 14
  - 1.3.3 Experimental Results 21
- 1.4 Thesis Structure 24

2 Apparent Reflection Point Formalism **25**
- 2.1 Wave Equation and Apparent Reflection Point 26
- 2.2 Relativistic Definition of Apparent Reflection Point 29
- 2.3 Basic Properties of Apparent Reflection Point 31
  - 2.3.1 Existence of Apparent Reflection Point 31
  - 2.3.2 Reconstruction of Reflected Radiation 32
  - 2.3.3 Causality Condition 33
- 2.4 Apparent Reflection Point and Boundary Conditions 35

3 Relativistic Spikes **37**
- 3.1 Relativistic Similarity for Collisionless Plasma 38
- 3.2 Relativistic Spikes and Skin Layer Motion 43
- 3.3 Theory of Apparent Reflection Point Motion 44
- 3.4 Relativistic Motion of Apparent Reflection Point 49
- 3.5 Microscopic Spike Scalings 52
- 3.6 Oblique Laser Incidence 53
  - 3.6.1 Oblique Incidence Equations 54
  - 3.6.2 P-polarized Laser Pulse 57
  - 3.6.3 S-polarized Laser Pulse 58
- 3.7 Numerical Simulations of Relativistic Spikes 60

4 High Harmonic Generation **65**
4.1 Electromagnetic Shock Waves 66
4.1.1 Generation of Electromagnetic Shock Waves 66
4.1.2 Relativistic Invariance of Shock Waves 68
4.2 Relativistic Doppler Effect 70
4.3 Universal Spectrum 72
4.3.1 Invariant Derivation of Harmonic Spectrum 73
4.3.2 The Concept of Universality 77
4.4 Physical Picture of High Harmonic Generation 78

5 Ultra-Short Pulses **81**
5.1 Pulse Generation 82
5.2 Duration and Intensity of Ultra-Short Pulses 84
5.3 Ultra-Short Pulse Structure 86
5.4 Relativistic Plasma Control 88

6 Summary **91**

A Vlasov Equation **93**

B Practicalities **95**

Bibliography **97**

Invited Talks, Conferences and Publications **103**

Acknowledgments **109**

Index **109**

Chapter 1

Introduction

1.1 Advent of Non-Linear Optics

The idea to intensify and use light is probably as old as mankind. A so called "burning-glass", a large convex lens that can concentrate rays of sunlight onto a small spot, heating up the area and thus resulting in ignition of the exposed surface, has been known since antiquity. Legend has it that Archimedes used a burning-glass[1] in 212 BC to focus sunlight onto the approaching Roman ships, causing them to catch fire, when Syracuse was besieged by Marcus Claudius Marcellus. The Roman fleet was supposedly incinerated, though eventually the city was taken and Archimedes was slain [1].

A breakthrough in the generation of intense coherent light was first achieved by the combination of geometric optics with quantum mechanics leading to the invention of the laser around 1960. In the following five years tabletop lasers already reached a power of 1 GW [2, 3]. However, the attempts to further intensify the laser light led to no significant progress. Non-linear effects which started playing a major role at high laser intensities put a limit on the amplification of intensity impairing the beam quality and even damaging the components of the amplifying systems.

However, the non-linear effects became not only a major problem of laser technology but also a subject of excitement in the physics community. In his Nobel lecture 1981 Bloembergen [4] pointed out that nonlinear optics had developed into a significant subfield of physics. The availability of tunable dye lasers made detailed nonlinear spectroscopic studies possible throughout the visible region of the spectrum, from 0.35 to 0.9 μm. Conversely, nonlinear

[1] Or more likely a large number of angled hexagonal mirrors

techniques extended the range of tunable coherent radiation. Harmonic generation, parametric down conversion and stimulated Raman scattering in different orders extended the range from the vacuum ultraviolet to the far infrared. As Bloembergen noticed [4], such nonlinear phenomena at optical frequencies are quite striking and can readily be calculated by combining the nonlinear constitutive relation with Maxwells equations. He also recalled that at the beginning of the XX$^{\text{th}}$ century Lorentz calculated the electric susceptibility by modeling the electron as a harmonic oscillator. If Lorentz had admitted some anharmonicity, he could have developed the field of nonlinear optics 100 years ago. In his Nobel lecture Bloembergen emphasized that the soft X-ray region still presented a challenge [4].

1.2 High-Order Harmonics from Gases

Four years after Bloembergen received the Nobel prize for physics laser technology made a new important step. The problem caused by intense laser radiation destroying optical elements was circumvented using a technique now known as "chirped pulse amplification" (CPA) [5]. Tabletop laser powers increased by factors of 10^3 to 10^5 making new classes of non-linear laser-matter interaction accessible. CPA is the current state of the art technique which all of the highest power lasers in the world utilize and which has made the generation of high-order harmonics a routine operation.

High harmonics[2] from rare gases were first observed in 1987 at moderate laser intensities of about $10^{13}\text{W}\cdot\text{cm}^{-2}$ [6, 7]. A semi-classical "three-step" model for the explanation of this phenomenon was proposed in [8] and later substantiated in [9].

According to this three-step-model (Fig. 1.1) the effective Coulomb potential binding valence electrons to the atomic core is temporarily suppressed around the oscillation peak of the laser electric field. As a result a valence electron can tunnel through or escape above the potential barrier formed by the superposition of the atomic Coulomb field and the instantaneous laser field.

The freed electron is moved away from the atomic core and then driven back to it by a linearly polarized laser field. The interaction of the returning electron with its parent ion may trigger several processes, including secondary electron emission, excitation of bound electrons and emission of a soft X-ray photon.

[2]More than 30 multiples of the laser frequency

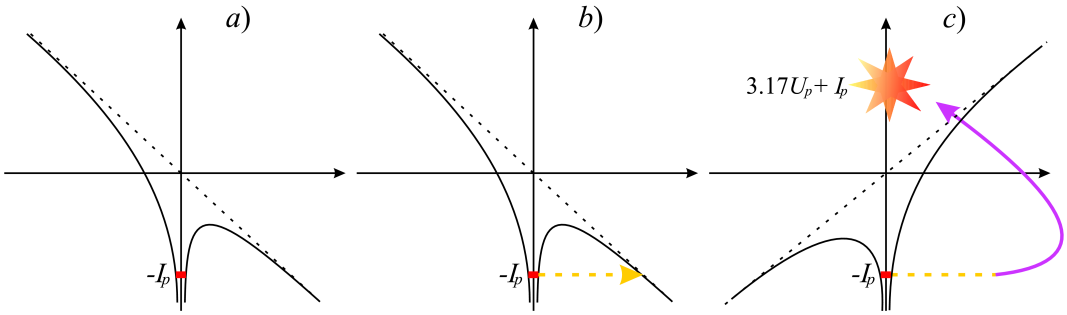

Figure 1.1: The three stages of the "three-step" Corkum model. See text for details.

The trajectory of the freed electron driven by a strong, linearly polarized optical field is described by the classical Hamiltonian

$$H = \frac{1}{2m_e}\left(\pi + \frac{e}{c}A(t)\right)^2, \tag{1.1}$$

where π is the canonical momentum. Since the electron has zero velocity at the time t_i of its release, one can readily check that the electron returns to the parent ion at t_r given as an implicit function of t_i by the equation

$$A(t_i)(t_r - t_i) = \int_{t_i}^{t_r} A(\tau)\, d\tau. \tag{1.2}$$

Since the electric field is known, one can solve this equation for t_i as a function of t_r. The result for a Gaussian wave packet is presented in Fig. 1.2 a. Evidently, several roots t_r can be found for a single t_i depending on how many oscillations the electron performs around the nucleus. Root branches, which belong to one half-period of the laser field, are painted in the same colour.

Due to the absorption of the returning electron by the parent atom at t_r, a photon with energy

$$\hbar\omega = \frac{e^2}{2m_e c^2}\left(A(t_r) - A(t_i)\right)^2 + I_p, \tag{1.3}$$

is emitted, where the first term in (1.3) is the kinetic energy of the returning electron, which can be found from Eq. (1.2), and I_p is the ionization potential, i.e. Eq. (1.3) is simply the energy conservation law. One can easily calculate this energy for every t_i. The result is presented in Fig. 1.2 b.

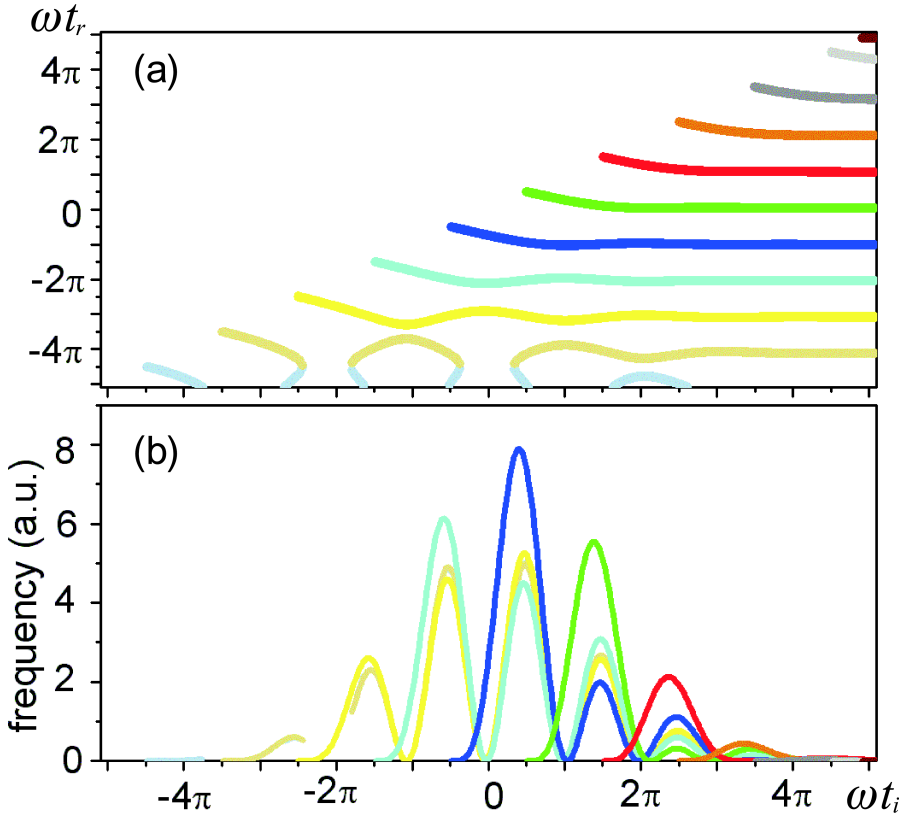

Figure 1.2: Solution of Eq. (1.2): (a) roots t_r for each t_i; (b) photon energy emitted at time t_r: $\hbar\omega(t) = e^2(A(t_r) - A(t_i))^2/2m_ec^2$ [10].

A simulation of the three-dimensional time-dependent Schrödinger equation (TDSE) [10] gives a very close result to what the classical picture shows (Fig. 1.3). In the simulations of the TDSE the total current generated due to the interaction between the hydrogen atom and the laser was calculated. The function $I(t, \omega)$ describing the intensity of radiation within the spectral interval $(\omega - \Delta\omega, \omega + \Delta\omega)$ (with $\hbar\Delta\omega = 15$ eV) at time t is plotted on the (t, ω)-plane by colour indicating the amplitude of I.

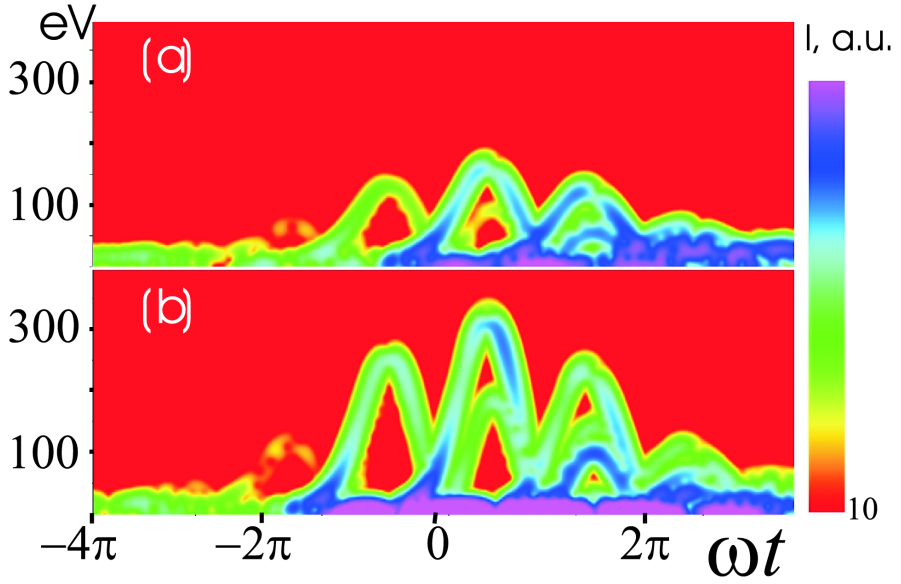

Figure 1.3: Spectral intensity (arbitrary units) vs time in TDSE simulations [10]: (a) $U_p = 44$ eV; (b) $U_p = 93$ eV. Compare with Fig. 1.2 b.

Eq. (1.3) predicts that for the optical field $A(t) = A_0 \cos(\omega_0 t)$ the maximum energy of emitted photons is

$$\hbar\omega_{max} = 3.17U_p + I_p, \tag{1.4}$$

where U_p is the ponderomotive potential

$$U_p[\text{eV}] = \frac{e^2 A_0^2}{4m_e c^2} = 9.3 \times 10^{-14} I[\text{W} \cdot \text{cm}^{-2}]\lambda_0^2[\mu\text{m}^2].$$

A direct application of the high-order harmonics is the generation of short pulses for high resolution experiments [11, 12]. The current state of technology allows the generation of pulses of several hundred attoseconds duration (1as $= 10^{-18}$s) applying a filter and letting a significant number of gas harmonics interfere.

In order to generate even shorter pulses more such harmonics are needed. Due to the expression (1.4) describing the number of high harmonics generated from gases, it is evident that the only route to shorter pulse durations involves higher laser intensities[3].

However, at intensities higher than $10^{16}\mathrm{W}\cdot\mathrm{cm}^{-2}$ the electron trajectory is disturbed by the magnetic field and, as a result, the electron misses the parent ion on its return. Applying even higher intensities leads to complete ionization of the gas molecules, thereby stopping any generation of high harmonics. In other words, a completely new medium is needed in order to support the interaction of laser radiation with matter at higher intensities. The plasma state of matter has been identified as such a promising medium, able to generate sufficient harmonics and to produce attosecond [13] and even sub-attosecond[4] pulses [14].

1.3 Coherent X-rays from Plasma

The first observation of high harmonic generation from plasma was accomplished in 1981 [15]. A solid target was irradiated by a CO_2-laser and turned into plasma. This resulted in the observation of a number of harmonics limited by the plasma frequency. A theoretical explanation of this phenomenon was proposed shortly afterwards [16].

A new range of laser intensities was opened up with the development of the CPA technique. This revived the interest in high harmonic generation from plasma. The ultra-short and intense pulses provided by CPA turn a solid target almost immediately into overdense plasma which starts performing a complicated motion. The plasma electron fluid experiences huge pressure from the electromagnetic radiation and starts moving, driven by the Lorentz force of the laser radiation and the Coulomb attraction to the ions. As a result, the radiation reflected from the plasma contains a high frequency component (Fig. 1.4).

The current understanding of high harmonic generation from plasma in the ultra-relativistic regime emerged as a result of gradual development of theoretical ideas, analysis of numerical simulations and experimental data. For this reason it is instructive to take a look at the evolution of ideas and controversies that prompted the search for new methods and theoretical approaches.

[3] or longer wavelengths. The latter is connected with technological difficulties.

[4] Such pulses are called zepto-second pulses, where 1zs= 10^{-21}s

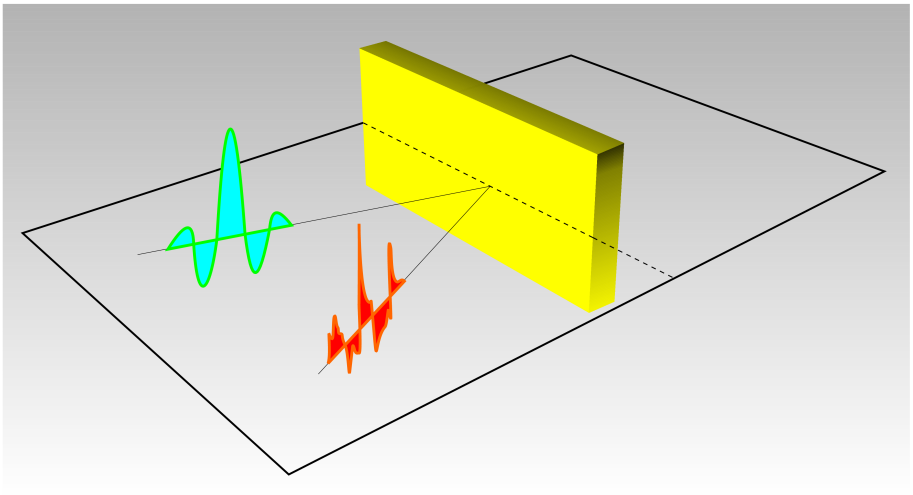

Figure 1.4: When a laser pulse of ultra-relativistic intensity irradiates a planar solid target it almost immediately turns into overdense plasma. The reflected radiation contains high frequencies.

1.3.1 First Theoretical Approaches to Relativistic Harmonics

While in classical optics the field amplitude is small enough so that the electron oscillation velocities are always much less than the speed of light c, with the advent of laser intensities above $10^{18}\mathrm{W{\cdot}cm^{-2}}$, the electron motion entered the ultra-relativistic regime. As a result, relativistic effects fundamentally change the electron response to light.

A new approach to the interaction of ultra-short and relativistically strong laser pulses with overdense plasma was needed and in 1993 such an approach was proposed [17]. The generation of high harmonics in this regime was interpreted as due to the Doppler effect produced by a reflecting charge sheet, formed in a narrow region at the plasma boundary, oscillating under the action of the laser pulse [17]. This "relativistic oscillating mirror" model predicts a cutoff harmonic number of $4\gamma_{max}^2$, where γ_{max} is the maximal relativistic factor of the mirror. However, the "oscillating mirror" cannot explain the generation of high-order harmonics from plasma in the relativistic regime for several reasons.

First, despite its name, the plasma mirror is transparent at surprisingly low γ-factors. In order to see this, let us consider a slab of plasma with density N_e moving with constant velocity v and relativistic γ-factor

$\gamma = 1/\sqrt{1-(v/c)^2} \gg 1$, which collides with a laser pulse of frequency ω_0 and dimensionless vector potential $a_0 = eA_0/m_e c^2$. In the reference frame co-moving with the plasma the vector potential of the laser pulse does not change its value a_0, the plasma density becomes N_e/γ and the laser frequency is increased to $2\gamma\omega_0$. Consequently, even for $a_0 \ll 1$ the slab becomes transparent if

$$\frac{N_e}{4\gamma^3 N_c} \leq 1, \tag{1.5}$$

where $N_c = m_e\omega_0^2/(4\pi e^2)$ is the critical density. As a result, the plasma mirror is opaque only for relativistic γ-factors less than

$$\gamma_{tr} = \left(\frac{N_e}{4N_c}\right)^{1/3}. \tag{1.6}$$

Therefore the relativistic Doppler effect could apply to explain the generation of harmonics from plasma only for harmonic numbers less than

$$n_D = 4\gamma_{tr}^2 = \left(\frac{2N_e}{N_c}\right)^{2/3}. \tag{1.7}$$

This Doppler cut-off related to plasma transparency is too low in order to interpret the results of numerical simulations and experimental data. The numerical simulations in [18] and [19] demonstrated the generation of a large number of harmonics, exceeding the plasma frequency. More recent numerical results produced over 1000 harmonics [14], while the current relativistic laser-matter interaction experiments deliver photons with over 3 keV energies [21, 20].

Secondly, the model of the ideal mirror assumes that the reflection is linear in the reference frame in which the mirror is at rest. This assumption is the corner stone in the derivation of the relation between the frequency of the incoming radiation ω_i and the frequency of the reflected radiation $\omega_r = 4\gamma^2\omega_i$. However, such linear response theory is not applicable to the plasma mirror for $a_0 \geq 1$ and, consequently, the relativistic oscillating mirror model is not applicable to relativistic intensity laser pulses due to the non-linear reflection in the reference frame of the mirror.

As a final remark let us notice that the relativistic mirror moves with constant velocity according to its definition and does work against the pressure of the electromagnetic radiation. For this reason in the laboratory reference frame the energy of the radiation reflected from the ideal mirror is $4\gamma^2$ times larger than the energy of the incident pulse. This violates the

energy conservation law for the laser-plasma interaction in which all energy is delivered into the system by the driving incident laser pulse.

Although the relativistic mirror model is not applicable for the explanation of high harmonic generation in the relativistic regime, this model is widespread in the physics community. One reason for this is that in the late nineties the relativistic mirror model was used in order to fit the spectrum of reflected radiation obtained by numerical simulations. It was found that only a couple of modes describing the plasma surface oscillations were needed to fit the shape of spectra observed numerically for various laser intensities and plasma densities. The small number of modes that were necessary for a good fit over rather wide ranges of densities and intensities was considered a reliable confirmation of the relativistic mirror model.

In reality, it is clear that an arbitrary spectrum can be obtained with a proper choice of modes. Moreover, as one of its major results, this Thesis demonstrates that the harmonic spectrum depends only on one parameter and can be described by a simple function. Therefore it is not surprising that such single-parametric dependence can be fitted by a small number of modes for wide ranges of laser intensities and plasma densities.

By the year 2004 a number of experimental [23]–[32] and theoretical [13], [33]–[37] results on relativistic laser-overdense plasma interaction were obtained. However, apart from the numerical fit of the spectrum as $I(\omega) \propto \omega^{-5}$ proposed in [18], no theoretical description of the harmonic spectrum was known. An attempt to calculate the harmonic spectrum was made in 1996. In [35] the laser-plasma interaction was modeled as reflection from a sharp plasma boundary (oscillating mirror), the motion of which was considered a harmonic function of time. This approach led to an analytical expression for the harmonic spectrum intensity.

The idea that the harmonic spectrum does not depend on a particular model for the motion of the plasma boundary but is described by a universal function was announced for the first time in 2004 [14]. Although the approximation used in [14] did not allow the finding of an exact analytical expression for this universal function, it suggested that the harmonic spectrum contains a long region decaying according to a power-law and this power-law decay was used to fit numerical results. The calculation of the spectrum in [14] showed that the saddle points defining the spectrum of high harmonics gain an imaginary part for frequencies exceeding $4\gamma_{max}^2\omega_0$, where γ_{max} is the maximal γ-factor of the plasma surface motion. This effect was interpreted as the end of the power-law decay of the harmonic spectrum. The present Thesis demonstrates that the power-law decay goes well beyond

these frequencies.

As a final remark notice that the analytical calculation performed in [14] relies on the boundary condition $\mathbf{E}_\perp = 0$, where $\mathbf{E}_\perp$ is the component of the electric field tangential to the plasma surface. However, this boundary condition is not relativistically invariant. Therefore, it is necessary to specify a particular reference frame in which this condition applies. A qualitatively new approach to ultra-relativistic laser-overdense plasma interaction was given in 2006 by the Theory of Relativistic Spikes [38, 39] to which this Thesis is devoted. This new approach avoids any phenomenological boundary conditions and obtains relativistically invariant results for the high harmonic spectrum.

1.3.2 Theory of Relativistic Spikes

Similarity theory for ultra-relativistic laser-plasma interaction was developed [40] in 2004 in order to derive scalings for the intensity of the focused harmonic radiation from concave plasmas. This theory[5] showed that the ultra-relativistic electron motion differs qualitatively from the collective motion of the plasma towards the laser pulse [38]. As a result the similarity theory evoked the idea of relativistic spikes.

The theory of relativistic spikes is based on the apparent reflection point formalism. This formalism described in Chapter 2 allows re-formulating any non-linear reflection as a problem of calculating the radiation emitted by an abstract moving surface. For ultra-relativistic overdense plasma the qualitative behaviour of this abstract surface comes from the motion of the plasma skin layer and demonstrates ultra-relativistic spikes in its γ-factor. Chapter 3 of this Manuscript examines the ultra-relativistic spikes. As a brief introduction to this subject, we summarize the basic physical ideas and results of the theory of relativistic spikes here.

Let us consider a laser pulse, linearly polarized in the y-direction, that is normally incident onto a slab of overdense plasma with surface in the (y, z)-plane. It is well known that the transverse momentum of an electron inside the skin layer is

$$p_y = \frac{eA_y(t, x)}{c}, \tag{1.8}$$

[5]The ultra-relativistic similarity theory is applicable to both overdense and underdense plasmas. For underdense plasmas in the context of electron acceleration this theory was developed in detail in [41].

where A_y is the y-component of the vector potential. Consequently, the x-component of electron velocity is

$$v_x = c\frac{p_x}{\sqrt{m_e^2c^2 + p_x^2 + (eA_y(t,x)/c)^2}} \tag{1.9}$$

Ultra-relativistic similarity theory [41] shows that if overdense plasma is irradiated by a laser pulse of ultra-relativistic intensity and dimensionless vector potential a_0 both the transverse momentum of electrons $p_y = eA_y/c$ and the momentum perpendicular to the plasma surface p_x scale as $m_e c a_0$, provided that the parameter $S = N_e/a_0N_c$ is held constant.

It is interesting that both momenta p_x and p_y result from apparently quite different physical processes. The momentum p_x is due to the radiation pressure which pushes the electron fluid and forces the Coulomb electron-ion attraction to start restoring the equilibrium. The momentum p_y is due to the surface current that does not allow the incident laser pulse to penetrate into the plasma. Nevertheless, these two momenta are of the same order of magnitude $m_e c a_0$.

Consequently the velocity of electrons inside the skin layer is about c and their relativistic γ-factor scales as a_0. However, this ultra-relativistic velocity is not directed perpendicular to the plasma surface. As a result, the value of the γ-factor corresponding to the electron motion that is normal to the plasma surface is

$$\gamma_x = \frac{1}{\sqrt{1-(v_x/c)^2}} = \sqrt{\frac{m_e^2c^2 + p_x^2 + (eA_y(t,x)/c)^2}{m_e^2c^2 + (eA_y(t,x)/c)^2}} \tag{1.10}$$

is not usually as large as a_0 but is of the order of unity.

However, when the vector potential at the point x passes through zero, the velocities of the electrons at this point and within a small neighbourhood are directed along the normal to the plasma surface (Fig. 1.5). Since the vector potential oscillates with frequency ω_0, the vector potential passes through zero at x according to the scaling $A_y \propto m_e c^2 a_0 \omega_0 t$. Therefore the electron velocity v_x at x is a smooth function reaching the maximum value $c\left(1 - O(a_0^{-2})\right)$. At the same moment when v_x reaches its maximum the corresponding γ-factor γ_x jumps[6] up to a_0 and the electrons located at x emit high frequency photons.

This means that each point of the ultra-relativistic skin layer contributes to the high harmonic generation when the zero of the vector potential passes

[6]These jumps are called ultra-relativistic spikes.

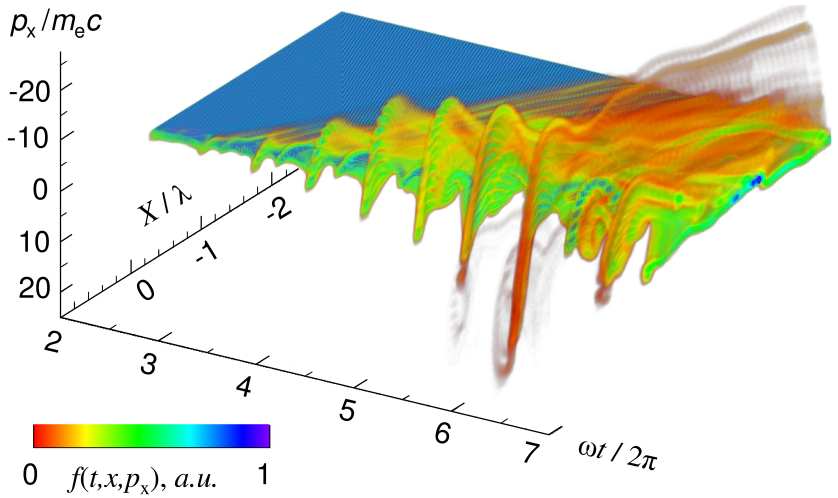

Figure 1.5: Electron distribution function $f(t, x, p_x)$ as a function of time, x-coordinate in direction of laser pulse propagation and corresponding electron momentum p_x [14]. Electron bursts towards the laser pulse caused by the zeros of the vector potential can clearly be observed. At the same moments of time v_x reaches its maximum, the corresponding γ-factor γ_x jumps up to a_0 and the electrons, located at the zero of the vector potential, emit high frequency photons.

through it. As a result, the outcoming radiation is accumulated during the whole time the zero of the vector potential travels through the skin layer. To understand this accumulation process one has to notice that the velocity of the zero of the vector potential coincides with the local phase velocity of the signal. On the other hand, the velocity of the vector potential's zero is the velocity of the radiation source. This means that the phase matching condition is automatically satisfied in the whole skin layer.

This physical picture has two important consequences. First of all, since the high harmonics are generated by the whole skin layer due to coherent emission of different parts at different times, the skin layer can radiate harmonics that are much shorter than its thickness. Secondly, since the whole relativistic skin layer is involved in this process, the high harmonic generation is robust and is not affected by the surface roughness, provided that it does not destroy the structure of the whole skin layer.

The accumulated radiation manifests itself in the form of electromagnetic shock waves ($a_0 \to +\infty$) propagating in vacuum in which the electric field E_r of the reflected wave depends on time as

$$E_r(t,x) = const_1 + const_2 \times (ct-x)^{1/3} \tag{1.11}$$

These shock-waves are distinctive in numerical simulations demonstrating the local steepening of the reflected electric field (Fig. 1.6). This local steepening according to the power law $(ct-x)^{1/3}$ is a characteristic feature of the ultra-relativistic γ-spike mechanism.

Contrary to the relativistic Doppler effect that compresses the pulses and causes a frequency upshift, a relativistic γ-spike leads to local steepness without any compression of the incident pulse. It is worth emphasizing that the compression of the pulse and the upshift of all frequencies makes the spectrum of the reflected radiation strongly dependent on the spectrum of the incidence laser pulse. On the other hand, the steepening due to the electromagnetic shock is a local phenomenon resulting in the universal spectrum of high harmonics, which can be calculated as the Fourier image of the electromagnetic shock:

$$|E_r(\omega)|^2 \propto \left| \int_{-\infty}^{+\infty} (ct-x)^{1/3} e^{i\omega t} dt \right|^2 \propto \frac{1}{\omega^{8/3}}, \tag{1.12}$$

where $E_r(\omega) = \int_{-\infty}^{+\infty} E_r(t,x) \exp(i\omega t) dt$. The electromagnetic shocks are

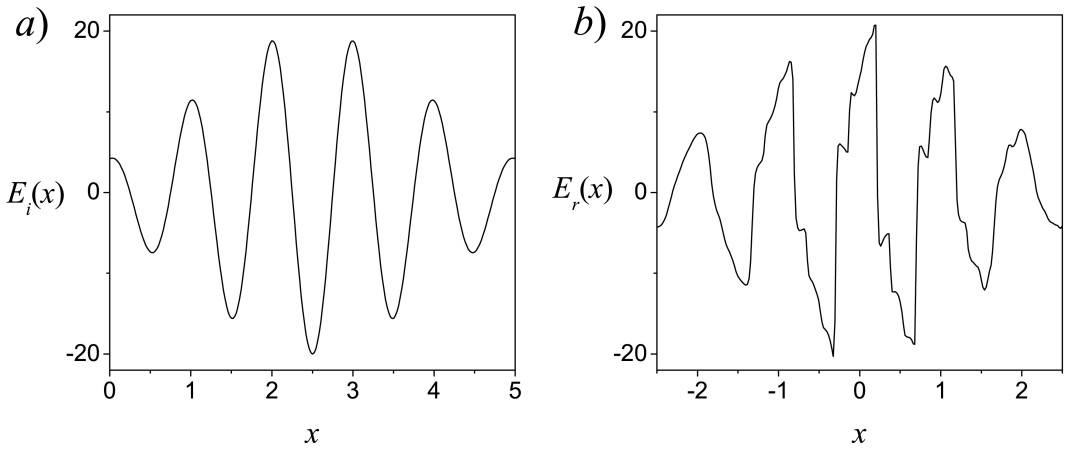

Figure 1.6: Numerical simulation with the particle-in-cell code VLPL[47] performed for the case of $a_0 = 20$ and $N_e = 90N_c$ demonstrates a) the incoming laser radiation and b) the reflected radiation containing electromagnetic shocks.

derived and discussed in detail in Chapter 4 of this Thesis.

The relativistic spikes allow us to derive a single analytical formula describing the whole universal spectrum of high harmonics:

$$|E_r(\omega)|^2 \propto \left(\frac{\omega_0}{\omega}\right)^{8/3} Ai^2\left(\frac{1}{N}\left(\frac{\omega}{\omega_0}\right)^{2/3}\right), \tag{1.13}$$

where $N = \alpha^{1/3} n_{cr}/2$, $n_{cr} = 2/(1 - v_s)$ and v_s is the velocity corresponding to the peak of the γ-spike. The theory of relativistic spikes proves that N scales as a_0^2. Ai is the well-known Airy function:

$$Ai(x) = \frac{1}{\sqrt{\pi}} \int_0^{+\infty} \cos\left(ux + \frac{1}{3}u^3\right) du, \tag{1.14}$$

the asymptotic expansion of which confirms Eq. (1.12) and demonstrates that for $\omega < \omega_{roll} = N^{3/2}\omega_0 \propto a_0^3\omega_0$ the spectrum decays as

$$|E_r(\omega)|^2 \propto \left(\frac{\omega_0}{\omega}\right)^{8/3}, \tag{1.15}$$

while for $\omega > \omega_{roll}$ the spectrum of high harmonics decays exponentially

$$|E_r(\omega)|^2 \propto \left(\frac{\omega_0}{\omega}\right)^3 \exp\left(-\frac{4}{3N^{3/2}}\frac{\omega}{\omega_0}\right). \tag{1.16}$$

The high harmonic spectrum predicted by (1.13) can be beautifully visualized in a numerical simulation (Fig. 1.7).

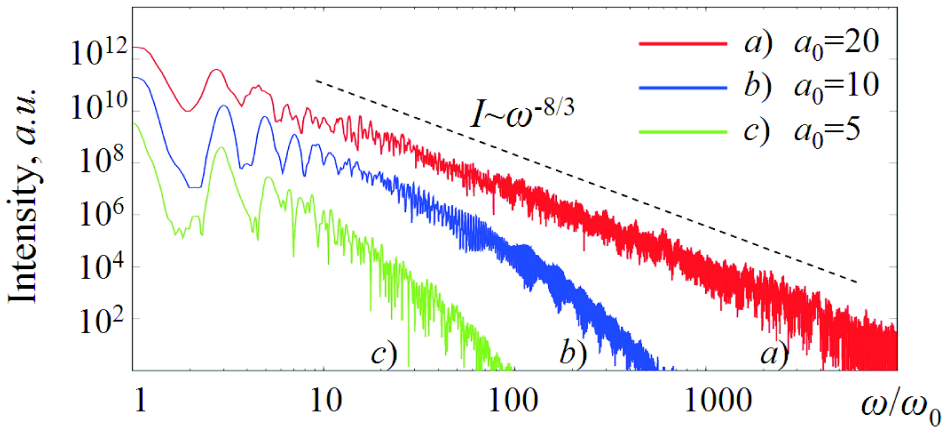

Figure 1.7: Spectra of the high harmonics generated by laser-overdense plasma interaction, produced by the particle-in-cell code VLPL [47]. These numerical simulations clearly demonstrate the power-law decay of the harmonic spectrum [14].

The origin of the a_0^3-roll-over can be illustrated physically using the idea of ultra-relativistic spikes. Let us estimate the duration of one pulse of high harmonics emitted at the boundary of a relativistic plasma. Since these harmonics are generated only during a γ-spike, the first photon is radiated at time t_1 when the position of the plasma surface is x_1 and the last one at time $t_1 + \Delta t_s$ when the position of the surface is x_2 (Fig. 1.8 b). However, since the photon moves with velocity c, which differs from the velocity of the γ-spike v_s, the first photon has come to the position x_3. As a result, the spatial delay between the first and the last photon radiated from the plasma surface is

$$\Delta l_{pulse} = x_3 - x_2 \approx (c - v_s)\Delta t_s = \frac{c\Delta t_s}{\gamma_s^2},$$

where $\gamma_s^2 = 1/(1 - (v_s/c)^2)$.

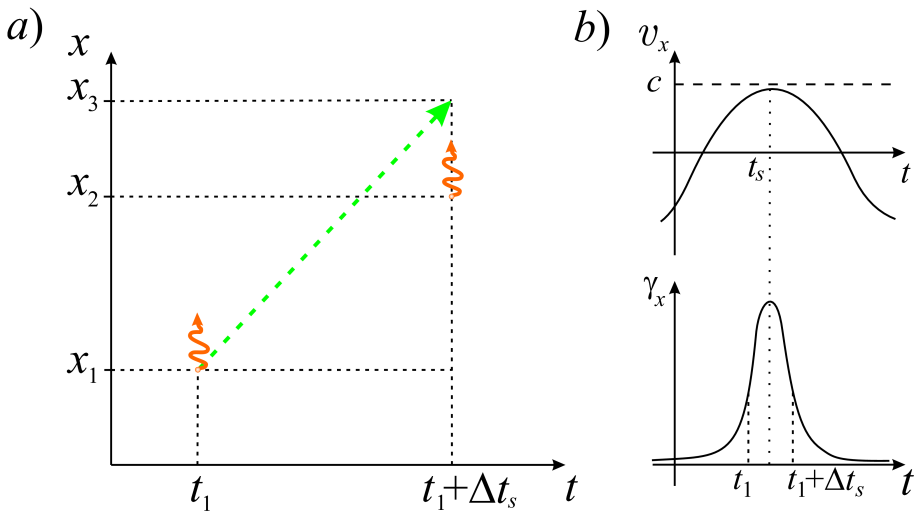

Figure 1.8: Physical illustration of the a_0^3 scaling for the roll-over harmonic frequency. See text for details.

In order to estimate this delay we calculate the width of the γ-spike. For this purpose we make use of the fact that the velocity v_x is a smooth function and expand it as a parabola around its maximum v_s (Fig. 1.8 b)

$$v_x(t) = v_s - c\alpha\left(\omega_0 t\right)^2 .$$

Consequently, the corresponding γ-factor is

$$\gamma^2(t) = \frac{1}{1-(v_x(t)/c)^2} \approx \frac{1}{1-(v_s/c)^2+2\alpha\left(\omega_0 t\right)^2},$$

which gives us the width of the γ-spike as

$$\Delta t_s \propto \frac{1}{\sqrt{\alpha}\omega_0\gamma_s},$$

where γ_s is the maximal relativistic factor of the γ-spike, which, as we pointed out previously, is proportional to a_0. As a result we obtain for the spatial duration of the harmonic pulse

$$\Delta l_{pulse} \propto \frac{1}{a_0^3}, \tag{1.17}$$

which corresponds to a number of a_0^3 harmonics in the frequency domain.

Chapter 4 of this manuscript is devoted to the detailed discussion of the universal harmonic spectrum. Nevertheless, it is worth emphasizing at this

point that the power law decay, the a_0^3-roll-over and the following exponential decay are all consequences of the same physical phenomenon and are obtained from the same formula (1.13).

As mentioned earlier the high harmonics from plasma have been identified as a promising source of ultra-short pulses. Since all high harmonics are locked in the time domain in the form of an electromagnetic shock, they are highly coherent. In other words their constructive interference results in the generation of extremely short pulses, the duration of which is defined by the harmonic spectrum (1.13). One readily sees that the pulse duration scales as

$$T \propto \frac{1}{\omega_{roll}} \propto \frac{1}{\omega_0 a_0^3}.$$

These short pulses are embedded in the low frequency background which has to be filtered out in order to reveal the high frequency content. As a result, the structure of the filtered pulses depends on the position of the filter relative to the position of the roll-over frequency [38]. Moreover, it is possible to control the development of ultra-short pulses by means of changing the polarization of the incident laser pulse in order to isolate single sub-attosecond pulses [39]. Chapter 5 studies these ultra-short pulses in detail.

Finally, let us point out that shortly after the publication of the major results of the theory of relativistic spikes, the predictions of this theory were confirmed experimentally [21, 22].

1.3.3 Experimental Results

The experiments confirming the theory of relativistic spikes were performed using the Vulcan Petawatt laser at the Rutherford Appleton Laboratories, which can readily reach peak intensities of about $10^{21}\mathrm{W{\cdot}cm^{-2}}$, delivering up to 600 J on a target in about 500 fs [21, 22]. After applying a plasma mirror which significantly increases the contrast of the experiment, the spectrum of the radiation generated by the plasma target was measured (Fig. 1.9).

The harmonic spectra were taken for two different intensities $(1.5\pm0.3)\times 10^{20}\mathrm{W{\cdot}cm^{-2}}$ (red trace on Fig. 1.9) and $(2.5\pm0.5)\times10^{20}\mathrm{W{\cdot}cm^{-2}}$ (blue trace). It was found that both the power-law decay part of the spectrum as well as the position of the roll-over frequency ω_{roll} are in agreement with the predictions of the theory of relativistic spikes. The coherent nature of the generated harmonics was demonstrated by the highly directional beamed

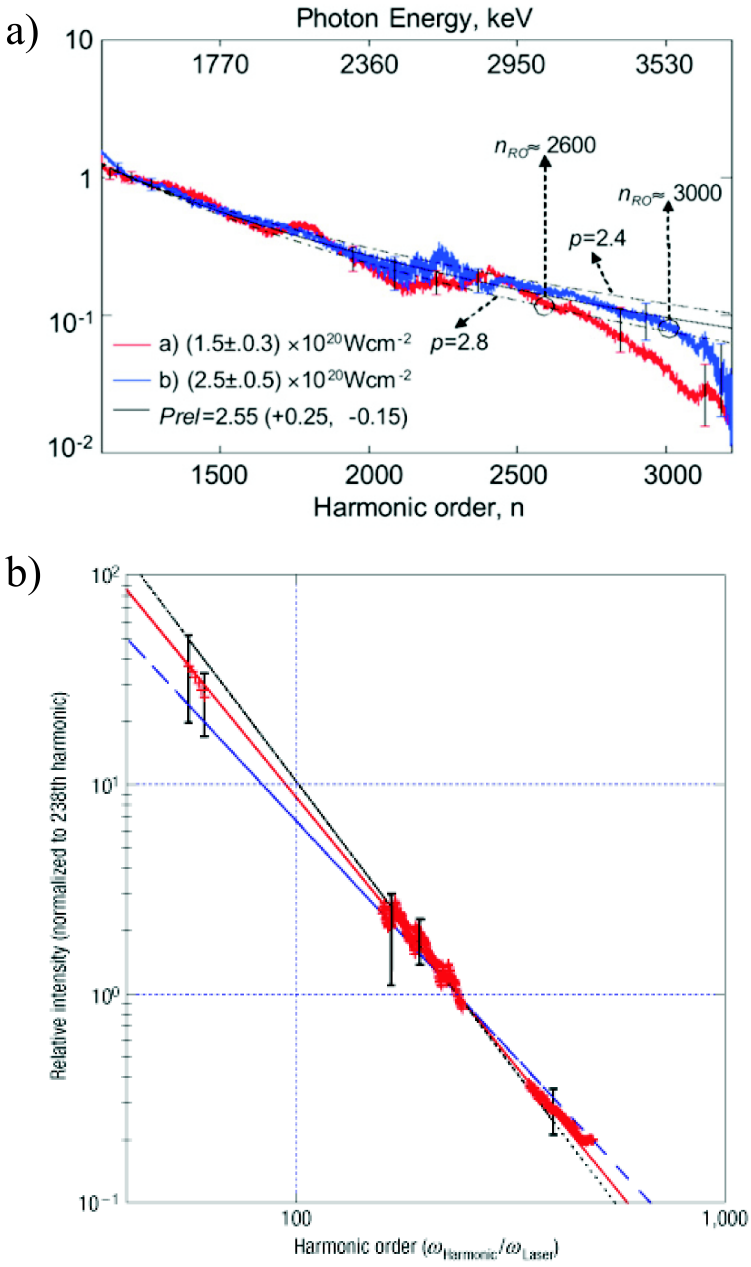

Figure 1.9: Power-law scaling in the relativistic limit obtained using the Vulcan Petawatt laser in the x-ray regime. a) 1200th–3200th order harmonics, corresponding to wavelengths of 9–3 Å; b) 60th–850th orders, corresponding to wavelengths of 17–1.2 nm. Figures from [21, 22].

emission, which for photon energy $h\nu > 1$ keV was found to be into a cone angle $\propto 4^o$ (Fig. 1.10), significantly less than the incident laser cone (20^o).

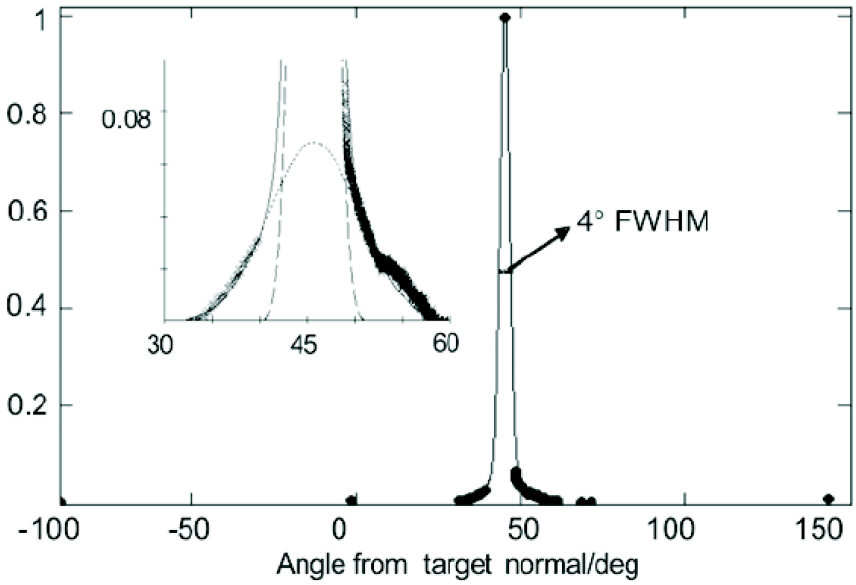

Figure 1.10: Angular distribution of > 1 keV x-ray signal under high contrast conditions. The signal is emitted into a narrow cone peaked in the specular direction at 45^o(the laser incidence angle is -45^o). Figure from [21].

It is interesting to notice that the number of harmonics generated in these experiments is huge. The wavelengths of the highest harmonics observed are only a couple of Ångströms. Thus, these harmonics have wavelengths comparable with the inter-atomic distances in solids. As we explained earlier in this Section, such high frequency harmonics are generated at the boundary of the relativistic plasma since the process of high harmonic generation is not affected by the plasma surface roughness and the whole bulk of the skin layer efficiently contributes to the generation of even the shortest harmonics. This point is discussed in detail in Chapter 3.

1.4 Thesis Structure

This Thesis is organized as follows. Every Chapter contains a brief introductory part, which points out the key issues considered in that Chapter.

Chapter 2 "Apparent Reflection Point Formalism" presents the new mathematical tools that are used in this Thesis. The apparent reflection point formalism introduced here enables one to study the non-linear processes of reflection. This mathematical approach allows the high harmonic generation from relativistic plasma to be studied in a relativistically consistent way.

Chapter 3 "Relativistic Spikes" examines the apparent reflection point dynamics for non-linear relativistic reflection from overdense plasma and obtains scalings characterizing the most important features of this dynamics. For the first time the apparent reflection point formalism is combined with the relativistic similarity theory. This consideration allows the role of the laser pulse polarization to be taken into account for the case of oblique laser pulse incidence which is applied in the high-power laser laboratories.

Chapter 4 "High Harmonic Generation" applies the results of the first two Chapters to derive the universal spectrum of the high harmonics. The new physical phenomenon of electromagnetic shocks, which is introduced here, is a distinctive feature of the relativistic laser-plasma interaction. The analytical description of the electromagnetic shock-waves, which points out the relation between the shocks and the universal harmonic spectrum, is obtained in this Thesis for the first time.

Chapter 5 "Ultra-Short Pulses" studies one of the most interesting applications of the plasma harmonics - the generation of ultra-short pulses. This Chapter demonstrates the generation of trains of zepto-second pulses with tunable structure and introduces the mechanism of Relativistic Plasma Control which allows isolating single zepto-second pulses.

Chapter 6 "Conclusions" contains a brief summary of the main results obtained here.

Chapter 2

Apparent Reflection Point Formalism

The theory of high harmonic generation at the boundary of an ultra-relativistic overdense plasma is based on the concept of an apparent reflection point (ARP). In this Chapter the notion of an apparent reflection point is introduced and the ARP formalism is discussed.

The main goal of this formalism is to highlight the connection between an incident laser pulse and reflection radiation, while hiding the details of the interaction in the background. This connection is obtained as a pure consequence of the $1D$ wave equation in vacuum. For this reason the concept of ARP is rather general and can be applied to various media. However, this method unfolds its full power when it is applied to high harmonic generation from overdense ultra-relativistic plasmas.

The ARP formalism is a new approach to problems concerning laser-matter interaction. In this Chapter we derive the master equation for apparent reflection point dynamics and study the properties of this equation related to Lorentz transformations. The ARP formalism relies on the tensor properties of the electromagnetic field and enables one to use the ideas of relativistic invariance in order to simplify the concrete problems of non-linear laser-matter interaction.

2.1 Wave Equation and Apparent Reflection Point

Let us consider a slab of matter irradiated by a laser. The specific nature of the irradiated matter is of no importance, since the formalism which is developed here is based only on the properties of the wave equation in vacuum and the universal relation between the current density and the vector potential following from the Maxwell equations.

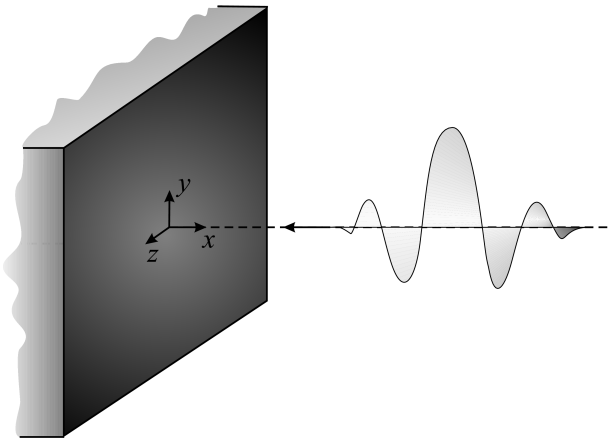

Figure 2.1: A slab of matter is irradiated normally by a laser pulse moving in x-direction. The directions y and z are tangential to the slab.

Choosing the direction of negative x to be the direction of laser pulse propagation, let us consider the tangential components of the vector potential of a laser pulse normally incident onto the slab. The vector potential satisfies the equation

$$\frac{1}{c^2}\frac{\partial^2 \mathbf{A}(t,x)}{\partial t^2} - \frac{\partial^2 \mathbf{A}(t,x)}{\partial x^2} = \frac{4\pi}{c}\mathbf{j}(t,x), \tag{2.1}$$

where

$$\mathbf{A}(t, x = -\infty) = 0 \tag{2.2}$$

and $\mathbf{j}$ is the tangential current density.

For the particular case of linear laser polarization (along the y-axis) we see that the y component of Eq. (2.1) satisfies the equation[1]

$$\frac{1}{c^2}\frac{\partial^2 A(t,x)}{\partial t^2} - \frac{\partial^2 A(t,x)}{\partial x^2} = \frac{4\pi}{c} j(t,x), \tag{2.3}$$

[1]We skip the indexes and write $A = \mathbf{A} \cdot \mathbf{e}_y$ and $j = \mathbf{j} \cdot \mathbf{e}_y$ for brevity.

the solution of which is

$$A(t,x) = 2\pi \int_{-\infty}^{+\infty} J\left(t,x,t',x'\right)\, dt'dx'. \tag{2.4}$$

Here

$$J\left(t,x,t',x'\right) = j\left(t',x'\right)\left(\Theta_- - \Theta_+\right),$$

where we have defined Θ_- and Θ_+ as

$$\Theta_- = \Theta\left(t - t' - \left|x - x'\right|/c\right); \quad \Theta_+ = \Theta\left(t - t' + \left(x - x'\right)/c\right)$$

and $\Theta(t)$ is the Heaviside step-function. Due to this choice of J, the vector potential $A(t,x)$ satisfies both Eq. (2.1) and the boundary condition at $x = -\infty$. Since the tangential electric field is

$$E = -\frac{1}{c}\frac{\partial A(t,x)}{\partial t},$$

from Eq. (2.4) one readily obtains

$$E(t,x) = \frac{2\pi}{c} \int_{-\infty}^{+\infty} \left(j(t - |x - x'|)/c, x') - j(t + (x - x')/c, x')\right) dx', \tag{2.5}$$

where $E = \mathbf{E} \cdot \mathbf{e}_y$ is the y-component of the electric field.

Note that both terms in Eq. (2.5) have clear mathematical and physical meaning: the first term is a partial solution of the inhomogeneous wave-equation, the second term is a solution of the homogeneous wave-equation. This term is necessary in order to satisfy the physical condition (2.2) of electromagnetic field decay inside the slab. The current is localized at the slab boundary, since for large negative x we have $|x - x'| = -(x - x')$ and $\lim_{x\to-\infty} E(t,x) = 0$.

A point requiring closer attention is the time dependence of the terms in Eq. (2.5). The first term always depends on the retarded time. The time dependence in the second term is quite different. At points located deep inside the slab the time in the second term is retarded, however in the area remote from the medium the second term depends on the advanced time.

The non-trivial time dependence of the second term can be understood physically. Indeed, long before the interaction and far away from the slab, i.e.

$$t \to -\infty, x \to +\infty$$

the electromagnetic field coincides with the incident laser pulse. Since for such t and x the first term in Eq. (2.5) vanishes, the second term

$$E_i(t,x) = -\frac{2\pi}{c}\int_{-\infty}^{+\infty} j(t+(x-x')/c, x')\,dx' \tag{2.6}$$

must represent the incident laser pulse. The source of this field in Eq. (2.6) is the electron current j, which is a function of the advanced time. In other words, the incident laser pulse is expressed through the current density which it is going to generate in the future.

Since the second term in Eq. (2.5) is the incident laser pulse, the first term is the electromagnetic field generated by the surface current induced in the medium. As a result, one sees that the reflected radiation in vacuum[2] is

$$E_r(t,x) = \frac{2\pi}{c}\int_{-\infty}^{+\infty} j(t-(x-x')/c, x')\,dx'. \tag{2.7}$$

The physical meaning of E_i and E_r just discussed motivates the definition of the apparent reflection point. Let us introduce the new vector field[3]

$$\Gamma(t,x) = \frac{2\pi}{c}\int_{-\infty}^{+\infty} (j(t-(x-x')/c, x') - j(t+(x-x')/c, x'))\,dx', \tag{2.8}$$

which is related to the incoming and reflected electric field in vacuum as

$$\Gamma(t,x) = E_i(t,x) + E_r(t,x). \tag{2.9}$$

The ARP is defined as the point $X(t)$, where the field $\Gamma(t,x)$ equals zero

$$\Gamma(t, X(t)) = 0. \tag{2.10}$$

[2]In other words, far from the slab, where $x \to +\infty$.

[3]Note that one obtains the field $\Gamma(t,x)$ from Eq. (2.5) by dropping out the sign of modulus inside the current density.

The zero of Γ is named apparent reflection point, since to an external observer in vacuum it appears that the reflected radiation originates from the reflection of the laser pulse at this point.

Note that the field Γ coincides with the electric field E in vacuum[4]. However, it should be emphasized that Γ does not coincide with the physical electric field E inside the matter. Neither does Γ satisfy the Maxwell equations there. However, one can check by direct substitution that the field Γ is a solution of the wave-equation in vacuum for all x.

Due to its connection with E_i and E_r, the ARP can be used to relate the reflected and incoming radiation. In order to use this connection efficiently however, we must first clarify the relativistic properties of the apparent reflection point.

2.2 Relativistic Definition of Apparent Reflection Point

Let us see what happens to the apparent reflection point if we change the frame of reference. For this purpose we consider a reference frame (t', x') moving with constant velocity u in the x direction. The Lorentz transformation describing this change of reference frame can be written as

$$x = \gamma(x' + c\beta t'); \quad ct = \gamma(ct' + \beta x'),$$

where $\beta = u/c$ and $\gamma = 1/\sqrt{1-\beta^2}$.

Since the definition of Γ in (2.9) does not depend on the reference frame, in the moving frame (t', x') we have

$$\Gamma'(t', x') = E_i'(t', x') + E_r'(t', x'), \tag{2.11}$$

where the electric field of the incident and reflected radiation in the moving frame transforms as

$$E_i' = rE_i; \quad E_r' = E_r/r, \tag{2.12}$$

with the transition factor

$$r = \sqrt{\frac{1+\beta}{1-\beta}}. \tag{2.13}$$

[4]Compare Eqs. (2.5) and (2.8) for $x \to +\infty$.

In the moving reference frame the ARP $X'(t')$ is defined again as the zero position of the field Γ':

$$\Gamma'(t', X'(t', r)) = 0. \tag{2.14}$$

In order to study the processes accompanying laser-matter interaction it is more convenient to work with fields and electric currents in the laboratory reference frame. Therefore let us notice that the apparent reflection point $X'(t', r)$, defined by Eq. (2.14), is not the image of the ARP $X(t) = X(t, 1)$ defined in the laboratory reference frame as the zero point of $\Gamma(t, x)$ (see Eq. (2.10)). Instead, if $X'(t', r)$ is the image of a point $X(t, r)$ obtained by the Lorentz transformation with the transition factor r, in the laboratory reference frame $X(t, r)$ satisfies the equation (see Eq. (2.12))

$$r^2 E_i(ct + X(t, r)) + E_r(ct - X(t, r)) = 0 \tag{2.15}$$

or equivalently

$$\frac{2\pi}{c} \int_{-\infty}^{+\infty} j(t - (X(t, r) - x)/c, x)\, dx = -r^2 E_i(ct + X(t, r)). \tag{2.16}$$

Thus, each Lorentz transformation (2.16) defines a point $X(t, r)$ which is characterized by the transition factor r of the Lorentz transformation. As a result, the whole set of Lorentz transformations defines a pool of points parametrized by r. These points have a clear physical meaning. According to Eq. (2.11) it appears to an external observer moving with velocity u, that the incoming laser radiation is reflected at the point

$$X'(t', r) = \gamma(X(t, r) - c\beta t); \quad ct' = \gamma(ct - \beta X(t, r)),$$

where $\beta = u/c$ and $\gamma = 1/\sqrt{1 - \beta^2}$.

As we have just seen, the relativistic definition (2.16) of the ARP provides a pool of apparent reflection points with a free parameter r. However, there is a relation between these different points $X(t, r)$. In order to formulate this relation, let us consider two such points $X(t_1, r_1)$ and $X(t_2, r_2)$, taken at such moments of time that the corresponding phases of the reflected field $\Psi(t, r) = ct - X(t, r)$ coincide

$$\Psi(t_1, r_1) = \Psi(t_2, r_2). \tag{2.17}$$

Using Eq. (2.15) one obtains

$$\frac{r_1^2}{r_2^2} = \frac{E_i(ct_2 + X(t_2, r_2))}{E_i(2ct_1 - ct_2 + X(t_2, r_2))}. \tag{2.18}$$

We can use Eq. (2.18) in order to calculate t_2 as a function of t_1, r_1 and r_2:

$$t_2 = T(t_1, r_1, r_2), \tag{2.19}$$

and to find the connection between these two points

$$X(t_1, r_1) = ct_1 - cT(t_1, r_1, r_2) + X(T(t_1, r_1, r_2), r_2). \tag{2.20}$$

Notice that Eq. (2.20) depends only on the shape of the initial pulse and does not contain any information about the laser-matter interaction leading to the generation of the reflected signal.

It is worth emphasizing that the free parameter r appears in all applications of the ARP-formalism. However, we will see that all final results depend only on invariants of the transformation (2.18) due to the relativistic invariance of the theory. Since all calculations depend on the reference frame in which the quantities involved in the formulas are expressed, the presence of an explicit parameter characterizing the frame of reference allows advantage to be taken of the Lorentz invariance.

The ARPs defined in this Section are the basis of the ARP-formalism. Indeed, in what follows we demonstrate that for large enough r the motion of $X(t, r)$ enables one to reconstruct the reflected radiation E_r.

2.3 Basic Properties of Apparent Reflection Point

In order to see how the reflected radiation can be reconstructed through the apparent reflection point $X(t, r)$, we study some basic properties of this point.

2.3.1 Existence of Apparent Reflection Point

First of all let us show that the ARP always exists. This means for Eq. (2.14) to always have a solution. In order to prove this, let us notice that since E_i' and E_r' satisfy the wave-equation in vacuum, they describe waves

propagating towards $x' = -\infty$ and $x' = +\infty$ correspondingly. As a result, the following integral representations are valid

$$E'_i(t', x') = \int E'_i(\omega) e^{-i\omega t' - ik(\omega)x'} d\omega; \quad E'_r(t', x') = \int E'_r(\omega) e^{-i\omega t' + ik(\omega)x'} d\omega,$$

where $k(\omega) = \omega/c$ since E'_i and E'_r are solutions of the $1D$-wave equation in vacuum. From Eq. (2.8) one reads[5]

$$\int_{-\infty}^{+\infty} \Gamma'(t', x') dx' = 0 \tag{2.21}$$

for all t. Since the integral in Eq. (2.21) equals zero, the function Γ' changes sign and passes through zero. In other words Eq. (2.14) has a solution. Consequently, the apparent reflection points $X(t, r)$ exist for arbitrary r.

It is worth emphasizing that since the physical electric field E satisfies the Maxwell equations, the integral representation for this field is

$$E'(t', x') = \int E'(\omega, k) e^{-i\omega t' - ikx'} d\omega dk, \tag{2.22}$$

where ω and k are independent variables. Consequently, although one can easily demonstrate the existence of zero points for Γ' if a static electric field is not present, one cannot prove the existence of zeros for E' for all t'.

2.3.2 Reconstruction of Reflected Radiation

The main idea behind the ARP-formalism is to reconstruct the radiation reflected from the slab. As we saw there is a relation between incoming and reflected signal provided by the apparent reflection points $X(t, r)$. Moreover, we demonstrated that the ARPs exist for all r. Yet the existence of $X(t, r)$ alone does not mean that we can obtain full information about E_r.

Indeed, let us rewrite Eq. (2.15) as

$$E_r(\Psi) = -r^2 E_i(\Phi), \tag{2.23}$$

where

$$\Psi(t, r) = ct - X(t, r) \quad \text{and} \quad \Phi(t, r) = ct + X(t, r).$$

[5]Since there is no static electrostatic field ($\omega = 0$) parallel to the slab neither in the incident nor in the reflected pulse.

Only if $\Psi(t,r)$ changes from $-\infty$ to $+\infty$ when t runs from $-\infty$ to $+\infty$, Eq. (2.23) can be used in order to restore the reflected pulse for all values of the phase $\psi = ct - x$. Since the reflected radiation propagates in $1D$ without change of shape or amplitude, E_r is defined everywhere, provided the dependence of E_r upon ψ is known.

It is clear that not every ARP lets $\Psi(t,r)$ satisfy this condition. However, we can readily identify ARPs which do. Indeed, if we choose r large enough[6] the apparent reflection point will always be located by a zero point of E_i, which propagates from $+\infty$ to $-\infty$. Consequently, $\Psi(t,r)$ changes from $+\infty$ to $-\infty$ as well. As a result E_r is restored for all phases ψ.

A significant role in the proof of the existence of apparent reflection points which allow the reconstruction of E_r is played by the transformation factor r. Therefore let us notice at this place that the parameter r arises due to the fact that the electric field transforms as a component of the electromagnetic tensor under Lorentz transformations [45]. An alternative consideration using the magnetic field components instead of the electric field is also possible.

However, an attempt to develop the ARP-formalism on the basis of the vector potential fails due to its different tensor properties. The Lorentz transformations do not change the relative values of the vector potential of the incident and reflected waves, and this results in difficulty proving that the reflected radiation can be reconstructed for all phases.

2.3.3 Causality Condition

For the apparent reflection points allowing reconstruction of the reflected radiation we can prove the very important property of causality.

Let us consider the derivative of Eq. (2.23) over time. We obtain

$$r^2 \left(c + \frac{dX(t,r)}{dt} \right) \frac{dE_i}{d\Phi} = - \left(c - \frac{dX(t,r)}{dt} \right) \frac{dE_r}{d\Psi}. \tag{2.24}$$

Note that at the moment dX/dt reaches c, $dE_i/d\Phi$ vanishes. In other words, the apparent reflection point $X(t,r)$ is then at the local maximum or minimum of $r^2 E_i$. However, this never happens if the parameter r is large enough. Consequently, the ARP velocity never equals the velocity of light:

$$\frac{dX(t,r)}{dt} \neq c. \tag{2.25}$$

[6] This means $\beta \to 1$

Eq. (2.25) is satisfied for all r larger than some threshold value r_{thresh}. In what follows we restrict our study to the case of $r > r_{thresh}$.

If the parameter r is chosen large enough one can demonstrate that $\dot{X}(t,r)$ is always less than c. Indeed, from Eq. (2.24) one obtains

$$\dot{X} = c\frac{1+\Delta}{1-\Delta}, \tag{2.26}$$

where

$$\Delta = r^2 \frac{dE_i/d\Phi}{dE_r/d\Psi}.$$

For large enough r we have $|\Delta| \gg 1$ and consequently the causality condition

$$\frac{dX(t,r)}{dt} < c$$

applies for the phase Ψ of the reflected radiation.

Let us remark that due to the denominator $dE_r/d\Psi$, Δ can pass through 1 for some Ψ, if r is not sufficiently large. However, the causality condition still applies for the given phase, if we pick the neighbouring zero of E_i, for which the derivative $dE_i/d\Phi$ has the opposite sign.

In conclusion let us notice that the change of apparent reflection point is automatically embedded in a proper parametrization. In order to demonstrate this, let us rewrite Eq. (2.23) in the form

$$E_r(\Psi) = -r^2 E_i(2ct - \Psi). \tag{2.27}$$

In this parametrization it is evident that one can restore the reflected radiation if for each value of the parameter Ψ one can find $t(\Psi)$ in order to satisfy Eq. (2.27). The apparent reflection point is now defined as an implicit function of time as

$$X(\Psi) = ct(\Psi) - \Psi.$$

We now demonstrate that Eq. (2.27) has a solution for all Ψ, if $r > r_{thresh}$. Notice that if Eq. (2.27) is solved for some Ψ_0 and $t_0 = t(\Psi_0)$ is known, then to first order Taylor expansion

$$(\Psi - \Psi_0)\frac{dE_r}{d\Psi} = -r^2\left[2c(t-t_0) - (\Psi - \Psi_0)\right]\frac{dE_i}{d\Phi} + O\left((\Psi - \Psi_0)^2\right).$$

In other words,

$$\begin{aligned} t(\Psi) - t(\Psi_0) &= -\frac{dE_r/d\Psi - r^2 dE_i/d\Phi}{2cr^2 dE_i/d\Phi}(\Psi - \Psi_0), \\ X(\Psi) - X(\Psi_0) &= -\frac{dE_r/d\Psi + r^2 dE_i/d\Phi}{2r^2 dE_i/d\Phi}(\Psi - \Psi_0). \end{aligned}$$

This solution exists for $dE_i/d\Phi \neq 0$, which coincides with our choice of $r > r_{thresh}$. For $dE_r/d\Psi = r^2 dE_i/d\Phi$, which corresponds to $\Delta = 1$, the second order of the Taylor expansion must be taken into account. One reads

$$\frac{1}{2}(\Psi - \Psi_0)^2 \frac{d^2 E_r}{d\Psi^2} = -2cr^2(t - t_0)\frac{dE_i}{d\Phi} - \frac{1}{2}r^2(\Psi - \Psi_0)^2 \frac{d^2 E_i}{d\Phi^2} + O\left((\Psi - \Psi_0)^3\right).$$

In other words,

$$\begin{aligned} t(\Psi) - t(\Psi_0) &= -\frac{d^2 E_r/d\Psi^2 + r^2 d^2 E_i/d\Phi^2}{4cr^2 dE_i/d\Phi}(\Psi - \Psi_0)^2, \\ X(\Psi) - X(\Psi_0) &= -\frac{d^2 E_r/d\Psi^2 + r^2 d^2 E_i/d\Phi^2}{4r^2 dE_i/d\Phi}(\Psi - \Psi_0)^2 - (\Psi - \Psi_0), \end{aligned}$$

and thus the solution $(X(\Psi), t(\Psi))$ exists for all phases Ψ.

2.4 Apparent Reflection Point and Boundary Conditions

In this Chapter we introduced the apparent reflection point formalism and examined its general properties. This advance was necessary in order to develop tools for the examination of relativistic laser-matter interactions without applying any phenomenological boundary conditions.

One reason to avoid such boundary conditions lies in the complexity of the non-linear interactions and the restrictions enforced by relativistic invariance. Not only are boundary conditions for such problems difficult to state but the ultra-relativistic laser radiation significantly perturbs the electron fluid density, which makes even the notion of a plasma boundary quite obscure.

Yet the major reason is that in our study of ultra-relativistic laser-matter interaction we are looking for universal relations. In other words, if we apply a boundary condition it has to be universal as well. The difficulty in finding

such boundary conditions is immense. To resolve this problem the idea of boundary conditions is replaced by the new theoretical approach - apparent reflection point formalism - introduced in this Chapter.

In conclusion we notice an interesting analogy between the presented ARP-formalism and the S-matrix formalism well-known from quantum mechanics [42]. The S-matrix connects the incident free particles with the outcoming ones obtained due to collision. Here we applied similar logic to the problem of laser-matter interactions and found the relation (2.23) between the incident laser pulse E_i propagating in vacuum and the reflected radiation E_r at a large distance from the reflecting matter.

In quantum mechanics the efficiency of the S-matrix formalism is revealed by two quite different types of applications. The S-matrix hides the details of the particle collision and often allows results of physical importance to be expressed through a limited set of parameters that can be measured experimentally. On the other hand, in order to express these parameters through the characteristics of the particle interaction, dynamic equations must be studied. However, if the parameters that are relevant to the problem have been calculated, postulated or derived from the experimental results, one can apply the S-matrix as a black-box, thus obtaining general results without having to give attention to how the parameters entering the theory relate to the microscopic Hamiltonian.

The same logic applies to the ARP-formalism. In the next Chapter we consider laser-matter interactions on the microscopic level in order to express the parameters characterizing the important features of apparent reflection point motion. Then we describe the non-linear relativistic reflection from overdense plasma through these parameters. We demonstrate how the combination of universal features of relativistic plasma dynamics with the ARP-formalism and the fundamental restrictions following from relativistic invariance lead to an understanding of the physics of non-linear relativistic reflection as a new class of universal phenomena.

Chapter 3

Relativistic Spikes

The apparent reflection point (ARP) formalism introduced in Chapter 2 allows general expressions to be obtained for the structure of the radiation reflected from the plasma as a result of laser-overdense plasma interaction. These expressions are based on the motion of a single point - the apparent reflection point.

Due to its importance for the reconstruction of the reflected radiation, this Chapter is given over to the derivation of scalings describing the dynamics of the apparent reflection point in relativistic laser plasma interactions. For this purpose the dynamics of a plasma driven by a laser pulse of relativistic intensity is analyzed.

The interaction of an intense laser pulse with a plasma is accompanied by a variety of complex non-linear phenomena and a number of instabilities [43]. When the laser pulse intensity is relativistic, strong relativistic non-linearities start playing an important role and evoke fascinating phenomena. There are several ways to approach this new physics. Firstly, due to sustained increase in computer power and corresponding reduction in the cost of computer resources, numerical simulations of relativistic laser plasma interaction have become available in many research laboratories and universities. Secondly, simplified theoretical models which can be studied analytically provide valuable clues to the understanding of relativistic plasma physics.

Apart from these obvious approaches there is a third one. As has recently been noticed, similarity theory can be developed in order to treat relativistic laser plasma interactions [40]. Relativistic similarity theory happens to be an efficient tool for the study of both underdense [41] and overdense [40] plasmas. In its generality this approach does not rely on artificial simplifying assumptions and often allows the derivation of scalings efficiently collating

experimental data and theoretical results. The similarity scalings are rigorous mathematical results representing intrinsic symmetry properties of the laser-plasma interaction [44].

In this Chapter we first apply similarity analysis in order to describe qualitatively the ARP motion. The thorough consideration given to the topic below shows that both the relativistic similarity theory itself and the first-order correction to it are of importance for the ARP motion. We demonstrate that the plasma dynamics is characterized by sharp, so called relativistic spikes in the relativistic γ-factor and smooth velocity. The microscopic analysis performed here connects the motion of the plasma electrons with the ARP dynamics. It is shown that the characteristic relativistic spikes determine the dynamics of the apparent reflection point at relativistic laser intensities, for both normal and oblique laser incidence. The ARP motion is demonstrated by numerical simulations.

3.1 Relativistic Similarity for Collisionless Plasma

In what follows we concentrate on laser plasmas involved in high-order harmonic generation (HHG). The standard way to generate high harmonics from overdense plasma is to expose a solid target to the focused radiation of a femtosecond laser (see Fig. 1.4). The target almost immediately turns into overdense plasma with MeV-range energy electrons and density around the solid state density. For these laser plasmas Coulomb collisions are negligible.

Indeed, for $T \leq m_e c^2$ the collision frequency is

$$\nu \propto \omega_{pe} \left(\frac{e^2 n_e^{1/3}}{T} \right)^{3/2} \ln \Lambda, \tag{3.1}$$

where ω_{pe} is the plasma frequency, T is the electron energy and $\ln \Lambda \approx 15$ is the Coulomb logarithm. Since the laser pulse duration is $\tau \propto 2\pi/\omega_0$, for $T \propto m_e c^2$ Eq. (3.1) gives rise to

$$\tau\nu \propto 2\pi \frac{\omega_{pe}}{\omega_0} \left(\frac{e^2 n_e^{1/3}}{T} \right)^{3/2} \ln \Lambda \approx 10^{-5} \ll 1 \tag{3.2}$$

for a laser wavelength of 800 nm and typical solid state density ($e^2 n_e^{1/3} \approx 4$ eV). Consequently on the time scale of the laser we can neglect the Coulomb

collisions and use a collisionless description by means of the relativistic Vlasov equation. Notice that for the case of interest the kinetic energy of the electrons is much larger than $m_e c^2$ and so the role of collisions is even less than estimated by Eq. (3.2).

For this reason, in order to derive the basic scalings of the relativistic similarity, we consider collisionless laser-plasma dynamics. Due to the short duration of the laser pulse, we neglect the ion motion in what follows.

In this work we apply a $1D3V$-description of the laser-plasma interaction. This means that the electron distribution function $f(t, \mathbf{x}, \mathbf{p})$ does not depend on y and z, but only the x-coordinate, corresponding to the direction of laser propagation. In other words there is transitional symmetry in the plasma plane. Of course, the y- and z-components of electron momentum play an important role in the electron dynamics and therefore are taken into account.

This $1D3V$-consideration is justified by the size of the laser beam spot R. Indeed, since the laser pulse cannot be focused to a spot size smaller than the laser wavelength λ_0, we can always assume that

$$k_0 R = \frac{2\pi}{\lambda_0} R \gg 1.$$

We start our analysis with consideration of the case of normal laser incidence. The case of oblique incidence is subject of Section 3.6.

Due to the transitional symmetry in the plasma plane, the tangential canonical momentum

$$\boldsymbol{\pi}_\perp = \mathbf{p}_\perp - e\mathbf{A}_\perp/c \tag{3.3}$$

is conserved. For this reason we have

$$\mathbf{p}_\perp = \frac{e\mathbf{A}_\perp}{c}, \tag{3.4}$$

where $\mathbf{A}_\perp = (A_y, A_z)$ is the vector potential tangential to the plasma, and $\mathbf{p}_\perp = (p_y, p_z)$ is the corresponding electron momentum. Eq. (3.4) follows from the fact that $\boldsymbol{\pi}_\perp = 0$ before the arrival of the normally incident laser pulse. Consequently, the kinetic state of the plasma is described by the electron distribution function $f(t, x, p_x)$, the evolution of which is given by the relativistic Vlasov equation[1]

$$\frac{\partial f}{\partial t} + \frac{\partial}{\partial x}(v_x f) + \frac{\partial}{\partial p_x}(F_x f) = 0. \tag{3.5}$$

[1]For the derivation of this equation see Appendix 1.

Here v_x is the relativistic electron velocity in the x-direction

$$v_x = \frac{p_x c}{\sqrt{m_e^2 c^2 + p_x^2 + (e\mathbf{A}_\perp/c)^2}}, \tag{3.6}$$

F_x is the Lorentz force acting on the electrons

$$F_x = -e\left(E_x + v_y B_z/c\right) = e\left(\frac{\partial \phi}{\partial x} - \frac{\mathbf{v}_\perp}{c} \cdot \frac{\partial \mathbf{A}_\perp}{\partial x}\right), \tag{3.7}$$

ϕ is the electrostatic potential and $\mathbf{v}_\perp = (v_y, v_z)$ is the tangential relativistic electron velocity

$$\mathbf{v}_\perp = \frac{e\mathbf{A}_\perp}{\sqrt{m_e^2 c^2 + p_x^2 + (e\mathbf{A}_\perp/c)^2}}. \tag{3.8}$$

In order to obtain a closed system of equations for the electromagnetic potential, we add the Poisson equation for ϕ and the wave equation for $\mathbf{A}_\perp$ [45]

$$\frac{\partial^2 \phi}{\partial x^2} = 4\pi e(N_e - \rho) \tag{3.9}$$

$$\frac{1}{c^2}\frac{\partial^2 \mathbf{A}_\perp}{\partial t^2} - \frac{\partial^2 \mathbf{A}_\perp}{\partial x^2} = \frac{4\pi}{c}\mathbf{j}_\perp. \tag{3.10}$$

Here N_e is the background ion density, coinciding with the unperturbed electron density, and

$$\rho = \int f(t, x, p_x) dp_x; \quad \mathbf{j}_\perp = -e \int \mathbf{v}_\perp f(t, x, p_x) dp_x. \tag{3.11}$$

Just before entering the plasma the vector potential of the laser pulse is

$$\mathbf{A}_\perp(t = 0) = \mathrm{Re}\left(\mathbf{a}(x/c\tau_0)e^{-ik_0 x}\right), \tag{3.12}$$

where $k_0 = \omega_0/c$ is the wavenumber.

If one fixes the initial laser envelope $\mathbf{a}(x)$, which means that incident laser pulses always have the same shape, the laser-plasma dynamics depends on three dimensionless parameters: the laser amplitude

$$a_0 = \max\left|\frac{e\mathbf{a}}{m_e c^2}\right|,$$

the pulse duration $\omega_0 \tau_0$ and the plasma density ratio N_e/N_c, where

$$N_c = \frac{m_e \omega_0^2}{4\pi e^2}$$

is the critical density.

The basic idea of ultra-relativistic similarity is that in the ultra-relativistic limit ($a_0^2 \gg 1$), the number of independent dimensionless parameters reduces to two: $\omega_0 \tau_0$ and S, where the similarity parameter S is defined as

$$S = \frac{N_e}{a_0 N_c}. \tag{3.13}$$

In order to demonstrate this key property of ultra-relativistic dynamics we introduce new dimensionless variables

$$\hat{t} = S^{1/2}\omega_0 t, \quad \hat{x} = S^{1/2} k_0 x, \quad \hat{p_x} = p_x / m_e c a_0, \tag{3.14}$$

$$\hat{\mathbf{A}}_\perp = \frac{e\mathbf{A}_\perp}{m_e c^2 a_0}, \quad \hat{\phi} = \frac{e\phi}{m_e c^2 a_0}, \quad \hat{\mathbf{E}}_\perp = \frac{eS^{-1/2}\mathbf{E}_\perp}{m_e c \omega_0 a_0}$$

and the new distribution function $\hat{f}$, defined as

$$f = \frac{N_e}{m_e c a_0} \hat{f}\left(\hat{t}, \hat{x}, \hat{p_x}, a_0, S, \hat{\tau}\right), \tag{3.15}$$

where

$$\hat{\tau} = S^{1/2}\omega_0 \tau_0. \tag{3.16}$$

The function $\hat{f}$ satisfies the equations

$$\frac{\partial \hat{f}}{\partial \hat{t}} + \frac{\partial}{\partial \hat{x}}(\hat{v}_x \hat{f}) + \frac{\partial}{\partial \hat{p}_x}(\hat{F}_x \hat{f}) = 0 \tag{3.17}$$

$$\frac{\partial^2 \hat{\phi}}{\partial \hat{x}^2} = 1 - \int \hat{f} d\hat{p}_x; \tag{3.18}$$

$$\frac{\partial^2 \hat{\mathbf{A}}_\perp}{\partial \hat{t}^2} - \frac{\partial^2 \hat{\mathbf{A}}_\perp}{\partial \hat{x}^2} = -\int \hat{\mathbf{v}}_\perp \hat{f} d\hat{p}_x, \tag{3.19}$$

where

$$\hat{v}_x = \frac{\hat{p}_x}{\sqrt{\hat{p}_x^2 + \hat{\mathbf{A}}_\perp^2 + a_0^{-2}}}; \quad \hat{\mathbf{v}}_\perp = \frac{\hat{\mathbf{A}}_\perp}{\sqrt{\hat{p}_x^2 + \hat{\mathbf{A}}_\perp^2 + a_0^{-2}}} \tag{3.20}$$

$$\hat{F}_x = \frac{\partial \hat{\phi}}{\partial \hat{x}} - \hat{\mathbf{v}}_\perp \cdot \frac{\partial \hat{\mathbf{A}}_\perp}{\partial \hat{x}}.$$

The initial condition for the vector potential becomes

$$\hat{\mathbf{A}}_\perp(\hat{t}=0) = \hat{\mathbf{a}}\left(\hat{x}/\hat{\tau}\right)\cos\left(S^{-1/2}\hat{x}\right). \tag{3.21}$$

Here $\mathbf{a}$ is a slowly varying envelope such that $\max|\hat{\mathbf{a}}| = 1$.

Eqs. (3.17) and (3.18) together with the initial condition (3.21) still depend on the initial laser polarization, which is assumed fixed[2], and on the dimensionless parameters $\hat{\tau}$, S and a_0. However, the parameter a_0 appears only in the expression for the electron velocity Eq. (3.20). In the limit $a_0^2 \gg 1$ one can write

$$\hat{v_x} = \frac{\hat{p}_x}{\sqrt{\hat{p}_x^2 + \hat{\mathbf{A}}_\perp^2}}; \quad \hat{\mathbf{v}}_\perp = \frac{\hat{\mathbf{A}}_\perp}{\sqrt{\hat{p}_x^2 + \hat{\mathbf{A}}_\perp^2}}. \tag{3.22}$$

Notice that in this limit the normalized distribution function $\hat{f}$ describing the interaction of the given laser pulse with the plasma does not depend on a_0. Moreover, for relativistic amplitudes $a_0^2 \gg 1$, the laser-plasma dynamics does not depend on a_0 and N_e/N_c separately. They merge into the single similarity parameter S instead.

This result has the following physical meaning. When the plasma density and the laser amplitude change simultaneously so that $S = const$, the laser-plasma dynamics remains similar. In particular, this basic relativistic scaling states that for different interactions with the same $S = const$, the plasma electrons move along similar trajectories and their momenta p_x scale as

$$p_x \propto a_0. \tag{3.23}$$

Since $\mathbf{p}_\perp \propto a_0$ as well (see Eq. (3.4)), both electron momentum components are of the same order of magnitude.

The parameter S characterizes the transparency[3] of a laser driven relativistic plasma. If $S \geq 1$ the laser radiation does not penetrate the plasma, yet the plasma becomes transparent for $S \leq 1$ [41].

[2]The role of polarization will be studied later in Chapter 5

[3]The parameter S is the only non-trivial parameter describing relativistic laser-plasma

3.2 Relativistic Spikes and Skin Layer Motion

The general similarity scaling (3.23) obtained in Section 3.1 leads to an intriguing physical picture of the electron fluid motion. In order to understand the qualitative features of this motion we consider a linearly polarized laser pulse for which $A_y = A$ and $A_z = 0$.

The scaling (3.23) shows that when we increase the dimensionless vector potential a_0 of the incident wave but keep the plasma overdense so that $S = const$, both p_x and p_y grow as a_0. This means that although inside the plasma the velocity of the electron fluid

$$v = c\sqrt{\frac{p_x^2 + p_y^2}{m_e^2c^2 + p_x^2 + p_y^2}} = c(1 - O(a_0^{-2})) \tag{3.24}$$

is about the speed of light at all times, the collective plasma motion in the direction of the laser pulse observed from outside the plasma is qualitatively different.

Let us project the electron motion in the laser pulse propagation direction and consider the electron fluid at point x. From Eqs. (3.4) and (3.23) it follows that the momentum of these electrons can be represented as

$$p_x(t, x) = m_e c a_0 \hat{p}_x(S, \hat{t}, \hat{x}); \tag{3.25}$$

$$p_y(t, x) = m_e c a_0 \hat{p}_y(S, \hat{t}, \hat{x}), \tag{3.26}$$

where $\hat{p}_x$ and $\hat{p}_y$ are universal functions, the detailed description of which is of no importance for us here. For the electron collective velocity $\beta_x(t)$ and γ-factor $\gamma_x(t)$ in the skin-layer motion one obtains

$$\beta_x(t) = \frac{p_x(t)}{\sqrt{m_e^2c^2 + p_x^2(t) + p_y^2(t)}} = \frac{\hat{p}_x(t)}{\sqrt{\hat{p}_x^2(t) + \hat{p}_y^2(t)}} + O(a_0^{-2}), \tag{3.27}$$

$$\gamma_x(t) = \frac{1}{\sqrt{1 - \beta_s^2(t)}} = \sqrt{1 + \frac{\hat{p}_x^2(t)}{\hat{p}_y^2(t)}} + O(a_0^{-2}). \tag{3.28}$$

interaction. It automatically takes into account that the plasma is driven by the laser pulse and treats the penetration of the radiation into the plasma dynamically and self-consistently. As a result the self-consistent transparency condition $S \leq 1$ differs significantly from the "moving mirror" model predictions; compare Eqs. (1.6) and (3.23)

It now becomes evident that when a_0 gets large, the relativistic γ-factor of the electrons increases and their velocities approach the speed of light (see Eq. (3.24)). However, the collective dynamics of the plasma boundary is significantly different. For large a_0 the plasma boundary motion does not enter the ultra-relativistic regime and its relativistic γ-factor $\gamma_x(t)$ is generally of the order of unity (see Eq. (3.28)). Yet there is one exception. If at the moment t_s it happens that

$$p_y(t_s, x) = 0, \tag{3.29}$$

we have

$$\gamma_x = \frac{1}{\sqrt{1-\beta_x^2}} = \sqrt{\frac{p_x^2 + m_e^2 c^2}{m_e^2 c^2}} \propto a_0. \tag{3.30}$$

So, the relativistic γ-factor of the electron fluid at point x jumps to $\gamma_x(t_s) \propto a_0$ and the duration of this relativistic γ-spike is

$$\Delta t \propto 1/(a_0 \omega_0). \tag{3.31}$$

One can find in just the same way that the velocity of the electron fluid element smoothly approaches the velocity of light as $\beta_x(t_s) = (1 - O(a_0^{-2}))$. Fig. 3.1 visualizes this behaviour.

One could suppose that this characteristic spikey behaviour is transferred to the motion of the apparent reflection point as well. Yet this picture is convincing only for a thin skin layer. Otherwise the thickness of the skin layer must be taken into account and the fact that different points of the skin layer get the spikes at different times would have to be examined carefully. The microscopic theory developed in the following sections of this Chapter addresses the finite thickness skin layer problem.

3.3 Theory of Apparent Reflection Point Motion

In order to start the analysis of the ARP dynamics one must choose the apparent reflection point which will be examined. In other words, we have to specify a value of the parameter r in Eq. (2.15). The final results concerning the reflected radiation are not affected by this choice, yet the difficulty in the derivation of the results can be reduced immensely by making the proper choice.

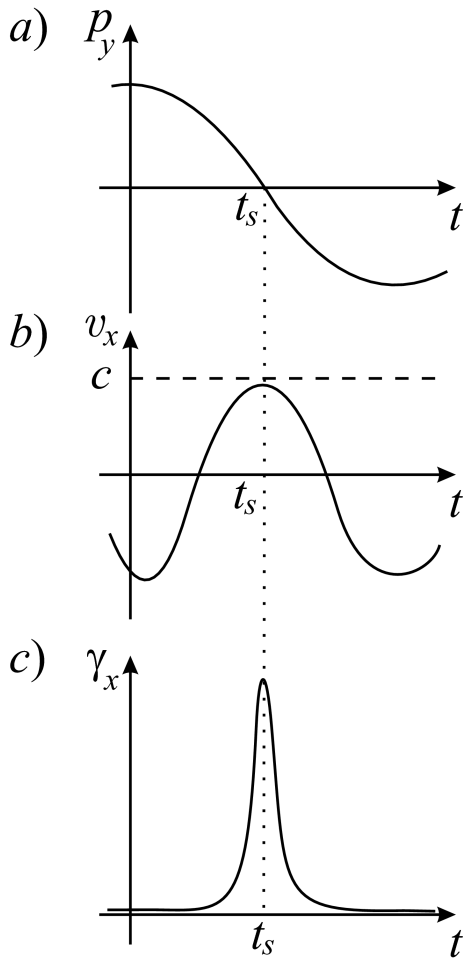

Figure 3.1: a) Tangential electron momentum; b) collective plasma skin-layer velocity and c) γ-factor. At the time when $p_y(t_s, x) = 0$ the γ-factor has a sharp spike, while the velocity v_x is a smooth function.

The ultra-relativistic similarity theory presented in Section 3.1 demonstrates that the ratio between the incident and reflected radiation does not depend on a_0 but is defined by S and $\hat{\tau}$ instead. As a result one can choose a threshold value r_{thresh} of r depending only on S, $\hat{\tau}$ in order to guarantee that Eq. (2.15) has a solution enabling one to reconstruct the reflected radiation. We are not interested in the value of r_{thresh}, yet we are going to consider r as an independent parameter satisfying the inequality $r > r_{thresh}$.

Let us start from the definition of the ARP position given as a solution of Eq. (2.16) which we re-write as

$$\int_{-\infty}^{+\infty} j\left(t^-, x\right)\, dx = -\frac{cr^2}{2\pi} E_i(ct + X(t,r)) \tag{3.32}$$

where

$$t^- = t - \frac{X(t,r) - x}{c}.$$

Differentiation of Eq. (3.32) with respect to t leads to

$$\frac{dX(t,r)}{dt} = c\frac{1+\Delta}{1-\Delta}, \tag{3.33}$$

where

$$\Delta = \frac{c^2 r^2}{2\pi D}\frac{dE_i}{d\Phi}, \tag{3.34}$$

$\Phi = ct + X(t)$ and the denominator D is

$$D = \int_{-\infty}^{+\infty} \frac{\partial}{\partial t^-} j(t^-, x)\, dx.$$

According to Eq. (3.33), dX/dt approaches the speed of light c only if $\Delta \to 0$. Since we can always choose r large enough in order to guarantee that the value of $E_i(ct + X(t,r))$ is close to zero, the value of $dE_i(ct + X(t,r))/d\Phi$ can be considered as a constant. Consequently, the value of dX/dt can approach the speed of light only if D becomes large.

In order to examine the value of D notice that the current density is

$$j(t^-, x) = -e \int v_y(t^-, x, p_x) f(t^-, x, p_x) dp_x, \tag{3.35}$$

where

$$v_y = \frac{eA_y(t^-, x)}{\sqrt{m_e^2c^2 + p_x^2 + e^2A^2(t^-, x)/c^2}}.$$

In what follows we will denote the denominator of this expression as

$$P(t^-, x, p_x) = \sqrt{m_e^2c^2 + p_x^2 + e^2A^2(t^-, x)/c^2}$$

and the dimensionless quantity p_x/P as

$$\xi(t^-, x, p_x) = p_x/P(t^-, x, p_x).$$

Differentiation of Eq. (3.35) yields

$$D = I_1 + I_2,$$

where

$$\begin{aligned} I_1 &= -e^2 \int_{-\infty}^{+\infty} \frac{A_y(t^-, x)}{P} \frac{\partial f(t^-, x, p_x)}{\partial t^-} dp_x dx \\ I_2 &= -e^2 \int_{-\infty}^{+\infty} f(t^-, x, p_x) \frac{\partial A_y(t^-, x)}{\partial t^-} \frac{m_e^2c^2 + p_x^2}{P^3} dp_x dx. \end{aligned}$$

Making use of the Vlasov equation (3.5) and integrating by parts, one obtains[4]

$$D = D_1 + D_2 + D_3 + D_4,$$

where

$$D_1 = -e^2 \int_{-\infty}^{+\infty} (1 + \xi) c p_x \frac{dK(t^-, x)}{dx} \mu M(t, x, p_x) dx dp_x \tag{3.36}$$

$$D_2 = -e^2 \int_{-\infty}^{+\infty} \frac{dF_x}{dp_x} K(t^-, x) P \mu M(t, x, p_x) dx dp_x \tag{3.37}$$

$$D_3 = -e^2 \int_{-\infty}^{+\infty} (1 + \xi) F_x K \mu M(t, x, p_x) dx dp_x \tag{3.38}$$

$$D_4 = -e^2 \int_{-\infty}^{+\infty} \frac{\partial A_y}{\partial t^-} \frac{m_e^2c^2}{m_e^2c^2 + (eA_y/c)^2} \frac{\mu M(t, x, p_x)}{P} dx dp_x, \tag{3.39}$$

[4]See Appendix 2 for details

using the notation

$$K(t^-, x) = \frac{A_y}{m_e^2 c^2 + (eA_y/c)^2}$$

$$\mu = \frac{1}{1 - v_x/c} = \frac{P^2}{m_e^2 c^2 + (eA_y/c)^2}(1 + \xi)$$

$$\frac{dF_x}{dp_x} = \frac{e^2}{c} A \frac{\partial A}{\partial x} \frac{p_x}{P^3}.$$

Finally, $M(t, x, p_x)$ is the electron counting function

$$M(t, x, p_x) = \sum_i \delta\left(p_x - p_i(t_i)\right) \delta\left(x - x_i(t_i)\right),$$

with

$$t_i = t - \frac{X(t, r) - x_i}{c}.$$

Since $\int M(t, x, p_x) dp_x$ related to the electron density scales as a_0, one can estimate the behaviour of $D_{1,2,3,4}$ according to the similarity scalings. Let us consider, for example, D_4. If the vector potential A has no zero point inside the plasma skin-layer one applies the scaling $A \propto a_0$ to obtain $D_4 \propto a_0^{-1}$.

If A has a zero point, the vicinity of the zero point in which $|A| \leq m_e c^2$ gives the main contribution to the integral estimated as

$$D_4 \propto a_0^3 \Delta l, \tag{3.40}$$

where Δl is the typical length on which $|A| \leq m_e c^2$. Thus, Δl is at least of the order of a_0^{-1} and, consequently, D_4 is at least as large as a_0^2.

The scalings for Δl and D_4 will be stated more precisely later in Section 3.4 of this Chapter. For now it is important to draw the conclusion that as a consequence of Eq. (3.33) the velocity of the ARP approaches c as a_0 goes to infinity:

$$\lim_{a_0 \to +\infty} v_s = c,$$

where v_s is the velocity of the apparent reflection point at the time of its local extremum. The asymptotic behaviour of γ_{ARP} for a_0 is examined in the next Section.

3.4 Relativistic Motion of Apparent Reflection Point

As we have just seen, in the ultra-relativistic limit $a_0 \to \infty$ the velocity of the apparent reflection point v_s approaches the speed of light c. In order to find the exact scaling for v_s when a_0 is large, we develop perturbation theory for the ARP dynamics.

For this purpose we use Eqs. (3.17) and (3.18) describing this dynamics. The perturbation theory we intend to develop presents the difference between the velocity of light and v_s as an expansion over $1/a_0^2$.

The zero-order approximation corresponds to $a_0 = \infty$ and the ARP position $\hat{X}^{(0)}(\hat{t}, r)$ is found from the following zero-order (over $1/a_0^2$) equations

$$\int \hat{v}_y^{(0)}(\hat{t}_0^-, \hat{x}) \hat{f}^{(0)}(\hat{t}_0^-, \hat{x}, \hat{p}_x) d\hat{x} d\hat{p}_x = -2r^2 \hat{E}_i(\hat{t} + \hat{X}^{(0)}(\hat{t}, r))$$

$$\frac{\partial \hat{f}^{(0)}(\hat{t}, \hat{x}, \hat{p}_x)}{\partial \hat{t}} + \frac{\partial}{\partial \hat{x}} \left(\hat{v}_x^{(0)} \hat{f}^{(0)}(\hat{t}, \hat{x}, \hat{p}_x) \right) + \frac{\partial}{\partial \hat{p}_x} \left(\hat{F}_x^{(0)} \hat{f}^{(0)}(\hat{t}, \hat{x}, \hat{p}_x) \right) = 0$$

$$\frac{\partial^2 \hat{\phi}^{(0)}}{\partial \hat{x}^2} = 1 - \int \hat{f}^{(0)}(\hat{t}, \hat{x}, \hat{p}_x) d\hat{p}_x$$

$$\frac{\partial^2 \hat{A}^{(0)}}{\partial \hat{t}^2} - \frac{\partial^2 \hat{A}^{(0)}}{\partial \hat{x}^2} = - \int \hat{v}_y^{(0)} \hat{f}^{(0)}(\hat{t}, \hat{x}, \hat{p}_x) d\hat{p}_x,$$

where

$$\hat{v}_y^{(0)} = \frac{\hat{A}}{\sqrt{\hat{p}_x^2 + \hat{A}^2}}; \quad \hat{v}_x^{(0)} = \frac{\hat{p}_x}{\sqrt{\hat{p}_x^2 + \hat{A}^2}}; \quad \hat{F}_x^{(0)} = \frac{\partial \hat{\phi}^{(0)}}{\partial \hat{x}} - \hat{v}_y^{(0)} \frac{\partial \hat{A}^{(0)}}{\partial \hat{x}}$$

and

$$\hat{t}_0^- = \hat{t} - \hat{X}^{(0)} + \hat{x}.$$

Note that the zero-order in the perturbation theory which we develop coincides with the ultra-relativistic similarity from Section 3.1. However for our purpose we need to go beyond the similarity theory and analyze the first-order approximation over $1/a_0^2$.

The first-order perturbation is a result of taking into account the finite value of $1/a_0^2$. In other words we look for $X(t, r)$ as

$$\hat{X}(\hat{t},r) = \hat{X}^{(0)}(\hat{t},r) + \hat{X}^{(1)}(\hat{t},r),$$

where $\hat{X}^{(1)}$ is due to the change in the velocity by

$$\hat{v}_y^{(1)} = -\frac{1}{2a_0^2}\frac{\hat{A}}{\left(\hat{p}_x^2+\hat{A}^2\right)^{3/2}}; \qquad \hat{v}_x^{(1)} = -\frac{1}{2a_0^2}\frac{\hat{p}_x}{\left(\hat{p}_x^2+\hat{A}^2\right)^{3/2}},$$

as well as to corrections to the distribution function $\hat{f}^{(1)}$, the electrostatic potential $\hat{\phi}^{(1)}$ and the vector potential $\hat{A}^{(1)}$. One easily obtains that these first-order corrections satisfy the following equations

$$\int \hat{v}_y^{(0)}(\hat{t}_0^-,\hat{x})\hat{f}^{(1)}(\hat{t}_0^-,\hat{x},\hat{p}_x)d\hat{x}d\hat{p}_x - \hat{X}^{(1)}S_X = -\int \hat{v}_y^{(1)}(\hat{t}_0^-,\hat{x})\hat{f}^{(0)}(\hat{t}_0^-,\hat{x},\hat{p}_x)d\hat{x}d\hat{p}_x, \tag{3.41}$$

where

$$S_X = \int \partial_{\hat{t}_0^-}\left(\hat{v}_y^{(0)}(\hat{t}_0^-,\hat{x})\hat{f}^{(0)}(\hat{t}_0^-,\hat{x},\hat{p}_x)\right)d\hat{x}d\hat{p}_x - 2r^2\partial_{\hat{t}}\hat{E}_i(\hat{t}+\hat{X}^{(0)}),$$

$$\frac{\partial \hat{f}^{(1)}}{\partial \hat{t}} + \frac{\partial}{\partial \hat{x}}\left(\hat{v}_x^{(0)}\hat{f}^{(1)}\right) + \frac{\partial}{\partial \hat{p}_x}\left(\hat{F}_x^{(0)}\hat{f}^{(1)}\right) = -\frac{\partial}{\partial \hat{x}}\left(\hat{v}_x^{(1)}\hat{f}^{(0)}\right) - \frac{\partial}{\partial \hat{p}_x}\left(\hat{F}_x^{(1)}\hat{f}^{(0)}\right), \tag{3.42}$$

where

$$\hat{F}_x^{(1)} = \frac{\partial\hat{\phi}^{(1)}}{\partial\hat{x}} - \hat{v}_y^{(0)}\frac{\partial\hat{A}^{(1)}}{\partial\hat{x}} - \hat{v}_y^{(1)}\frac{\partial\hat{A}^{(0)}}{\partial\hat{x}},$$

and

$$\frac{\partial^2\hat{\phi}^{(1)}}{\partial\hat{x}^2} + \int \hat{f}^{(1)}d\hat{p}_x = 0 \tag{3.43}$$

$$\frac{\partial^2\hat{A}^{(1)}}{\partial\hat{t}^2} - \frac{\partial^2\hat{A}^{(1)}}{\partial\hat{x}^2} + \int \hat{v}_y^{(0)}\hat{f}^{(1)}d\hat{p}_x = -\int \hat{v}_y^{(1)}\hat{f}^{(0)}d\hat{p}_x. \tag{3.44}$$

Let us take a closer look at the structure of Eqs. (3.41)–(3.44). One immediately observes that the source terms for the first-order corrections are proportional to a_0^{-2}, and consequently so are $\hat{X}^{(1)} = a_0^{-2}\hat{X}_1$, $\hat{f}^{(1)}$, $\hat{\phi}^{(1)}$ and $\hat{A}^{(1)}$. Moreover, since a_0 only appears in the form of the factor $1/2a_0^2$, the

typical time scale on which $\hat{X}$, $\hat{f}$, $\hat{\phi}$ and $\hat{A}$ change does not depend on a_0, but is defined by the laser frequency ω_0.

It is interesting to observe that the perturbation theory always gives a solution for $\hat{X}^{(1)}$ if the value of r is chosen large enough in order to ensure that the coefficient S_X does not vanish. Let us therefore remember at this point that we have already met this choice of r in Section 3.3.

We can now formulate the basic properties of the ultra-relativistic ARP motion. Taking into account the $O(1/a_0^2)$ corrections, the ARP follows the trajectory

$$X(t,r) = S^{-1/2}k_0^{-1}\left(\hat{X}_0\left(\hat{t},r,S,\hat{\tau}\right) + a_0^{-2}\hat{X}_1\left(\hat{t},r,S,\hat{\tau}\right)\right). \tag{3.45}$$

Consequently, the v_s reaches the velocity of light according to the scaling

$$v_s = c(1 - F(t_s,r,S,\hat{\tau})a_0^{-2}), \tag{3.46}$$

where F does not depend on a_0, and $\hat{t}_s$ is the moment of local extremum. We can also observe that the function $\hat{X}^{(1)}$, which is a solution of Eq. (3.41), is smooth. Therefore, around the time $\hat{t}_s$, the ARP velocity can be expanded as

$$\frac{dX}{dt} = v_s - c\alpha(t_s,r,S,\hat{\tau})\omega_0^2(t-t_s)^2, \tag{3.47}$$

where $F\alpha > 0$, due to Eq. (2.25). This expansion is valid for all t in the time interval

$$|t - t_s| \ll 1/\omega_0, \tag{3.48}$$

the duration of which does not depend on a_0 but can be affected by S, r and $\hat{\tau}$.

The expansion (3.47) provides a direct estimation of the γ-factor of the ARP. One immediately sees from Eq. (3.47) that the height of the γ-spike scales as

$$\gamma_{\mathrm{ARP}} \propto a_0 \tag{3.49}$$

and the duration of this γ-spike is

$$\Delta t_\gamma \propto \frac{1}{a_0\omega_0}. \tag{3.50}$$

Thus, while the characteristic time of velocity change around the maximum does not depend on a_0, the characteristic width of the γ-spike scales proportional to $1/a_0$.

Let us now return to the results for the γ-spike scalings of the electron skin-layer motion that were obtained in Section 3.2. One sees that the scalings (3.27) and (3.28) describing the collective plasma skin-layer dynamics coincide with the scalings we have just obtained for the formally defined apparent reflection point. Although surprising at first glance, this result is physically clear. Since the reflection from overdense plasma is related to the vicinity of the critical surface (with $n = a_0 n_{cr}$), the ARP motion comes about from the skin-layer oscillations.

3.5 Microscopic Spike Scalings

The γ_{ARP} scaling (3.49) should also be present in the microscopic ARP dynamics we studied in Section 3.3, i.e. in Eq. (3.33). Yet in order to estimate the precise scaling of the integral D in Eq. (3.34) one needs to understand the behaviour of the vector potential inside the plasma skin layer.

We saw from the scaling for D_4 (see Eq. (3.40)) that the ARP moves towards the incident laser pulse with velocity close to the velocity of light when the function $A(t^-, x)$ goes through zero[5] inside the plasma. On the other hand, the perturbation theory we developed shows that v_s is close to c only for a very short time $\Delta t_\gamma \propto 1/a_0$. This means that the zeros of the function $A(t^-, x)$ move in the plasma with velocity of the order of ca_0, since they cover a length of $1/k_0$ according to similarity[6], during the time Δt_γ. This observation allows us to obtain the correct scaling for γ_{ARP}.

If $Q(t)$ is the coordinate of a point at which $A(t^-, x)$ has a fixed value one reads

$$\left(1 - \frac{1}{c}\frac{dX(t,r)}{dt}\right)\frac{\partial A(t^-, Q(t))}{\partial t^-} + \frac{dQ(t)}{dt}\left(\frac{1}{c}\frac{\partial A(t^-, Q(t))}{\partial t^-} + \frac{\partial A(t^-, Q(t))}{\partial x}\right) = 0, \tag{3.51}$$

which follows from the differentiation of $A(t^-, x) = const$ with respect to time. However if the constant is of the order of or less than $m_e c^2$, then $dQ/dt \propto ca_0$ and

[5] Or, more exactly, gets a value of the order of $m_e c^2$

[6] We are interested in scalings over a_0 and therefore skip the multipliers depending on S and $\hat{\tau}$.

$$\frac{dA(t^-,x)}{dx} = \frac{1}{c}\frac{\partial A(t^-,Q(t))}{\partial t^-} + \frac{\partial A(t^-,Q(t))}{\partial x} = O\left(\frac{1}{a_0^2}\right) \tag{3.52}$$

at $x = Q(t)$. This means that the full derivative of $A(t^-,x)$ is in essence zero at all points where $A(t^-,x)$ is of the order of $m_e c^2$. From here one readily obtains that $A(t^-,x)$ is not only small simultaneously in the whole skin layer but also has the same (up to corrections of the order of $O(a_0^{-2})$) value throughout the layer.

Now we can find the exact scaling for $D_{1,2,3,4}$ (see Eqs. (3.36)-(3.39)). The integrals D_1 and D_2 scale as a_0^2 and are of no interest for the question at hand. The value of D_4 scales as a_0^3 since Δl does not depend on a_0 (see 3.40). The main contribution to D_3 when A_y is of the order of $m_e c^2$ inside the relativistic skin layer can be written as[7]

$$D_3 = \frac{4eA_y}{\left(m_e^2c^2 + (eA_y/c)^2\right)^2}\int \Theta(p_x)p_x M(t,x,p_x)\partial_x\phi(t^-,x)dp_x dx, \tag{3.53}$$

where $\Theta(p_x)$ is Heaviside's function. From Eq. (3.53) one reads that D_3 scales as a_0^4 and changes its sign when A_y passes through zero. However, if the major term changes between large positive and negative values, this would mean that the ARP velocity jumps from $-c$ to almost c during a time interval of the order of $1/\omega_0 a_0$. Yet this contradicts the scalings obtained from the similarity theory. For this reason the integral in Eq. (3.53) equals zero.

Consequently, the γ_{ARP} scaling (3.49) is also present in the microscopic ARP dynamics.

3.6 Oblique Laser Incidence

Until now we have considered the interaction of a laser pulse with overdense plasma in the case of normal laser incidence. This approach let us concentrate on the dynamical features of relativistic laser plasma interactions and ignore the geometrical issues of the problem, such as the role of the angle of incidence Θ and the difference between P- and S-polarization. In a realistic laboratory experiment however, the case of oblique incidence is the most

[7] In order to derive Eq. (3.53) we take into account that $A_y(t^-,x)$ can be considered as a constant inside the skin layer.

common one. Therefore, in what follows, we derive incidence angle scalings which allow the results obtained for normal incidence to be transformed into those for the oblique case.

Geometrically it is clear that oblique incidence can be reduced to normal one by changing the frame of reference. Indeed, this can be done by applying the Lorentz transformation corresponding to the reference frame moving with velocity

$$v = c \sin \Theta. \tag{3.54}$$

However, this transformation causes a change in the values of parameters of the plasma as well as in those of the laser pulse. In the new reference frame the plasma density is $n/\cos\Theta$ and the electrons and ions move with velocity $-v$ until the laser pulse disturbs their motion. The laser pulse frequency transforms into $\omega_0 \cos\Theta$, while the laser vector potential a_0 remains unchanged for both S- and P-polarized laser pulses.

The transformation of the reference frame results in a change in the equations describing the plasma dynamics. In the moving frame not only the current produced by the laser-driven electrons, but also a constant ion current

$$\mathbf{j}_i = -en_i c \tan\Theta \ \mathbf{e}_z \tag{3.55}$$

must be taken into account. Moreover, the plasma electrons now have initial momentum

$$p_0 = -m_e c \tan\Theta \tag{3.56}$$

in the direction of the Lorentz transformation. The presence of the ion current does not allow us to reduce the problem of oblique incidence to the case of normal laser incidence in a straightforward way. However, this reduction can be done for both P- and S-polarizations by means of a special approach discussed below.

3.6.1 Oblique Incidence Equations

Let us write down all equations describing the laser-plasma interaction in the moving reference frame[8] for arbitrary laser polarization. The Vlasov

[8]According to the common notation, in relativistically transformed equations all transformed quantities are marked with $'$. In what follows we drop out $'$ for brevity. This causes no confusion.

equation in the new reference frame is[9]

$$\frac{\partial f}{\partial t} + \frac{\partial}{\partial x}(v_x f) + \frac{\partial}{\partial p_x}(F_x f) = 0, \tag{3.57}$$

where

$$F_x = e\left(\frac{\partial \phi}{\partial x} - \mathbf{v}_\perp \cdot \frac{\partial \mathbf{A}_\perp}{\partial x}\right); \quad v_x = \frac{cp_x}{P(t,x,p_x)} \tag{3.58}$$

and

$$P(t,x,p_x) = \sqrt{m_e^2 c^2 + p_x^2 + (eA_y/c)^2 + (p_0 + eA_z/c)^2}.$$

The Maxwell equations in this reference frame can be written as

$$\frac{\partial^2 \phi}{\partial x^2} = 4\pi e(N_e - \rho), \tag{3.59}$$

$$\frac{1}{c^2}\frac{\partial^2 \mathbf{A}_\perp}{\partial t^2} - \frac{\partial^2 \mathbf{A}_\perp}{\partial x^2} = \frac{4\pi}{c}\left(\mathbf{j}_i + \mathbf{j}_\perp\right), \tag{3.60}$$

where $\mathbf{j}_i$ is the ion current density (3.55) and

$$\mathbf{j}_\perp = -e\int \mathbf{v}_\perp f(t,x,p_x)dp_x,$$

with

$$v_y = \frac{eA_y}{P(t,x,p_x)}; \quad v_z = \frac{cp_0 + eA_z}{P(t,x,p_x)}. \tag{3.61}$$

Since the effects of the Lorentz transformation occur in two quite different places, in the Maxwell equations through the ion current $\mathbf{j}_i$ and in the Vlasov equation through p_0, the treatment of the equation of motion in this form is difficult.

However, it is clear that these two effects, despite their different appearance, have the same origin. The problem is in the inconvenient representation. The major difficulty is related to the ion current. The value of this term is large and this makes direct comparison with the normal incidence case impossible. Another obstacle is that the ion current is significant even far from the skin layer. In other words this current is not negligible far from the region where the physical processes take place.

[9]For derivation see Appendix 1.

In order to resolve the ion current problem and to represent the laser-plasma dynamics uniformly[10] we take the following approach. We introduce a new set of variables Π and $\mathbf{E}_\perp$ defined as

$$\Pi = -\frac{1}{c}\frac{\partial \phi}{\partial t}, \quad \mathbf{E}_\perp = -\frac{1}{c}\frac{\partial \mathbf{A}_\perp}{\partial t}. \tag{3.62}$$

The Maxwell equations can now be rewritten in the following form

$$\frac{\partial \phi}{\partial t} = -c\Pi, \quad \frac{\partial \mathbf{A}_\perp}{\partial t} = -c\mathbf{E}_\perp, \tag{3.63}$$

$$\frac{\partial^2 \Pi}{\partial x^2} = 4\pi e R, \tag{3.64}$$

$$\frac{1}{c^2}\frac{\partial^2 \mathbf{E}_\perp}{\partial t^2} - \frac{\partial^2 \mathbf{E}_\perp}{\partial x^2} = \frac{4\pi}{c}\mathbf{J}_\perp, \tag{3.65}$$

where

$$\begin{aligned} R &= \frac{1}{c}\frac{\partial \rho}{\partial t} = -\frac{1}{c}\int \left(\frac{\partial v_x}{\partial x} f + v_x \frac{\partial f}{\partial x}\right) dp_x, \\ \mathbf{J}_\perp &= -\frac{1}{c}\frac{\partial \mathbf{j}_\perp}{\partial t} = \frac{e}{c}\int \frac{\partial \mathbf{v}_\perp}{\partial t} f dp_x + \frac{e}{c}\int \mathbf{v}_\perp \frac{\partial f}{\partial t} dp_x. \end{aligned}$$

Rewriting Maxwell's equations as Eqs. (3.63)–(3.65) gives significant advantages. Firstly, Eqs. (3.63)–(3.65) explicitly show that only the skin layer region is important in order to calculate the electromagnetic field generated by the plasma. Secondly, in their standard form the Maxwell equations contain infinite electron and ion currents in the plasma. Since these currents have opposite signs, the infinite magnetic fields they generate cancel each other, giving a finite result. Eqs. (3.63)–(3.65) exclude these infinite currents and work with the finite values from the very beginning. Thirdly, note that Maxwell's equations rewritten with Π, ϕ, $\mathbf{A}_\perp$ and $\mathbf{E}_\perp$, together with the Vlasov equation provide us with a closed set of equations of motion in which all effects of the Lorentz transformation enter through the initial conditions. The information about the ion current, which compensates the electron current until the laser pulse hits the target, is hidden in the initial conditions for Π, ϕ, $\mathbf{A}_\perp$, $\mathbf{E}_\perp$.

[10] In other words our procedure reduces the effect of the Lorentz transformation only to that on the Vlasov equation.

We can now study the problem of transformation to normal laser incidence. The case of oblique incidence could be reduced to the normal one if, despite the additional electron momentum p_0, we are still able to recover the characteristic ARP motion which we derived in Section 3.4.

In what follows we separately consider the cases of P- and S-polarized light and show that in the ultra-relativistic regime $a_0^2 \cos^2\Theta \gg 1$ the problem of laser-plasma interaction under oblique laser incidence is equivalent to the case of normal incidence.

3.6.2 P-polarized Laser Pulse

Let us consider first the case of P-polarized light. The initial conditions for this geometry, set at a time just before the laser pulse hits the plasma are

$$\begin{aligned}
&\phi(t=0)=0, \quad \Pi(t=0)=0\\
&A_y(t=0)=0, \quad E_y(t=0)=0\\
&A_z(t=0)=\mathrm{Re}\left(a(x/\tau_0)e^{-ik_0x}\right)\\
&E_z(t=0)=\mathrm{Re}\left((i\omega_0 a(x/\tau_0)/c-\dot{a}(x/\tau_0)/(c\tau_0))\,e^{ik_0x}\right).
\end{aligned}$$

To take advantage of this representation of the Maxwell-Vlasov equations let us examine the zero and first orders of these equations over the small parameter $1/(a_0^2\cos^2\Theta)$.

Notice that $A_y = E_y = 0$ for all times which follows from the equations of motion. This means that P-polarization does not change due to the reflection. In order to find the dimensionless equations for all values involved in Eq. (3.63)–(3.65) one applies the following scalings

$$\Pi \propto a_0, \quad \phi \propto a_0, \quad E_z \propto a_0, \quad A_z \propto a_0, \tag{3.66}$$

which can readily be checked by direct substitution into Eqs. (3.63) and neglecting terms of the order of $1/(a_0^2\cos^2\Theta)$.

The zero-order approximation corresponds to the relativistic similarity theory, since all terms due to the new reference frame vanish in the equations for Π, ϕ, $\mathbf{A}_\perp$, $\mathbf{E}_\perp$ and f. This means that in the zero order approximation over $1/(a_0^2\cos^2\Theta)$ the ARP motion coincides with that for normal incidence with a rescaled value of the similarity parameter

$$S_\Theta = \frac{S}{\cos^3\Theta}. \tag{3.67}$$

Just as in the perturbation theory we developed in Section 3.4 the first-order approximation over $1/(a_0^2\cos^2\Theta)$ gives corrections to the ARP velocity which enable one to calculate[11] the velocity v_s. One easily obtains

$$v_s = c\left(1 - \frac{F}{a_0^2\cos^2\Theta} - \frac{\tan\Theta}{a_0}C - \frac{\tan^2\Theta}{a_0^2}C_P\right), \tag{3.68}$$

where the function $F(t_s, r, S_\Theta, \hat{\tau})$ coincides with the function F, which enters the ARP dynamics for normal laser incidence (see Eq. 3.22), C and C_P are universal functions depending on the same variables as does F, $\hat{\tau} = S_\Theta^{1/2}\omega_0\tau_0$.

Due to the causality property of the ARP motion the constant C must vanish and we obtain for the motion of the apparent reflection point[12]

$$X(t) = X(t_s) + c(1 - F_P a_0^{-2})(t - t_s) - c\alpha(t_s, r, S_\Theta, \hat{\tau})\omega_0^2\frac{(t-t_s)^3}{3}, \tag{3.69}$$

with

$$F_P = \frac{F}{\cos^2\Theta} + C_P\tan^2\Theta. \tag{3.70}$$

Eq. (3.69) demonstrates that we retain the same characteristic ARP motion as in the case of normal laser incidence. In other words, by means of a Lorentz transformation, we reduced the oblique to normal incidence in the ultra-relativistic regime $a_0^2\cos^2\Theta \gg 1$.

3.6.3 *S*-polarized Laser Pulse

In analogy to *P*-polarized laser light, we can now examine the *S*-polarization. The initial conditions for this geometry, set at a time just before the laser-plasma interaction, are

[11] Note that for *P*-polarization the first-order approximation over $\tan\Theta/a_0$ causes the generation of even-order harmonics. Even-order harmonic generation from a different perspective is discussed in [19].

[12] Otherwise the term $\tan\Theta/a_0$ can change sign, and since α is a function of $\cos\Theta$ only, F_P and $F_P\alpha$ change sign as well. However, if $F_P\alpha$ becomes negative, the ARP velocity equals the speed of light at some moment of time t. This violates Eq. (2.25).

$$\Pi(t=0)=0, \quad \phi(t=0)=0,$$
$$A_z(t=0)=0, \quad E_z(t=0)=0,$$
$$A_y(t=0)=\mathrm{Re}\left(a(x/c\tau_0)e^{-ik_0x}\right),$$
$$E_y(t=0)=\mathrm{Re}\left((i\omega_0 a(x/c\tau_0)/c-\dot{a}(x/c\tau_0)/(c\tau_0))e^{-ik_0x}\right).$$

In order to obtain the zero-order equations over $1/(a^2\cos^2\Theta)$ we assume

$$\Pi \propto a_0, \phi \propto a_0, A_y \propto a_0, E_y \propto a_0 \tag{3.71}$$

with $A_z = E_z = 0$ which satisfies the initial conditions and happens to be correct in the lowest order of the perturbation theory. As a result, we come to the similarity theory equations describing the normal incidence with the dimensionless parameter S_Θ (see Eq. (3.67)).

The specific feature of S-polarizations reveals itself in the first order of the perturbation theory in which the terms of the order of $\tan\Theta/a_0$ are taken into account. One sees that in the first order of the perturbation theory E_z obeys the following equation

$$\frac{\partial^2\hat{E}_z}{\partial\hat{t}^2}-\frac{\partial^2\hat{E}_z}{\partial\hat{x}^2}=\hat{J}_z, \tag{3.72}$$

where

$$A_z = \frac{m_e c^2\tan\Theta}{e}\hat{A}_z, \quad E_z=\frac{S^{1/2}m_e c\tan\Theta}{e}\hat{E}_z,$$
$$\hat{J}_z = \int\left(\frac{(1+\hat{A}_z)\hat{A}_y\hat{E}_y-\hat{E}_y}{P_0^3}\hat{f}^{(0)}-\frac{1+\hat{A}_z}{P_0}\left(\partial_{\hat{x}}(\hat{v}_x^0\hat{f}^{(0)})+\partial_{\hat{p}_x}(\hat{F}_x^0\hat{f}^{(0)}\right)\right)d\hat{p}_x d\hat{x},$$

where $P_0=\sqrt{1+\hat{p}_x^2+\hat{A}_y^{(0)2}}$.

One can see that the change of the polarization is given by the following scaling

$$\left(\frac{E_z}{E_y}\right)^2=\frac{\tan^2\Theta}{a_0^2}W\left(S_\Theta,\omega_0\tau_0\right), \tag{3.73}$$

where W is a universal function of S_Θ and $\omega_0\tau_0$.

Repeating the perturbation procedure in analogy with the case of P-polarization, one obtains the characteristic ARP motion once again. One sees that the parameter F defining v_s is rescaled as

$$F_S = \frac{F}{\cos^2\Theta} + C_S \tan^2\Theta. \tag{3.74}$$

Thus we come to the conclusion that in the ultra-relativistic regime, when $a_0^2 \cos^2\Theta \gg 1$ the problem of oblique laser incidence can be reduced to normal incidence by means of a Lorentz transformation. As a consequence of that, the subsequent studies by means of the ARP formalism will be based on the assumption of normal laser incidence.

3.7 Numerical Simulations of Relativistic Spikes

In order to conclude this Chapter on ultra-relativistic spikes, we finally demonstrate that one can also study the motion of the apparent reflection point numerically and visualize the analytical results we obtained so far. For this one needs to record the incident and the reflected electric fields at some point in vacuum ("external observer" position) at a series of moments. Being solutions of the wave-equation in vacuum, these fields can then be easily traced to arbitrary x and t. If we take the position of the external observer to be located at $x = 0$, then to find the ARP position x_{ARP}, we solve numerically the implicit equation defining x_{ARP}:

$$E_i(ct + x_{\mathrm{ARP}}) + E_r(ct - x_{\mathrm{ARP}}) = 0, \tag{3.75}$$

where E_i and E_r are the tangential components of the incoming and reflected electric field respectively, at the position of the external observer ($x = 0$).

Here the incoming field is an input and the outgoing one is calculated as a result of the laser-plasma interaction by a $1D$ particle-in-cell code [47]. In all simulations a laser pulse with a Gaussian envelope $a = a_0 \exp(-t^2/\tau_0^2)\cos(\omega_0 t)$, duration $\omega_0\tau_0 = 4\pi$ and dimensionless vector potential a_0 is incident onto a plasma layer with a step density profile. The plasma slab is initially positioned between $x_R = -1.5\lambda_0$ and $x_L = -3.9\lambda_0$, where $\lambda_0 = 2\pi/\omega_0$ is the laser wavelength.

In Fig. 3.2 one can see the results of a simulation for the case of laser pulse amplitude $a_0 = 20$ and plasma density $N_e = 90N_c$. Fig. 3.2 a) shows the oscillatory motion of the apparent reflection point. The corresponding

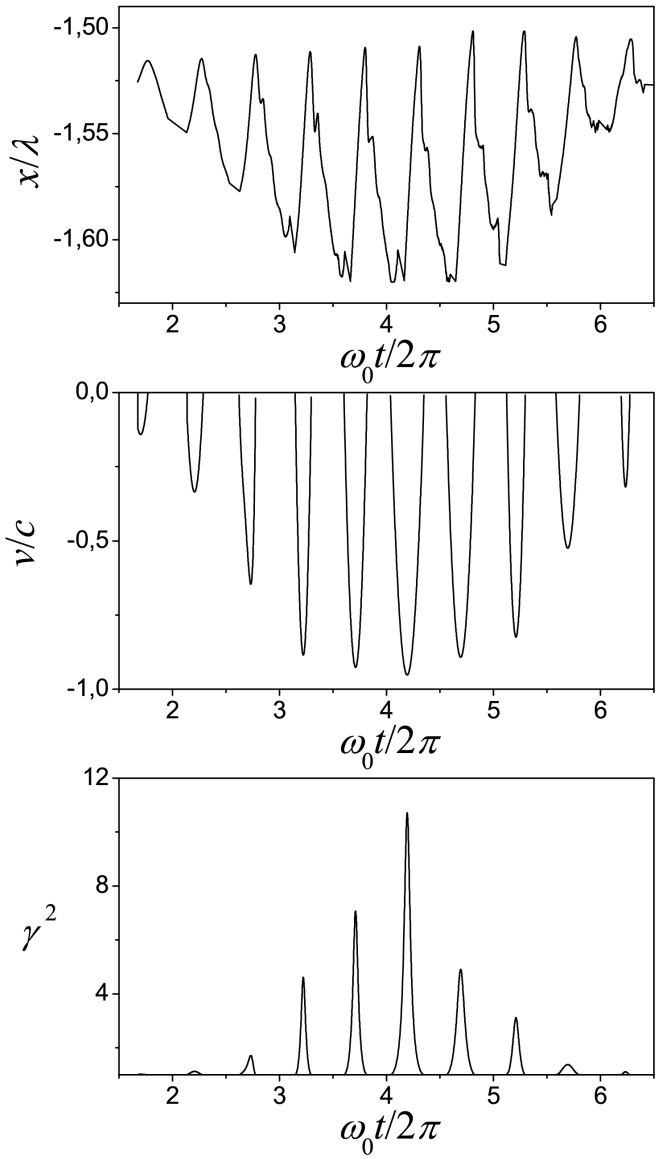

Figure 3.2: $1D$ particle-in-cell simulation results for the parameters $a_0 = 20$ and $N_e = 90N_c$, simulated with the particle-in-cell code VLPL [47]. a) Oscillatory motion of the ARP, b) Velocity $v_{\mathrm{ARP}}(t) = dx_{\mathrm{ARP}}(t)/dt$; only the negative velocities are shown. Notice that the ARP velocity is a smooth function around its maxima. c) The corresponding γ_{ARP} contains sharp spikes, which coincide with the velocity extrema.

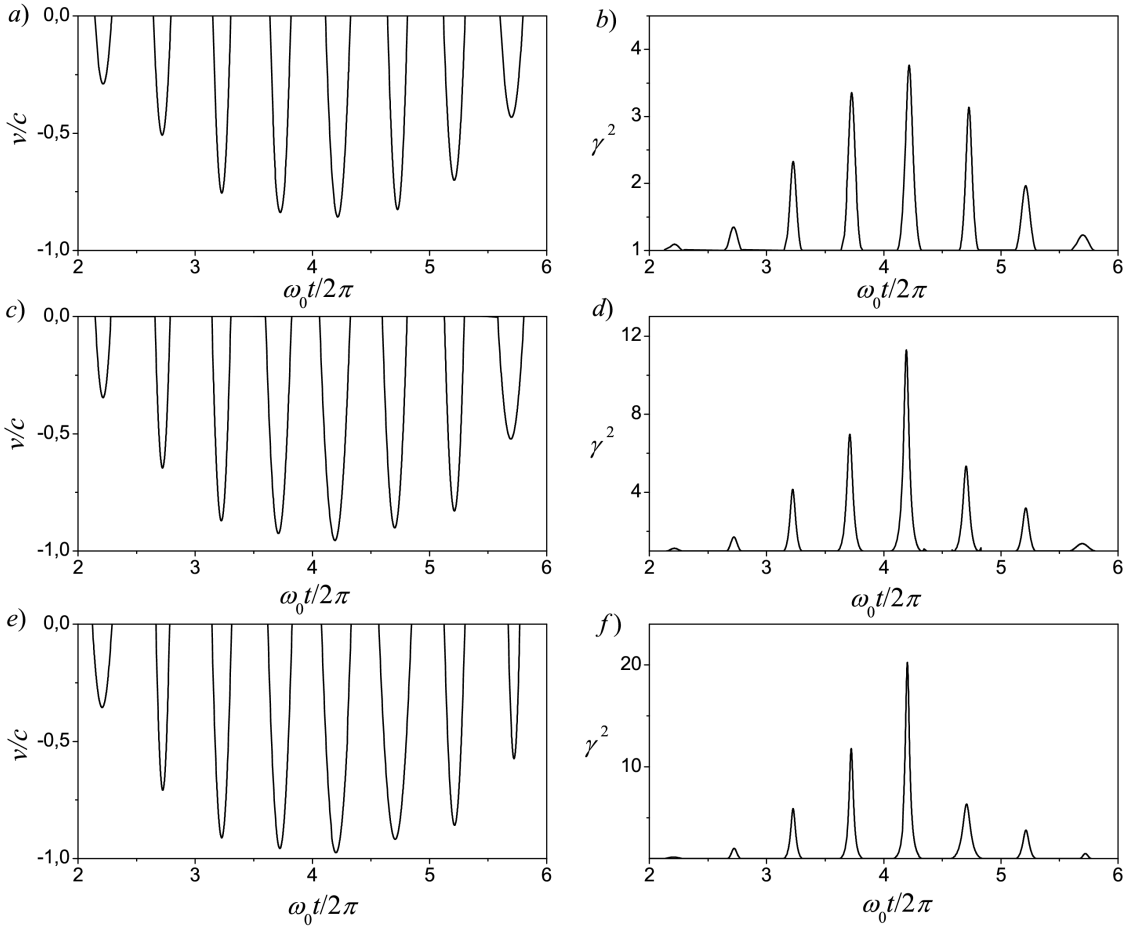

Figure 3.3: $1D$ particle-in-cell simulations with the code VLPL [47] allow the study of the γ-factor and the velocity of the apparent reflection point for three different sets of parameters with fixed $S = 4.5$: a) and b) $a_0 = 10$, c) and d) $a_0 = 20$, e) and f) $a_0 = 30$.

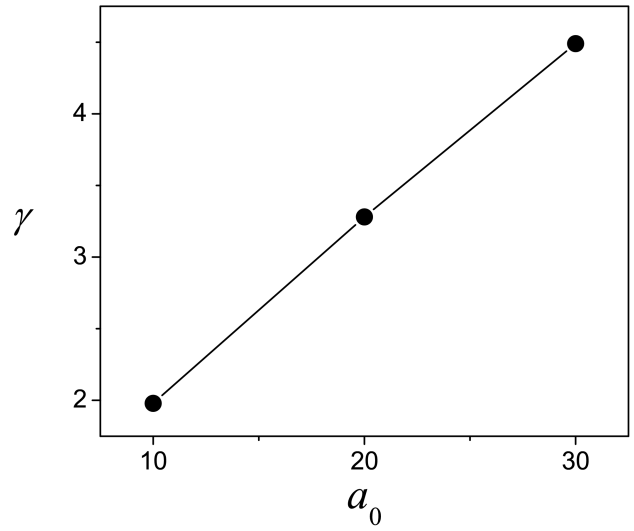

Figure 3.4: Numerical simulation with the $1D$ particle-in-cell code VLPL [47] shows the scaling (3.49). Here are depicted the maximal γ-spike vs. a_0 for $S = 4.5$

velocity $v_{\rm ARP}$ (Fig. 3.2 b) and γ-factor $\gamma_{\rm ARP}$ (Fig. 3.2 c) are calculated from the trajectory of the ARP motion by direct differentiation over time. Since only the ARP motion towards the laser pulse is of importance for the reflection, we cut out the positive ARP velocities and calculate only the negative ones. Notice that the ARP velocity is a smooth function around its maximum. At the same time, the γ-factor $\gamma_{\rm ARP}(t)$ contains sharp spikes, which coincide with the velocity extrema.

In Fig. 3.3 one can see the results of three simulations for laser pulse amplitudes of $a_0 = 10, 20, 30$ and plasma densities $N_e = 45N_c, 90N_c, 135N_c$ respectively, so that the similarity parameter $S = 4.5$. The results for the ARP velocities are presented in Fig. 3.3 a, c and e. The corresponding γ-factors $\gamma_{\rm ARP}(t) = 1/\sqrt{1 - v^2_{\rm ARP}(t)/c^2}$ are presented in Fig. 3.3 b, d and f. The dependence of the γ-spike height upon the laser amplitude a_0 for the three sets of simulation parameters is presented in Fig. 3.4. One can observe with good accuracy the linear scaling $\gamma_{\rm ARP} \propto a_0$ obtained analytically from the similarity theory (see Eq. (3.49)) and the microscopic theory for the motion of the apparent reflection point.

Chapter 4

High Harmonic Generation

With the new formalism developed in Chapters 2 and 3 we can now analyze the radiation reflected from the plasma. Indeed, the electric field irradiating the slab and the reflected one are unambiguously connected through the apparent reflection point, the motion of which was described quantitatively in Chapter 3.

In this Chapter we apply the ARP-formalism and the knowledge about the ARP motion to show that the radiation reflected from the plasma contains coherent high harmonics (high frequency radiation), the intensities of which decay as $I(\omega) \propto \omega^{-8/3}$. This power-law decay rolls over into exponential decay at frequencies proportional to a_0^3.

These harmonics form electromagnetic shock waves propagating in vacuum. A thorough investigation of the harmonic spectrum demonstrates its universality and results in an analytical expression for the intensity and phase of all high harmonics.

This Chapter demonstrates that the generation of high harmonics from relativistic plasma is not a result of the relativistic Doppler effect (so called "relativistic oscillating mirror" model) and provides the physical mechanism leading to the radiation of high harmonics.

As we have already seen in Chapter 3 oblique incidence is equivalent to normal incidence for ultra-relativistic laser intensities. Therefore, we consider only the normal geometry for the sake of brevity.

4.1 Electromagnetic Shock Waves

In this Section we examine how the reflected radiation looks in the time domain. For this purpose we combine the information about the dynamics of the apparent reflection point with the restrictions following from the relativistic invariance. In order to emphasize the distinction between dynamic information and relativistic invariance we separate the consideration of these two issues. First, we use the dynamic information in order to describe the time structure of the reflected radiation. Then we demonstrate that the results we obtained are relativistically invariant.

4.1.1 Generation of Electromagnetic Shock Waves

Let us first apply the ARP formalism in order to analyze the reflected electric field. Eq. (2.23) implies the following relation between the field derivatives

$$\frac{dE_r(\Psi)}{d\Psi} = -r^2 \frac{c + \dot{X}(t,r)}{c - \dot{X}(t,r)} \frac{dE_i(\Phi)}{d\Phi}. \tag{4.1}$$

In the vicinity of an ultra-relativistic γ-spike we use Eq. (3.47) in order to obtain for the ARP position $X(t)$ and the reflected phase $\Psi(t)$

$$X(t,r) = X(t_s) + c(1 - Fa_0^{-2})(t - t_s) - c\alpha\omega_0^2 \frac{(t - t_s)^3}{3} \tag{4.2}$$

and

$$\Psi(t) = \Psi(t_s) + cFa_0^{-2}(t - t_s) + c\alpha\omega_0^2 \frac{(t - t_s)^3}{3}. \tag{4.3}$$

Note that for

$$|\Psi(t) - \Psi(t_s)| \gg \left(\frac{3F^3}{\alpha}\right)^{1/2} \frac{c}{a_0^3\omega_0} \tag{4.4}$$

the linear term in Eq. (4.3) is negligible. The change of phase $\delta\Psi = \Psi(t) - \Psi(t_s)$ corresponds to the time change

$$t - t_s = \left(3\delta\Psi / c\alpha\omega_0^2\right)^{1/3}. \tag{4.5}$$

During the short time interval of the relativistic γ-spike the field of the incident pulse remains nearly unchanged. Substituting its value $E_i(\Phi(t_s))$ in Eq. (4.1) one reads

$$\frac{dE_r(\Psi)}{d(\delta\Psi)} = \frac{2r^2}{\alpha^{1/3}} \left(\frac{c}{3\omega_0^2 \delta\Psi} \right)^{2/3} \left(\frac{dE_i(\Phi)}{d\Phi} \right)_{\Phi=\Phi(t_s)} . \tag{4.6}$$

Integration of this ordinary differential equation gives the reflected electric field

$$E_r(\Psi) = -r^2 E_i(\Phi(t_s)) - \left(\frac{3r^2c^2}{\alpha\omega_0^2} \right)^{1/3} \left(\frac{dE_i(\Phi)}{d\Phi} \right)_{\Phi=\Phi(t_s)} \times (\delta\Psi)^{1/3} . \tag{4.7}$$

Since the phase dependence of the $1D$-wave describing the reflected wave propagating in vacuum is known, one can see that after the relativistic γ-spike, the reflected radiation gets the (quasi)singularity

$$E_r(x,t) = const_1 + const_2 \times (ct - x)^{1/3}. \tag{4.8}$$

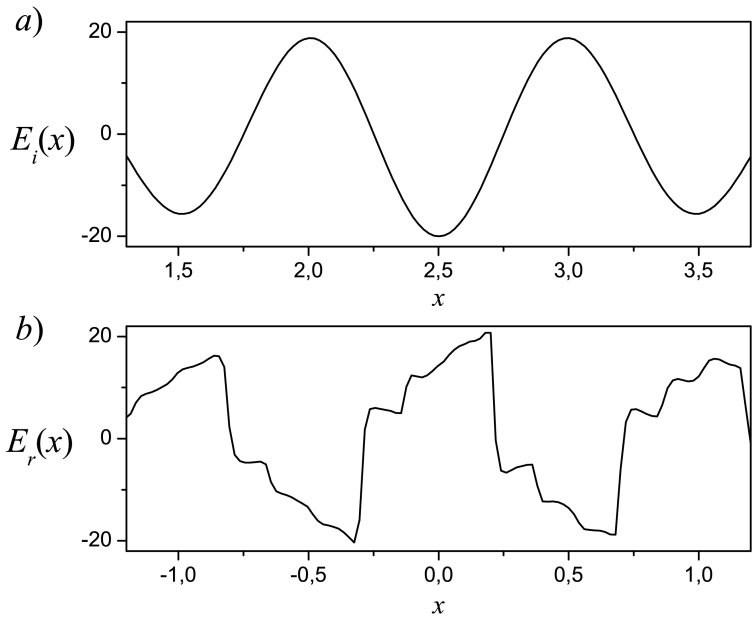

Figure 4.1: Numerical simulation with the particle-in-cell code VLPL [47] demonstrates the electromagnetic shocks. a) Incoming laser radiation. For the vector potential $a_0 = 20$ and electron density $N_e = 90N_c$ one obtains b) reflected radiation with shocks.

This means that the relativistic γ-spike turns the reflected electromagnetic field into an electromagnetic shock wave, in which the electric field has (almost) infinite derivatives at some points.

The possibility of developing electromagnetic shock waves as a result of the interaction of an electromagnetic field with a non-linear media is discussed in [46]. However, the width of the shocks presented in [46] is much larger than the laser wavelength. On the contrary, the width of the ultra-relativistic electromagnetic shocks discussed here is much less than the wavelength which allows their consideration as a new physical phenomenon.

The shock-wave behaviour of the reflected electric field can be observed in a numerical simulation. After the interaction of the incoming pulse (Fig. 4.1 a)) with the plasma slab, the particle-in-cell code VLPL[47] calculated the reflected signal. Fig. 4.1 b) demonstrates the resulting electromagnetic shocks propagating in vacuum.

Eq. (4.8) is valid for $const \times \lambda/a_0^3 \ll |ct-x| \ll \lambda$, where the first inequality is due to Eq. (4.4). The second inequality is connected with the range of validity of the expansion (3.47).

Therefore it is possible to study the contribution of the ultra-relativistic shock wave to the spectrum of the reflected radiation in the frequency domain

$$\omega_0 \ll \omega \ll a_0^3 \omega_0 / const. \tag{4.9}$$

The harmonic spectrum is given by

$$E_r(\omega) = \int E_r(x,t) e^{-i\omega t} dt. \tag{4.10}$$

Consequently, applying Eq. (4.8), one obtains for the harmonic intensity

$$|E(\omega)|^2 \propto \left| \int (ct-x)^{1/3} e^{-i\omega t} dt \right|^2 \propto \frac{1}{\omega^{8/3}}. \tag{4.11}$$

Note that the spectrum (4.11) applies to a large number of harmonics. According to Eq. (4.9) this number is proportional to a_0^3.

4.1.2 Relativistic Invariance of Shock Waves

A closer look at Eq. (4.8) shows that the coefficients of the shock wave depend on the relativistic transition factor r. However, this dependence is only apparent. In reality this expression is relativistically invariant to the ARP transformation (2.18). In order to demonstrate this, we study the different terms in Eq. (4.8).

We first notice that if $r \to +\infty$ the apparent reflection point approaches the zero of the incident electric field E_i that is located at the value of the phase Φ_0. However, $r^2 E_i(\Phi(t_s))$ remains unchanged since it equals $E_r(\Psi(t_s))$ and the phase $\Psi(t_s)$ of the reflected wave is not affected by the ARP transformation. At the same time the value of $dE_i(\Phi(t_s))/d\Phi$ approaches the value of E_i's derivative at its zero point[1].

It remains to prove that the coefficient $r^2/\alpha^{1/3}$ is invariant under the ARP transformation. Since we are interested in the case when the ARP is close to the zero point of E_i with the phase Φ_0, one can expand the incident field near Φ_0 and rewrite Eq. (2.18) as

$$\frac{r^2}{r_0^2} = \frac{ct_0 + X(t_0, r_0) - \Phi_0}{2ct - ct_0 + X(t_0, r_0) - \Phi_0}. \tag{4.12}$$

Eq. (4.12) defines t_0 as a function of t, r_0 and r. We are interested in this solution at those times when the ARP has a large relativistic γ-factor. According to Eq. (4.2) the derivative of the function

$$\Psi(t_0, r_0) = ct_0 - X(t_0, r_0) = \psi_0 \tag{4.13}$$

over time is negligible[2] and, as a result, it can be considered constant for this time interval. Consequently, one finds

$$t_0 = \left(\frac{r}{r_0}\right)^2 t - \tau_0, \tag{4.14}$$

where

$$\tau_0 = \frac{1}{2c}\left(1 - \left(\frac{r}{r_0}\right)^2\right)(\psi_0 + \Phi_0)$$

The substitution of the ARP motion given by Eq. (4.2) for both apparent reflection points $X(t, r)$ and $X(t_0, r_0)$ in Eq. (2.17) gives rise to the following invariants of the ARP transformation. The relativistic factors for both points γ_0 and γ and the respective curvatures of the velocity around its maximum α_0 and α satisfy the following equalities

$$\begin{aligned} r\gamma &= r_0\gamma_0, \\ r^6\alpha &= r_0^6\alpha_0. \end{aligned} \tag{4.15}$$

[1] If E_i and its first derivative happen to vanish simultaneously one can choose a phase that differs from Φ_0 in order to avoid the degenerate case.

[2] We recall that we have $\partial_{t_0}\psi(t_0) \propto a_0^{-2}$ in the neighbourhood of the spike.

The scalings in Eqs. (4.15) demonstrate that the coefficient $r^2/\alpha^{1/3}$ in Eqs. (4.7) and (4.8) is invariant under the ARP transformation and thus the whole expression of the shock wave is invariant.

4.2 Relativistic Doppler Effect

As we have just seen in Section 4.1.1 a large number of harmonics is present in the radiation reflected from the plasma. Since these harmonics result from reflection at the boundary of a moving medium it seems plausible that they occur due to the relativistic Doppler effect. The main idea of this explanation is that due to reflection from an ideal mirror moving with relativistic velocity v and corresponding relativistic factor $\gamma = 1/\sqrt{1-(v/c)^2}$, the frequency ω_0 of the incoming laser pulse is up-shifted to

$$\omega_{refl} = r^2\omega_0, \tag{4.16}$$

where r is the transition factor defined by Eq. (2.13)[3]. In just the same way, the whole spectrum of the laser pulse gets a $4\gamma^2$-upshift, while the pulse duration shortens by the same factor.

As already discussed in Chapter 1, the Doppler effect scheme has several critical drawbacks. Among these is the fact that the relativistic mirror gets transparent for surprisingly low γs and the linear reflection used to derive Eq. (4.16) is not applicable for relativistic intensities ($a_0 \geq 1$).

However, in what follows we apply the ARP formalism to this toy model ignoring its drawbacks. A reason for this consideration is that in the direct comparison between the electromagnetic shocks and the Doppler effect one can identify the physics of the shock formation. This comparison highlights the difference between the oscillating mirror relying on the Doppler effect and the processes resulting in high harmonic generation at boundaries of real plasmas.

Let us consider the reflection of a laser pulse from an ideal conductor moving with constant velocity v towards the laser pulse. The boundary condition describing this interaction is[4]

$$A_y(t, x = vt) = 0, \tag{4.17}$$

[3]This expression is usually written in the limit $\gamma \to +\infty$ in which $r^2 \approx 4\gamma^2$.

[4]This boundary condition is invariant under Lorentz (x,t)-transformation.

where $x = vt$ is the position of the mirror at time t.

This boundary condition has a clear physical meaning. To see this let us calculate the total derivative of Eq. (4.17) over time

$$\frac{\partial A_y}{\partial t} + v \left(\frac{\partial A_y}{\partial x} \right)_{x=vt} = 0, \tag{4.18}$$

which can be rewritten equivalently as

$$(E_y + vB_z)_{x=vt} = 0. \tag{4.19}$$

The last expression gives the Lorentz force acting on the electrons. In the ideal conductor the finite Lorentz force would generate an infinite current.

In order to apply the ARP formalism to the Doppler-effect scenario one has to characterize the motion of the ARP. This motion can be described in an arbitrary reference frame convenient for the calculation and then be transformed to the laboratory reference frame. Note that in the reference frame moving with velocity v Eq. (4.19) can be rewritten as

$$E_y(t, x = 0) = 0. \tag{4.20}$$

Eq. (4.20) shows that in the reference frame, in which the conductor is at rest, the electric field equals zero on the surface of the conductor. In order to apply the ARP formalism one needs to know the position of the zero points of the field Γ' defined in Section 2.2. However, E_y coincides with Γ in vacuum. Since in this reference frame the mirror is at rest, so is the apparent reflection point. As a result, in the laboratory reference frame the coordinate of the ARP, corresponding to the reference frame in which the conductor is at rest, moves as

$$X(t, r) = vt. \tag{4.21}$$

where

$$r = \sqrt{\frac{c+v}{c-v}}.$$

Note that in the frame in which the conductor is at rest, the position of the apparent reflection point coincides with the position of photon generation. This is not the case in the laboratory frame, where the photons are generated by the surface current at the point moving with constant velocity v, while the ARP is involved in a rather complicated motion. The reason for this is

that the point lying on the mirror surface is the one where $A_y = 0$, while the ARP makes Γ vanish (see Eq. (2.8)).

Let us now use the apparent reflection point from Eq. (4.21) in order to calculate the radiation reflected from the mirror. From Eq. (4.1) one obtains

$$\frac{dE_r}{d\Psi} = -r^4 \frac{dE_i}{d\Phi}. \tag{4.22}$$

Integrating this ordinary differential equation one easily derives

$$E_r(\Psi) = -r^4 \int \frac{dE_i}{d\Phi} \frac{d\Psi}{d\Phi} d\Phi = -r^2 E_i(\Phi) \tag{4.23}$$

and finally

$$E_r(\Psi) = -r^2 E_i(r^2 \Psi). \tag{4.24}$$

The derivation of Eq. (4.24) gives important clues about the difference between the mirror model and the shock wave formation. Indeed, the relativistic Doppler Effect is a consequence of the integration of $dE_i/d\Phi$, while $(c + \dot{X})/(c - \dot{X})$ is constant. On the other hand the shock formation is the result of the integration of $(c + \dot{X})/(c - \dot{X})$, while $dE_i/d\Phi$ is constant. The Doppler effect causes shortening of the pulse by a factor of r^2, as one can clearly see from Eq. (4.24). This shortening leads to the up-shift given by Eq. (4.16). On the contrary, the high harmonics inside the shock waves are the result of the local steepening of the electromagnetic field. The manifestation of this steepening is the harmonic spectrum of Eq. (4.11).

4.3 Universal Spectrum

So far we have seen that the radiation reflected from the plasma contains harmonics with very high frequencies. As we have just demonstrated, this harmonic generation does not result from the relativistic Doppler effect, which compresses the incoming signal. Far more is it due to local steepening of the reflected field propagating in vacuum in the form of electromagnetic shock waves (Fig. 4.1). The shocks gave an idea about the form of the harmonic spectrum (see Eq. (4.11)). In this Section we want to obtain an analytical expression describing the harmonic radiation and explain the physical processes inside the ultra-relativistic plasma, which lead to the generation of this radiation.

4.3.1 Invariant Derivation of Harmonic Spectrum

For this purpose we again apply the ARP-formalism, which provides a connection between the incident and reflected electric fields at the apparent reflection point (see Eq. (2.27)):

$$E_r(\Psi) = -r^2 E_i(2ct - \Psi), \tag{4.25}$$

where

$$\Psi = ct - X(t, r).$$

We find that the Fourier spectrum of the electric field $E_r(t, x = 0)$ is

$$E_r(\Omega) = -\frac{r^2}{c\sqrt{2\pi}} \int_{-\infty}^{+\infty} \mathrm{Re}\left[E\left(\frac{ct + X(t,r)}{c\tau_0}\right) e^{-i\omega_0 t - i\omega_0 X(t,r)/c)}\right] e^{-i\Omega\Psi/c} d\Psi, \tag{4.26}$$

where E is the slow envelope of the incident laser pulse. Note that since $X(t, r)$ enters directly the integrand in Eq. (4.26), profound knowledge of the ARP dynamics is needed in order to calculate the spectrum of the reflected radiation.

We proceed by rewriting Eq. (4.26) in dimensionless units using the parameters $\tau = \omega_0\Psi/c$, $\tau' = \omega_0 t$, $n = \Omega/\omega_0$ and $x(\tau') = (\omega_0/c)X(t, r)$. For the evaluation of Eq. (4.26) let us notice that the investigation of $E_r(\Omega)$ is equivalent to the investigation of the function

$$f(n) = f_+(n) + f_-(n), \tag{4.27}$$

where

$$f_\pm = \int g(\tau' + x(\tau')) e^{\pm i(\tau' + x(\tau')) - in\tau}\, d\tau \tag{4.28}$$

and

$$g(\tau' + x(\tau')) = -\frac{r^2}{2c\sqrt{2\pi}} E\left(\frac{ct + X(t,r)}{c\tau_0}\right). \tag{4.29}$$

We recall that, for the physical parameters we investigate, the envelope E, and consequently the function g, are both changing slowly[5]. Making use of the retardation relation we re-write Eq. (4.28) as

[5] In other words $|dg(\tau')/d\tau'| \ll 1$.

$$f_{\pm} = \int g(\tau' + x(\tau'))e^{i\tau'(-n\pm1)+ix(\tau')(n\pm1)}\,(1 - x'\,(\tau'))\,d\tau'. \tag{4.30}$$

Since we are interested in describing the spectrum of high harmonics we wish to examine the integral (4.30) for very large n. Note that for large harmonic numbers n the exponent in the integrand oscillates rapidly. Therefore, the main contribution to this integral comes from the extremal points of the phase

$$\Theta(\tau') = \tau'(-n \pm 1) + x(\tau')(n \pm 1). \tag{4.31}$$

The phase derivative $d\Theta/d\tau'$ changes sign in the vicinity of those moments τ'_s for which the ARP velocity $x'(\tau'_s) \approx 1$ (Fig. 4.2 a).

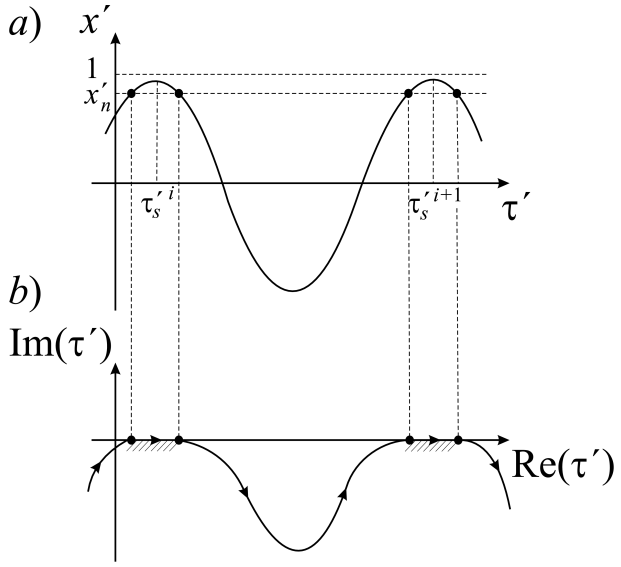

Figure 4.2: ARP dynamics and path integration in (4.30). a) Velocity $x'(\tau')$ of the ARP; $x'_n = (n-1)/(n+1)$ are the saddle points corresponding to $d\Theta/d\tau' = 0$. b) The integration path is shifted from the real axis to the complex plane everywhere except in the neighbourhoods of τ'_s (dashed regions).

These points will be denoted τ'_s in what follows since they coincide with the moments of γ-spiking in the ARP-dynamics. For all τ' that are not too close to one of the τ'_s, we can now shift the path over which we integrate to the complex plane everywhere except in the neighbourhoods of τ'_s (Fig. 4.2 b). The contributions of the parts remote from the real axis are exponentially

small. We can shift the path to the complex plane till the derivative equals zero or we find a singularity of the phase Θ.

To calculate the contribution of the τ_s'-neighbourhoods to the integrals in Eq. (4.30) we can now apply the knowledge about the ARP-dynamics acquired in Chapters 2 and 3. According to Eq. (3.47) at the vicinity of the spiking points τ_s', the following expansion of $x(\tau)$ is applicable

$$x(\tau') = x(\tau_s') + v_s(\tau_s')(\tau' - \tau_s') - \frac{\alpha(\tau_s')}{3}(\tau' - \tau_s')^3. \tag{4.32}$$

Substitution of Eq. (4.32) into $f_\pm(n)$ yields

$$f_\pm(n) = \sum_{\tau_s'} f_\pm(\tau_s', n), \tag{4.33}$$

where the sum is over all times τ_s',

$$f_+(\tau_s', n) = g\left(\tau_s' + x(\tau_s')\right) \exp(i\Theta_+(\tau_s', n)) F(\tau_s', n), \tag{4.34}$$

$$f_-(\tau_s', n) = g\left(\tau_s' + x(\tau_s')\right) \exp(i\Theta_-(\tau_s', n)) F(\tau_s', -n), \tag{4.35}$$

$$F(\tau_s', n) = \frac{4\sqrt{\pi}}{\alpha^{1/3}(\tau_s') n^{4/3}} Ai\left(\frac{n - n_{cr}(\tau_s')}{N n^{1/3}}\right), \tag{4.36}$$

$$\Theta_\pm(n) = \pm(\tau_s' + x(\tau_s')) + n(x(\tau_s') - \tau_s'). \tag{4.37}$$

Here $n_{cr} = 2/(1 - v_s)$ and $N = \alpha^{1/3} n_{cr}/2$. In Eq. (4.36) Ai is the well-known Airy-function, defined as

$$Ai(x) = \frac{1}{\sqrt{\pi}} \int_0^{+\infty} \cos\left(ux + \frac{1}{3}u^3\right) du. \tag{4.38}$$

Note that due to the scaling in Eq. (3.47) N scales proportional to a_0^2.

At this point we can use the relativistic transformation for the apparent reflection point in order to simplify Eq. (4.34). First of all, we choose r to be large enough and locate the ARP by a zero point of the incident laser pulse. Since the slow envelope is a real valued function this means that

$$\tau_s' + x(\tau_s') = \pi/2 + \pi k, \tag{4.39}$$

where k is an integer number. For the harmonic phase one obtains from Eq. (4.37)

$$\Theta(n) = n(x(\tau_s') - \tau_s'). \tag{4.40}$$

Two things about the harmonic phase $\Theta(n)$ are worth emphasizing. First we notice that this phase is invariant under the ARP transformation. And second, since the phase depends linearly on n, all high harmonics are in phase.

Note that n_{cr} and α transform as r^{-2} and r^6 respectively. As a result, the coefficient $r^2/\alpha^{1/3}$ on the right-hand side of Eq. (4.34) is invariant as also is N. The term related to n_{cr} in the argument of the Airy function gives a non-invariant contribution that decays as r^{-2} as r goes to $+\infty$. This means that this term is a non-selfconsistent contribution of high-order terms and must be dropped out in order to keep the leading order self-consistent. The fact that the n_{cr} related term gives only high-order corrections to the spectrum and can be dropped out can be checked also by a direct expansion of the Airy function without consideration of relativistically invariant perturbation theory[6].

Having combined Eqs. (4.33)–(4.39) one obtains the desired analytical expression for the spectrum of radiation generated by the plasma. For the intensity of the n^{th} harmonic we obtain

$$I_n \propto \left| F\left(n\right) e^{i\Theta(n)} \right|^2 = F^2(n), \tag{4.41}$$

where the harmonic phase is given by Eq. (4.40) and

$$F(n) = \frac{8\sqrt{\pi}}{n^{4/3}} Ai\left(\frac{n^{2/3}}{N}\right). \tag{4.42}$$

Fig. 4.3 represents the spectrum calculated numerically according to Eq. (4.41). One can notice that the spectrum contains two qualitatively different parts and a transition region. In order to demonstrate explicitly these two quite different laws of high harmonic intensity decay, we apply asymptotic representations of the Airy function.

For $n < N^{3/2}$ we can substitute the value of the Airy function[7] at $x = 0$ in Eq. (4.41), and obtain

$$I_n \propto \frac{1}{n^{8/3}}. \tag{4.43}$$

For $n > N^{3/2}$ Eq. (4.36) can be rewritten as

$$I_n \propto \frac{r^2}{\alpha^{1/3}} \frac{N^{1/2}}{n^3} \exp\left(-\frac{4n}{3N^{3/2}}\right). \tag{4.44}$$

[6]This approach was used in [38].

[7]$Ai(0) = \sqrt{\pi}/(3^{2/3}\Gamma(2/3)) = 0.629$, $Ai'(0) = -3^{1/6}\Gamma(2/3)/(2\sqrt{\pi}) = -0.459$

In other words the high harmonic intensity decays according to a power-law (4.43) and at frequencies

$$\omega_{roll} = N^{3/2}\omega_0 \tag{4.45}$$

rolls over into exponential decay (4.44).

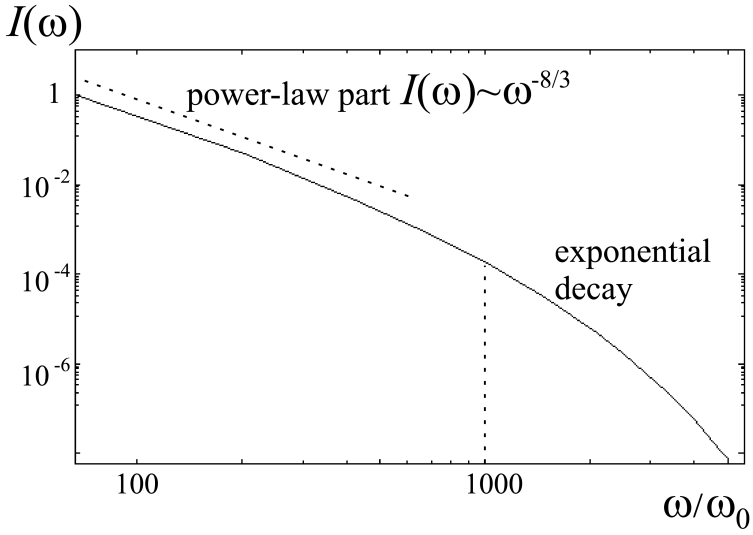

Figure 4.3: Spectrum of radiation calculated according to Eq. (4.41) for $N = 100$.

Eqs. (4.41) and (4.43) take into account the contribution of only one spike. If there are many spikes, the slow envelope of the spectrum remains unchanged, yet destructive interference among harmonics from different spikes may cause even order harmonics vanish. This effect is not due to the specific features of the relativistic laser-plasma interaction, but rather results from the symmetry of the equations of motion. In Section 3.6 we saw that even-order harmonics are generated for P-polarization [19]. The amplitude of even harmonics diminishes if the intensity of the incident laser pulse grows. In the case of S-polarization only odd harmonics are present in the harmonic spectrum [19].

4.3.2 The Concept of Universality

The most important feature of the high harmonic spectrum is its universality. This means that the shape of the spectrum depends on the single parameter N that encapsulates information relevant to non-linear ultra-relativistic reflection causing the generation of high harmonics.

In order to understand this concept let us return to the calculation of the spectrum from Eq. (4.30). Due to the observation that the main contribution to the spectrum comes from the spiking times τ_s' when the ARP velocity approaches the velocity of light, we applied the expansion (4.32), which led to the Airy-expression for the harmonic spectrum. It is essential to understand that we actually only made use of the fact that the ARP-velocity is a smooth function around its extremum. Since the harmonics are generated only during a very short interval of time at the γ-spiking, the precise shape of the ARP-velocity is irrelevant. This shape depends on the details of the laser-plasma interaction. Yet the behaviour around the velocity extremum is universal – all smooth functions resemble parabolas if zoomed at their extrema. Therefore, the high harmonic spectrum is universal (Fig. 4.3).

It is important to understand that the apparent reflection point formalism is intentionally designed to speak about the physics of high harmonic generation from plasmas in simple terms. The physics discussed in the next Section gives insight into the fascinating processes that result in the generation of high energy photons inside ultra-relativistic skin layers.

4.4 Physical Picture of High Harmonic Generation

As we saw in Section 4.2 high harmonic generation from relativistic plasmas yielding the universal harmonic spectrum depicted in Fig. 4.3 cannot be explained by the toy model of relativistic oscillating mirror. In order to conclude this Chapter addressing high harmonic generation, we discuss the physical processes which cause the radiation of harmonics from relativistic plasmas.

We demonstrated in Chapter 3 that the spikes in the γ-factor of the apparent reflection point are due to the zeros of the function $A(t^-, x)$, where $t^- = t - (X(t,r) - x)/c$ and $X(t,r)$ is the ARP position. In order to advance our understanding of high harmonic generation we have to study the dynamics of these zeros.

Let $Z(t)$ be the coordinate of a zero point of the function $A(t^-, x)$. In other words

$$A(t^-, Z(t)) = 0. \tag{4.46}$$

Differentiating Eq. (4.46) with respect to t we obtain

$$\frac{\partial A(t^-,Z)}{\partial t^-}\left(1-\frac{1}{c}\frac{dX}{dt}+\frac{1}{c}\frac{dZ}{dt}\right)+\frac{\partial A(t^-,Z)}{\partial Z}\frac{dZ}{dt}=0, \tag{4.47}$$

where $t^- = t - X(t)/c + Z(t)/c$, which means that

$$\frac{dZ}{dt} = -\frac{c - dX(t,r)/dt}{1 + c\partial_Z A(t^-,Z)/(\partial_{t^-} A(t^-,Z))}.$$

The scalings for $dZ/dt \propto ca_0$ and $c - dX/dt \propto a_0^{-2}$ obtained in Chapter 3 yield

$$\frac{c\partial_Z A(t^-,Z)}{\partial_{t^-} A(t^-,Z)} = -1 + O(a_0^{-3}), \tag{4.48}$$

or, in other words,

$$\frac{dZ}{dt^-} = -\frac{\partial_{t^-} A(t^-,Z)}{\partial_Z A(t^-,Z)} = c(1 + O(a_0^{-3})). \tag{4.49}$$

Eq. (4.49) demonstrates that the zero of $A(t,x)$ moves inside the ultra-relativistic skin-layer with the velocity of light. This means that if $A(t, x_{A=0}(t)) = 0$ inside the ultra-relativistic skin layer, then

$$\frac{dx_{A=0}}{dt} = c\left(1 + O(a_0^{-3})\right). \tag{4.50}$$

Before discussing the consequences of Eq. (4.50) notice that this result is due to the fact that the γ-factor of the ARP gets large if the zero of the vector potential is in rather dense $\propto a_0$ ultra-relativistic plasma. This follows from the scaling for D_4 derived in Section 3.5. Consequently in the diluted pre-plasma and non-ultrarelativistic plasma behind the skin layer that contribute to D_4 negligibly, the velocity of $x_{A=0}$ can differ from c significantly.

Eq. (4.50) has two interesting consequences. First, one sees that when the zero of the vector potential $x_{A=0}$ approaches an electron with $p_x > 0$, $p_x \gg m_e c$ the electron starts moving with $v_x \approx c$. This means that the electron and the zero of the vector potential start running together until the Coulomb attraction makes p_x become non-ultrarelativistic and subsequently change sign. As a result the cloud of fast electrons leave the skin layer and fly towards the incident laser pulse. This effect visualizes the ultra-relativistic spikes in numerical simulations (Fig. 1.5).

Secondly, one sees that a narrow band localized at $x_{A=0}$, the width of which is proportional to $1/(k_0 a_0)$, moves towards the laser pulse and radiates. Since the velocity of this band coincides with the speed of light,

different portions of the whole skin layer radiate coherently. Indeed, the phase matching condition is satisfied automatically, since the phase velocity of the radiation coincides with the velocity of the vector potential zeros. This phase matching condition can be seen from the scaling for D_4 in Chapter 3 which shows how the whole bulk of the skin layer contributes to the integral.

It is interesting to notice that the zero of the vector potential runs through the whole skin layer since the sign of the vector potential changes at each point. As a result, the emitted radiation is due to effects in the whole skin layer and is not influenced by the surface roughness.

Moreover, since the different parts of the ultra-relativistic skin layer coherently radiate at different times with the proper retardation, the duration of pulses that can be produced from the reflected radiation is not limited by the skin layer thickness. We examine the physics of these pulses in the the next Chapter.

In conclusion, let us recall that the formulas derived for the spectrum of high harmonics depend on the similarity parameter S defined in Chapter 3. We saw that the initial state of the laser-plasma system is characterized by the dimensionless similarity parameter $S = N_e/a_0 N_c$. However, the laser-plasma interaction diffuses the plasma boundary and, as we have just seen, clouds of fast electrons can leave the skin layer moving towards the incoming laser light (Fig. 1.5).

As a result the physical processes we discuss do no relate to the initial state of the system directly, but are connected with the area and the state of the plasma where the laser radiation is reflected. It is worth emphasizing that the location of this area is coupled with the unperturbed plasma density, but the properties of the plasma in the area of reflection are mainly dictated by the incident radiation. The generation of high harmonics occurs in the area with density[8] $N_e \propto a_0 N_c$, since the vector potential cannot have running zeros in dense plasma regions and the incident radiation is not able to reach the denser plasma parts. Finally, although the geometrical position of the reflection point depends on S, the process of reflection is only weakly dependent on the similarity parameter. For this reason we can expect that the dependence upon S in experimental conditions is weak as well. This looks especially plausible for laser installations generating not too short laser pulses.

[8]Notice the so called "local" S-parameter is about 1 in the region of reflection.

Chapter 5

Ultra-Short Pulses

In the previous Chapters we developed a self-consistent theory describing the generation of high frequency radiation in the laser-overdense plasma interaction. We demonstrated the equivalence between the normal and oblique incidence cases in the relativistic limit and, therefore, restricted our consideration to the case of normal incidence for brevity. This approach brought our studies as far as to get a grip on the physical mechanism behind the harmonic generation process and to derive an analytical expression describing the universal spectrum of radiation.

Our analysis showed that the thickness of the relativistic skin layer does not restrict the duration of the high frequency pulses that can be extracted from high frequency radiation produced at the boundary of a relativistic plasma. It became evident that the surface roughness does not prevent the generation of high harmonics. This means that HHG at plasma surfaces is a promising candidate for advanced time-resolved metrology, an area in particular need of ultra-short pulses of high intensity.

In this Chapter we examine the generation of ultra-short (sub-attosecond) pulses. We demonstrate the generation of trains of pulses with tunable structure and derive scalings for the pulse duration and intensity. The understanding we have developed concerning the short time intervals and physical conditions prevailing when high harmonic generation occurs, in turn provides a mechanism for efficient managing of the pulse generation. This Relativistic Plasma Control allows the isolating of single intense sub-attosecond pulses.

5.1 Pulse Generation

In Fourier-analysis it is well-known that a large number of coherent frequencies sum up to form short pulses in the time domain. In fact if all harmonics are of equal intensity[1] and have the same phase[2] the Fourier transformation returning the signal to the time domain produces a delta-function, a pulse of infinitely short duration. So long as either the harmonics are not coherent or their intensities differ, the resulting pulse will be of finite duration.

The high harmonics generated due to the interaction of a relativistically intense laser pulse with a slab of overdense plasma fulfill the first requirement: as demonstrated in Chapter 4 these harmonics are highly coherent. Moreover the frequencies which can be generated are unprecedentedly high. Consequently, the constructive interference of these harmonics could lead to the generation of unprecedentedly short pulses.

In order to generate such pulses one typically filters out the low order harmonics. However two competing effects have to be taken into account. Applying filters of too short a bandwidth leads to broadening of the pulses. On the other hand, due to the power-law decay of the spectrum, the low frequency harmonics are the most intense. Therefore, if too broad a filter is applied, the dominating signal occurs in the low harmonic range, which again results in broadening of the generated pulses. As a result, proper filtering has to balance these opposing trends in order to find a trade-off corresponding to short pulses of optimal duration.

A numerical example for the generation of a sub-attosecond pulses by filtering the reflected radiation is shown in Fig. 5.1. It is interesting to notice that the short pulses appear as a pulse train, twice per laser period. As we saw in Chapter 3 the reason for this effect is that the harmonic generation occurs at those moments of time, when the tangential vector potential $\mathbf{A}_\perp$ vanishes. For the generation of harmonics from plasma driven by a linearly polarized laser pulse, this happens twice per laser period.

Since the harmonic intensities are not constant but decay according to the law (4.41) derived in Chapter 4, the shape of the harmonic spectrum determines the properties of ultra-short pulses such as duration, structure and intensity. In what follows we analyze these properties.

[1] This corresponds to a perfectly flat spectrum in the frequency domain

[2] or linearly shifted phase $\phi = const \times \omega$

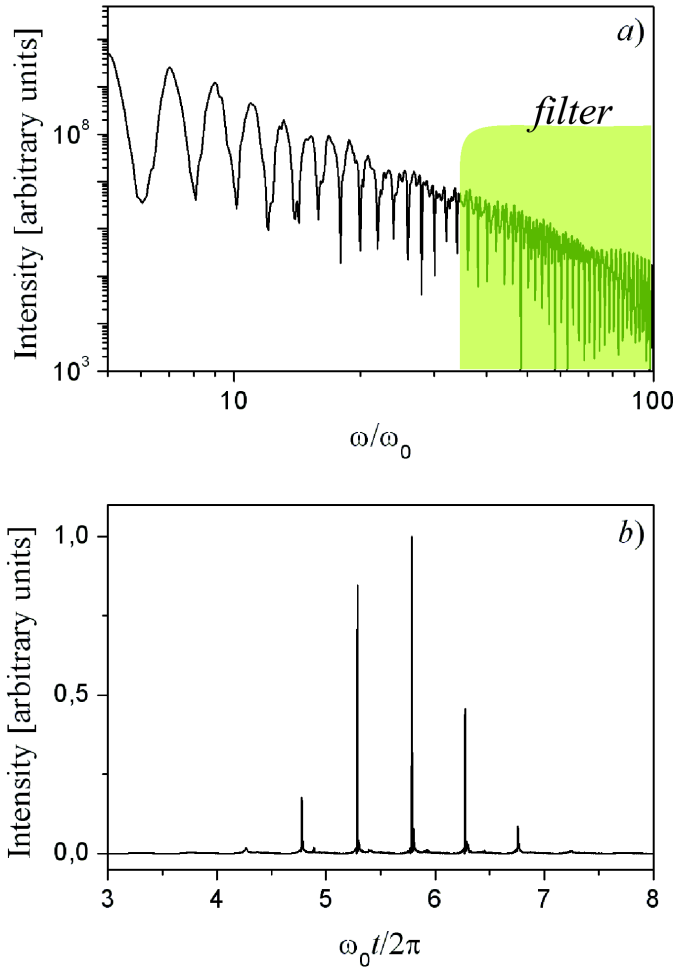

Figure 5.1: Numerical demonstration of ultra-short pulse generation. The applied filter (highlighted region in a)) lets through only frequencies greater than Ω_f [38]. The train of short pulses generated is given in b). The simulation is performed with the particle-in-cell code VLPL [47] for laser vector potential $a_0 = 20$ and plasma density $N_e = 90$.

5.2 Duration and Intensity of Ultra-Short Pulses

Let us estimate the minimal pulse duration, determined by the high harmonic spectrum. The broad spectrum band up to ω_{roll} corresponds to a generated pulse duration scaling as

$$T \propto \frac{2\pi}{\omega_{roll}} \propto \frac{2\pi}{\omega_0}\frac{1}{N^{3/2}}. \tag{5.1}$$

Since N is proportional to a_0^2 we obtain

$$T \propto \frac{1}{a_0^3}. \tag{5.2}$$

Thus the relativistic high harmonics allow the production of pulses with very favorable duration scaling, due to the high spectrum roll-over.

Magnifying the plotting scale for the ultra-short pulses reveals their duration. For the parameters of the interaction ($a_0 = 20$, $N_e = 30N_c$) the pulse in Fig. 5.2 is only 300 zeptoseconds long (1 zs $= 10^{-21}$ s). The possibility of generating pulses of such unprecedented duration was suggested for the first time in [14].

The intensity of the filtered ultra-short pulses depends on the filter position and width. Now we are going to estimate the energy and peak intensity of the optimal duration pulse. This pulse contains Δn ($\Delta n \leq n_{roll} = N^{3/2}$) harmonics. All of these harmonics are coherent which means that in order to estimate the peak intensity of the pulse one has to add up the electric fields[3] rather than the intensities as is done for incoherent radiation. For this reason one finds the following scalings for optimal pulse energy W , peak intensity I_p and duration T

$$W \propto \frac{\Delta n}{n_{roll}^{8/3}}\frac{I_0}{\omega_0}, \quad I_p \propto \left(\frac{\Delta n}{n_{roll}^{4/3}}\right)^2 I_0, \quad T \propto \frac{W}{I_p} \propto \frac{1}{\Delta n}\frac{1}{\omega_0}. \tag{5.3}$$

where I_0 the intensity of the incident laser pulse.

From the scaling for T one sees that the best choice of Δn is to be chosen of the same order of magnitude as n_{roll}. This choice gives rise to

$$I_p \propto \omega_0^2, \quad W \propto \omega_0^4/I_0^{3/2}. \tag{5.4}$$

[3]This is the central idea of coherent harmonic focusing that can be used in order to reach the Schwinger limit [49].

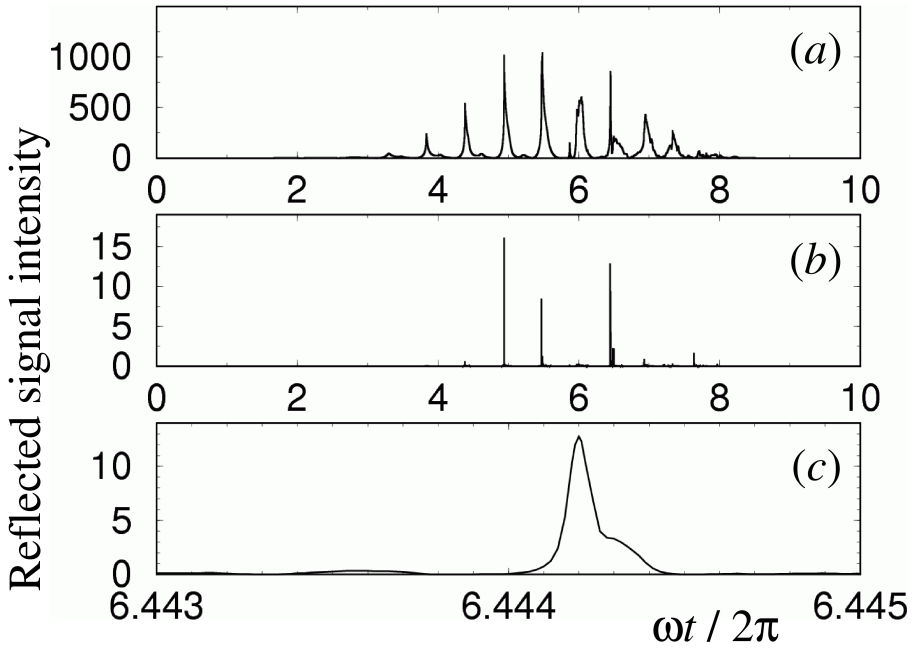

Figure 5.2: Zeptosecond pulse train obtained with the particle-in-cell code VLPL [47]: a) temporal structure of the reflected radiation, (b) zeptosecond pulse train seen after spectral filtering, (c) one of the zeptosecond pulses drawn against an expanded time-scale; its FWHM duration is about 300 zs [14].

The surprising feature of Eq. (5.4) is that the intensity of the optimal duration pulse depends only on the laser frequency.

5.3 Ultra-Short Pulse Structure

Not only the duration and intensity but also the structure of the filtered ultra-short pulses depends on the high harmonic spectrum. In order to demonstrate this effect let us apply a high-frequency filter that suppresses all harmonics with frequencies below Ω_f and study how the relative position of Ω_f and the spectrum roll-over frequency ω_{roll} (see Eq. (4.45)) affects the duration of the resulting (sub)attosecond pulses.

According to Eq. (4.41), the electric field of the pulse after the filtration is

$$E \propto \mathrm{Re} \int\limits_{\Omega_f/\omega_0}^{+\infty} F(n) e^{int}\, dn. \tag{5.5}$$

The structure of the filtered pulses depends on the position of the filter threshold Ω_f. In the case $1 \ll \Omega_f \ll \omega_{roll}$, we use Eq. (4.43) and rewrite Eq. (5.5) as

$$E \propto \mathrm{Re} \int\limits_{\Omega_f/\omega_0}^{+\infty} \frac{e^{int}}{n^{4/3}}\, dn = \left(\frac{\omega_0}{\Omega_f}\right)^{1/3} \mathrm{Re}\left[P(\Omega_f t)\right], \tag{5.6}$$

where the function P

$$P(x) = \int\limits_{1}^{+\infty} \frac{e^{iyx}}{y^{4/3}}\, dy \tag{5.7}$$

gives the slow envelope of the pulse.

It follows from expression (5.6) that the electric field of the filtered pulse decreases very slowly with the filter threshold as

$$E \propto \frac{1}{\Omega_f^{1/3}}. \tag{5.8}$$

The pulse duration decreases as $1/\Omega_f$. At the same time, the fundamental frequency of the pulse is Ω_f. Therefore the pulse is hollow when $\Omega_f \ll \omega_{roll}$, i.e. its envelope is not filled with electric field oscillations. One possible

application of these pulses is to study atom excitation by means of a single strong kick.

The pulse structure changes significantly when the filter threshold is placed above the spectrum roll-over. For $\Omega_f \gg \omega_{roll}$ we use Eqs. (4.44) and (5.5) to obtain

$$E \propto \left(\frac{\omega_0}{\Omega_f}\right)^{3/2} \exp\left(-\frac{2}{3N^{3/2}}\frac{\Omega_f}{\omega_0}\right) \mathrm{Re}\left[\frac{e^{i\Omega_f t}}{-2/\left(3N^{3/2}\right)+i\omega_0 t}\right]. \tag{5.9}$$

The amplitude of these pulses decreases rapidly when Ω_f grows. However, the pulse duration $\propto 1/a_0^3\omega_0$ does not depend on Ω_f. Since the fundamental frequency of the pulse grows as Ω_f, the pulses obtained with an above-ω_{roll}

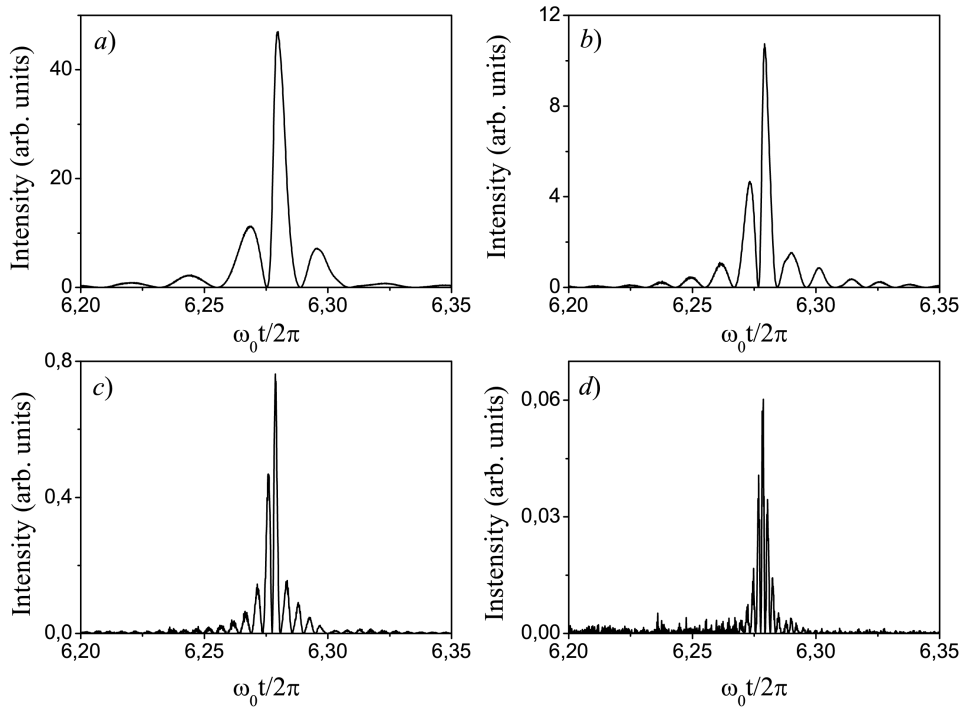

Figure 5.3: The structure of the ultra-short pulses depends on the position Ω_f of the filter. The figures present this dependence for $a_0 = 20$ and $N_e = 90N_c$ and filter positions: a) $\Omega_f = 20\omega_0$, b) $\Omega_f = 40\omega_0$, (c) $\Omega_f = 100\omega_0$, d) $\Omega_f = 200\omega_0$; $\Delta\omega = 2\omega_0$ [38].

filter are filled with electric field oscillations. Therefore, these pulses are suitable to study the resonance excitation of ionic and atomic levels.

This idea about the tunable pulse structure can be visualized numerically. Using the particle-in-cell code VLPL [47] one can study the structure of the generated pulses in its dependence on the filter position. We apply a filter with the filter function $f(\omega) = 1 + \tanh((\omega - \Omega_f)/\Delta\omega)$. It lets through frequencies above Ω_f and suppresses the lower ones. The results are presented in Fig. 5.3. One can see clearly that if the applied filter is set before the spectrum roll-over, the ultra-short pulses are hollow (Fig. 5.3 a). As the position of the filter is shifted to higher frequencies (Fig. 5.3 b,c) the pulse structure changes till finally the pulse is filled with oscillations when only above-ω_{roll} harmonics are allowed through the filter (Fig. 5.3 d).

5.4 Relativistic Plasma Control

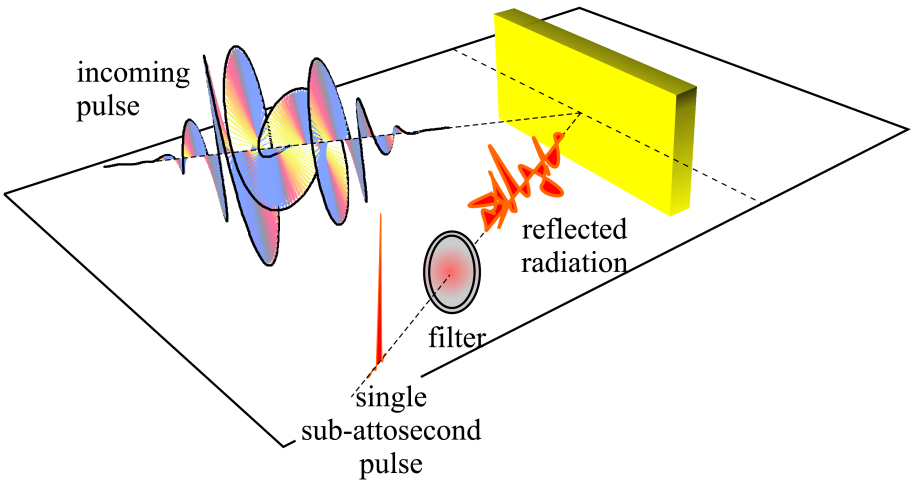

Figure 5.4: Geometry for relativistic plasma control of attosecond plasma surface dynamics. The polarization of the high intensity driving pulse is prepared in such a way that $\mathbf{A}_\perp$ vanishes only once. The high harmonics are generated only at this moment. As a result after proper filtering of the reflected radiation, a single ultra-short pulse can be isolated.

The generation and properties of the attosecond pulses just discussed are consequences of the properties of the high harmonics spectrum. These properties were obtained in the framework of the theory of relativistic spikes. Yet the observation that the high harmonics are generated only during a

γ-spike not only leads to an analytical derivation of the high harmonic spectrum, but also provides a powerful tool for control of the plasma motion. This control is based on the intrinsic connection between the plasma electron dynamics and the laser pulse, which drives this dynamics.

Indeed, as we noticed in Chapter 3, the moment of γ-spiking and, consequently, of high harmonic generation, corresponds to a zero of the tangential vector potential $\mathbf{A}_\perp$. In other words, controlling the polarization of the laser pulse leads to efficient control of the harmonic generation. In particular, if the polarization of the laser allows only one zero of $\mathbf{A}_\perp$ per laser pulse, we can produce an isolated ultra-short pulse. This tool for control of the laser-driven plasma dynamics was presented for the first time in [39] and named Relativistic Plasma Control.

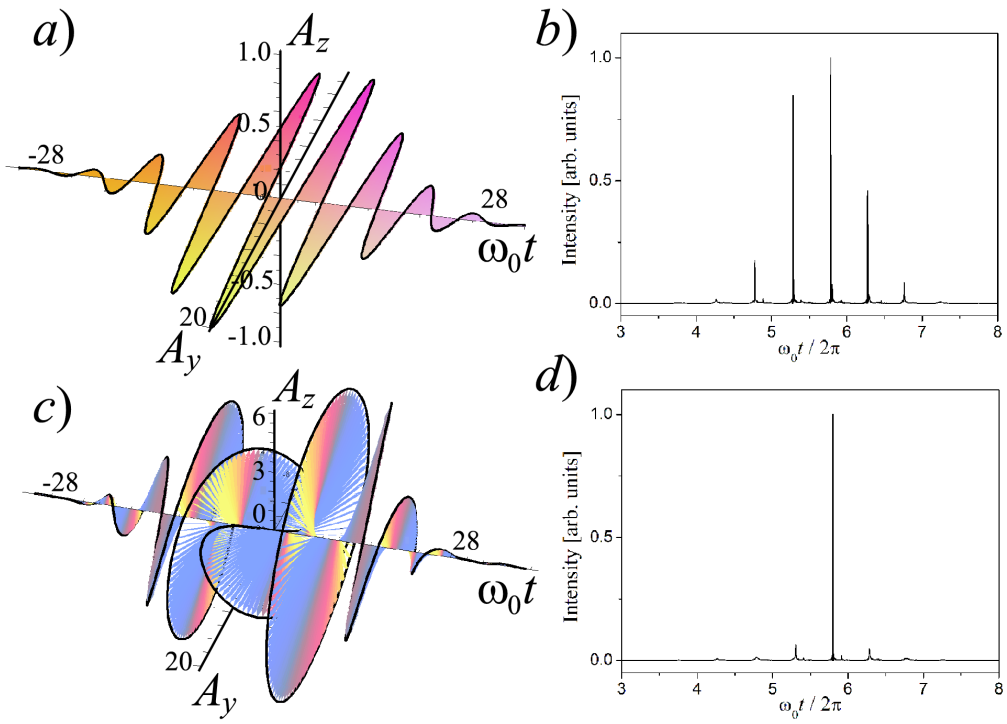

Figure 5.5: Demonstration of relativistic plasma control. Linearly polarized laser pulse with $a_0 = 20$ a) generates a train of ultra-short pulses b), appearing twice per laser period. Polarization-managed pulse c), with mixed polarization (y-polarization with $a_y = 20$ and frequency ω_0, z-polarization with $a_z = 6$ and frequency $\omega_z = 1.25\omega_0$, the phase shift between both polarizations is $\Delta\phi = \pi/8$), generates an isolated ultra-short pulse d).

The relativistic plasma control can be demonstrated numerically by a $1D$ particle-in-cell simulation with the code VLPL [47]. The plasma density for this simulation is $N_e = 90N_c$. For a linearly polarized pulse (Fig. 5.5 a) the filtered radiation contains a train of sub-attosecond pulses (Fig. 5.5 b) as already discussed in Section 5.1. However, if the polarization is changed, so that the vector potential crosses the zero-axis only once (Fig. 5.5 c), the reflected radiation contains only one sub-attosecond pulse (Fig. 5.5 d). This pulse is generated at the moment of the γ-spike corresponding to the zero of the vector potential.

It is important to notice, that the light pressure acting on the plasma slab in the case of a linearly polarized pulse (Fig. 5.5 a) differs only slightly from the light pressure in the case of the laser pulse with a single crossing $\mathbf{A}_\perp \approx 0$ (Fig. 5.5 c). However, the harmonic output as well as the whole plasma electron dynamics changes significantly. In other words, the high harmonic generation is not a result of the light pressure acting on the plasma, but rather the result of the relativistic spikes.

To conclude, let us observe that relativistic plasma control is a general tool for managing the relativistic plasma dynamics. The generation of harmonics and ultra-short pulses depends on the number of zero points of $\mathbf{A}_\perp$. In particular, the choice of elliptical laser polarization, for which $\mathbf{A}_\perp$ does not vanish, provides no opportunity for harmonic generation.

Chapter 6

Summary

The theory of relativistic spikes developed in this Thesis presents a new physical mechanism of high harmonic generation at the boundary of an overdense relativistic plasma. This is the first time, the laser plasma theory has proposed both a physical mechanism and an analytical approach that predict the universal power-law decay and the scaling for the roll-over of the high harmonic spectrum generated in relativistic laser–plasma interactions. These theoretical advances of the theory of relativistic spikes have been confirmed experimentally.

The theoretical foundation of this work is sufficient to demonstrate the robustness of the high harmonic generation process, which prevails in practical experiments where various imperfections occur. Indeed, this Thesis shows that the high harmonic emission caused by the relativistic spikes is not sensitive to surface roughness. This fact has enabled the experimental observation of high harmonics of unprecedentedly high frequencies in agreement with the theoretical predictions.

The relativistically invariant apparent reflection point formalism, developed in this work, encapsulates the features of ultra-relativistic laser-plasma interaction relevant to the generation of high energy coherent photons. This formalism puts the analytical theory of high harmonic generation on a firm mathematical footing and states that the relativistic γ-factor of the apparent reflection point has sharp ultra-relativistic spikes. These spikes originate from the electron motion inside the skin layer and are due to zeros of the vector potential.

Each ultra-relativistic spike causes the generation of an electromagnetic shock wave, which is a (quasi)singularity in the electric field of the reflected radiation

$$E_r(x,t) = const_1 + const_2 \times (ct - x)^{1/3}.$$

These shock waves contain coherent high harmonics with the universal power-law spectrum

$$I(\omega) \propto 1/\omega^{8/3},$$

describing the intensity $I(\omega)$ of the harmonic with frequency ω. The power-law scaling for $I(\omega)$ continues up to a roll-over frequency ω_{roll}

$$\omega_{roll} \propto I_0^{3/2}/\omega_0^2,$$

where I_0 and ω_0 are the intensity and frequency of the incident laser pulse.

The spectrum of the high harmonics is universal and depends neither on the shape of the incident laser pulse nor on the subtle details of the ultra-relativistic laser-plasma interaction, which leads to generation of harmonics. The full analytical description of the spectrum including the power-law decay and the exponential decay above the roll-over is obtained.

The theory of high harmonic generation at the boundary of relativistic plasmas predicts that the whole skin layer is in a coherent state, thereby enabling it to generate high harmonics with wavelengths that are much shorter than both the size of the surface roughness and the skin layer thickness. A mechanism to control the generation of high harmonics and produce single ultra-short pulses is proposed. Consequently, relativistic spikes resulting in high harmonic generation from plasma surfaces are a promising physical phenomenon that can be used in order to develop X-ray time-resolved metrology.

In conclusion, the main result obtained in this Dissertation is the theoretical prediction and examination of a new physical phenomenon: ultra-relativistic γ-spikes developing in ultra-relativistic laser-plasma interaction. This new physical phenomenon provides us with a robust mechanism to generate coherent radiation and even isolated ultra-short X-ray pulses in the soft and hard X-ray regions.

Appendix A

Vlasov Equation

In this Appendix the one-dimensional Vlasov equation (3.5) for the case of planar symmetry is derived. We start from the standard relativistic 3-dimensional Vlasov equation

$$\left(\partial_t + \mathbf{v}\cdot\partial_{\mathbf{r}} + \mathbf{F}\cdot\partial_{\mathbf{p}}\right)\mathcal{F}(t,\mathbf{p},\mathbf{r}) = 0, \tag{A.1}$$

where $\mathbf{F}$ is the Lorentz force

$$\mathbf{F} = -e(\mathbf{E} + \mathbf{v}\times\mathbf{B}/c) \tag{A.2}$$

and the electron distribution function $\mathcal{F}(t,\mathbf{p},\mathbf{r})$ depends on all 3 coordinates $x,\ y,\ z$ and momenta $p_x,\ p_y,\ p_z$. Due to

$$\nabla_{\mathbf{p}}\cdot\mathbf{F} = -\frac{e}{c}\nabla_{\mathbf{p}}\cdot(\mathbf{v}\times\mathbf{B}) = -\frac{e}{c}\mathbf{B}\cdot(\nabla_{\mathbf{p}}\times\mathbf{v}) + \frac{e}{c}\mathbf{v}\cdot(\nabla_{\mathbf{p}}\times\mathbf{B}) = 0 \tag{A.3}$$

we can re-write Eq. (A.1) in the following convenient form

$$\frac{\partial\mathcal{F}}{\partial t} + \frac{\partial}{\partial\mathbf{r}}\cdot(\mathbf{v}\mathcal{F}) + \frac{\partial}{\partial\mathbf{p}}\cdot(\mathbf{F}\mathcal{F}) = 0. \tag{A.4}$$

Let us now consider the particular case of planar symmetry, for which $\mathcal{F}$ does not depend on y and z. Eq. (A.4) can be written in the form

$$\frac{\partial\mathcal{F}}{\partial t} + \frac{\partial}{\partial x}(v_x\mathcal{F}) + \frac{\partial}{\partial\mathbf{p}}\cdot(\mathbf{F}\mathcal{F}) = 0. \tag{A.5}$$

Integration of Eq. (A.5) over p_y and p_z gives

$$\frac{\partial}{\partial t}I_f + \frac{\partial}{\partial x}I_v + \frac{\partial}{\partial p_x}I_F = 0, \tag{A.6}$$

where

$$I_f = \int \mathcal{F}\ dp_y dp_z; \quad I_v = \int v_x \mathcal{F}\ dp_y dp_z; \quad I_F = \int F_x \mathcal{F}\ dp_y dp_z.$$

note that in order to derive Eq. (A.6) we made use of the fact that

$$\int \frac{\partial}{\partial p_y}(F_y \mathcal{F})\ dp_y dp_z = 0;$$

$$\int \frac{\partial}{\partial p_z}(F_z \mathcal{F})\ dp_y dp_z = 0.$$

In order to simplify Eq. (A.6) we now use the integrals of motion due to the transitional symmetry in the plasma plane

$$\boldsymbol{\pi}_\perp = \mathbf{p}_\perp - e\mathbf{A}_\perp/c = const. \tag{A.7}$$

As a result, the electron distribution function is

$$\mathcal{F}(t, x, \mathbf{p}) = f(t, x, p_x)\delta(\mathbf{p}_\perp - \boldsymbol{\pi}_\perp - e\mathbf{A}_\perp/c). \tag{A.8}$$

Substituting Eq. (A.8) into Eq. (A.6) we obtain an equation for the $1D$ electron distribution function $f(t, x, p_x)$.

In the case of normal laser incidence we have $\boldsymbol{\pi}_\perp = 0$ and as a result we obtain that the $1D$ electron distribution function satisfies

$$\frac{\partial f}{\partial t} + \frac{\partial}{\partial x}(v_x f) + \frac{\partial}{\partial p_x}(F_x f) = 0, \tag{A.9}$$

where v_x and F_x are defined by Eqs. (3.6) and (3.7).

In the case of oblique laser incidence we perform a Lorentz transformation to a moving reference frame. As a result $\boldsymbol{\pi}_\perp = p_0 \mathbf{e}_z$, where p_0 is defined by Eq. (3.56) as discussed in Section 3.6. Consequently, one readily obtains Eq. (3.57).

It is important to emphasize that, although the electron distribution function f does not depend on $\mathbf{p}_\perp$, the electron dynamics is still three-dimensional. The tangential components of the electron momentum enter the Vlasov-Maxwell equations through $\mathbf{A}_\perp$.

Finally, let us notice that the Vlasov equation (A.9) can easily be derived if one keeps in mind that this equation is a continuity equation in the (x,p_x)-space. Indeed, the number of particles in a fixed volume $dxdp_x$ can change only due to a flow of particles in the x-direction with velocity v_x or due to a flow in the p_x-direction with velocity F_x.

Appendix B

Practicalities

The derivation of Eqs. (3.36)-(3.39) makes use of the Vlasov equation (3.5) in order to express the time derivative of the distribution function as

$$\frac{\partial f}{\partial t^-} = -\frac{\partial}{\partial x}(v_x f) - \frac{\partial}{\partial p_x}(F_x f).$$

Our goal is to obtain expressions which contain only f, rather than its derivatives. In order to do this we integrate the term $\partial_{p_x}(F_x f)$ by parts. For the term $\partial_x(v_x f)$ we make use of the transformation[1]

$$\int g(t^-,x)\frac{\partial}{\partial x}f(t^-,x,p_x)dp_x dx = \\ -\int f\frac{d}{dx}\left(\frac{g(t^-,x)}{1-v_x/c}\right)dxdp_x - \int f\frac{d}{dp_x}\left(\frac{g(t^-,x)}{1-v_x/c}\frac{F_x}{c}\right)dxdp_x.$$

Notice that since t^- depends on x, one must distinguish between the total derivative d/dx and the partial one $\partial/\partial x$.

In order to estimate the behavior of the final results it is not convenient to have integrals of the form $\int g(t^-,x)f(t^-,x,p_x)dxdp_x$, since the function

$$f(t^-,x,p_x) = \sum_i \delta\left(p_x - p_i(t^-)\right)\delta\left(x - x_i(t^-)\right)$$

counts one and the same particle many times. Instead, we rewrite our integrals using the electron counting function

$$M = \sum_i \delta\left(p_x - p_i\left(t - X(t)/c + x_i/c\right)\right)\delta\left(x - x_i\left(t - X(t)/c + x_i/c\right)\right)$$

[1]Here $g(t^-,x)$ is a probe function.

as

$$\int g(t^-, x) f(t^-, x, p_x) dx dp_x = \int g(t^-, x) M(t, x, p_x) \mu dx dp_x,$$

where $\mu = 1/(1 - v_x/c)$.

Bibliography

[1] Lucian, *Works*, Loeb Classical library, 9 volumes (1921)

[2] Michael D. Perry and Gerard Mourou, *Terawatt to Petawatt Subpicosecond Lasers*, Science **264**, 917 (1994)

[3] Gerard A. Mourou and Donald Umstadter, *Extreme Light*, Scientific American, May 2002

[4] N. Bloembergen, Nobel Lecture, *From Nobel Lectures, Physics 1981-1990*, Editor-in-Charge Tore Frängsmyr, Editor Gösta Ekspång, World Scientific Publishing Co., Singapore, 1993

[5] D. Strickland, G. Mourou, *Compression of amplified chirped optical pulses*, Optics Communications **56**, 219 (1985)

[6] A. McPherson, G. Gibson, H. Jara, U. Johann, T. Luk, I. McIntyre, K. Boyer and C. Rhodes, *Studies of multiphoton production of vacuum-ultraviolet radiation in the rare gases*, J. Opt. Soc. Am., **4**, 595 (1987)

[7] M. Ferray, A. L'Huillier, X. Li, L. Lompre, G. Manfray and C. Manus, *Multiple-harmonic conversion of 1064 nm radiation in rare gases*, J. Phys. B: At. Mol. Opt. Phys. **21**, L31 (1988)

[8] P. Corkum, *Plasma perspective on strong field multiphoton ionization*, Phys. Rev. Lett., **71**, 1994 (1993)

[9] M. Lewenstein, Ph. Balcou, M. Yu. Ivanov, A. L'Huiller and P. Corkum, *Theory of high-harmonic generation by low-frequency laser fields*, Phys. Rev. A, **49**, 2117, (1994)

[10] A. Pukhov, S. Gordienko, T. Baeva, *Temporal Structure of Attosecond Pulses from Intense Laser-Atom Interactions*, Phys. Rev. Lett., **91**, 173002 (2003)

[11] M. Bellini, S. Cavalieri, C. Corsi, and M. Materazzi, *Phase-locked, time-delayed harmonic pulses for high spectral resolution in the extreme ultraviolet*, Optics Letters **26**, 1010 (2001)

[12] P. Tzallas, D. Charalambidis, N. A. Papadogiannis, K. Witte, G. D. Tsakiris, *Direct observation of attosecond light bunching*, Nature **426**, 267 (2003)

[13] L. Plaja, L. Roso, K. Rzazewski, and M. Lewenstein, *Generation of attosecond pulse trains during the reflection of a very intense laser on a solid surface*, J. Opt. Soc. Am. B, **15**, 1904 (1998)

[14] S. Gordienko, A. Pukhov, O. Shorokhov, T. Baeva, *Relativistic Doppler Effect: Universal Spectra and Zeptosecond Pulses*, Phys. Rev. Lett., **93**, 115003 (2004)

[15] R. L. Carman, D. W. Forslund, J. M. Kindel, *Visible Harmonic Emission as a Way of Measuring Profile Steepening*, Phys. Rev. Lett., **46**, 29 (1981)

[16] B. Bezzerides, R. D. Jones and D. W. Forslund, *Plasma Mechanism for Ultraviolet Harmonic Radiation Due to Intense CO_2 Light*, Phys. Rev. Lett., **49**, 202 (1982)

[17] S. V. Bulanov, N. M. Naumova, F. Pegoraro, *Interaction of an ultrashort, relativistically strong laser pulse with an overdense plasma*, Phys. Plasmas **1**, 745 (1994)

[18] P. Gibbon, *Harmonic Generation by Femtosecond Laser-Solid Interaction: A Coherent Water-Window Light Source?*, Phys. Rev. Lett., **76**, 50 (1996)

[19] R. Lichters, J. Meyer-ter-Vehn, A. Pukhov, *Short-pulse laser harmonics from oscillating plasma surfaces driven at relativistic intensity*, Phys. Plasmas **3**, 3425 (1996)

[20] B. Dromey, S. Kar, C. Bellei, D. C. Carroll, R. J. Clarke, J. S. Green, S. Kneip, K. Markey, S. R. Nagel, P. T. Simpson, L. Willingale, P. McKenna, D. Neely, Z. Najmudin, K. Krushelnick, P. A. Norreys and M. Zepf, *Bright Multi-keV Harmonic Generation from Relativistically Oscillating Plasma Surfaces*, Phys. Rev. Lett., **99**, 085001 (2007)

[21] M. Zepf, B. Dromey, S. Kar, C. Bellei, D. C. Carroll, R. J. Clarke, J. S. Green, S. Kneip, K. Markey, S. R. Nagel, R. T. Simpson, L. Willingale, R. McKenna, D. Neely, Z. Najmudin, K. Krushelnick and P. A. Norreys, *High harmonics from relativistically oscillating plasma surfacesa high brightness attosecond source at keV photon energies*, Plasma Phys. Control. Fusion **49**, B149 (2007)

[22] B. Dromey, M. Zepf,A. Gopal, K. Lancaster, M. S. Wei, K. Krushelnick, M. Tatarakis, N. Vakakis, S. Moustaizis, R. Kodama, M. Tampo, C. Stoeckl, R. Clarke, H. Habara, D. Neely, S. Karsch and P. Norreys, *High harmonic generation in the relativistic limit*, Nature Physics **2**, 456-459 (2006)

[23] U. Teubner, C. Wülker, W. Theobald, E. Förster, *X-ray spectra from high-intensity subpicosecond laser produced plasmas*, Phys. Plasmas **2**, 972 (1995)

[24] S. Kohlweyer, G. D. Tsakiris, C. G. Wahlström, C. Tillmana and I. Mercera, *Harmonic generation from solid-vacuum interface irradiated at high laser intensities*, Optics Communications **117**, 431 (1995)

[25] D. von der Linde, T. Engers, G. Jenke, P. Agostini, G. Grillon, E. Nibbering, A. Mysyrowicz and A. Antonetti, *Generation of high-order harmonics from solid surfaces by intense femtosecond laser pulses*, Phys. Rev. A, **52**, R25-R27 (1995)

[26] P. A. Norreys, M. Zepf, S. Moustaizis, A. P. Fews, J. Zhang, P. Lee, M. Bakarezos, C. N. Danson, A. Dyson, P. Gibbon, P. Loukakos, D. Neely, F. N. Walsh, J. S. Wark and A. E. Dangor, *Efficient Extreme UV Harmonics Generated from Picosecond Laser Pulse Interactions with Solid Targets*, Phys. Rev. Lett., **76**, 1832 (1996)

[27] U. Teubner, D. Altenbernd, P. Gibbon, E. Förster, A. Mysyrowicz, P. Audebert, J.-P. Geindre, J. C. Gauthier, R. Lichters and J. Meyer-ter-Vehn, *Observation of VUV radiation at wavelengths in the ω_p- and $2\omega_p$-wavelength range emitted from femtosecond laser-plasmas*, Optics Communications **144**, 217 (1997)

[28] M. Zepf, G. D. Tsakiris, G. Pretzler, I. Watts, D. M. Chambers, P. A. Norreys, U. Andiel, A. E. Dangor, K. Eidmann, C. Gahn, A. Machacek, J. S. Wark and K. Witte, *Role of the plasma scale length*

in the harmonic generation from solid targets, Phys. Rev. E, **58**, R5253 - R5256 (1998)

[29] A. Tarasevitch, A. Orisch, D. von der Linde, Ph. Balcou, G. Rey, J.-P. Chambaret, U. Teubner, D. Klöpfel and W. Theobald, *Generation of high-order spatially coherent harmonics from solid targets by femtosecond laser pulses*, Phys. Rev. A, **62**, 023816 (2000)

[30] I. Watts, M. Zepf, E. L. Clark, M. Tatarakis, K. Krushelnick, A. E. Dangor, R. M. Allott, R. J. Clarke, D. Neely and P. A. Norreys, *Dynamics of the Critical Surface in High-Intensity Laser-Solid Interactions: Modulation of the XUV Harmonic Spectra*, Phys. Rev. Lett., **88**, 155001 (2002)

[31] U. Teubner, G. Pretzler, Th. Schlegel, K. Eidmann, E. Förster and K. Witte, *Anomalies in high-order harmonic generation at relativistic intensities*, Phys. Rev. A, **67**, 013816 (2003)

[32] U. Teubner, K. Eidmann, U. Wagner, U. Andiel, F. Pisani, G. D. Tsakiris, K. Witte, J. Meyer-ter-Vehn, Th. Schlegel and E. Förster, *Harmonic Emission from the Rear Side of Thin Overdense Foils Irradiated with Intense Ultrashort Laser Pulses*, Phys. Rev. Lett., **92**, 185001 (2004)

[33] E. Esarey, A. Ting, P. Sprangle, D. Umstadter, X. Liu, *Nonlinear analysis of relativistic harmonic generation by intense lasers in plasmas*, IEEE Transactions on Plasma Science **21**, 95 (1993))

[34] S. Hüller and J. Meyer-ter-Vehn, *High-order harmonic radiation from solid layers irradiated by subpicosecond laser pulses*, Phys. Rev. A, **48**, 3906 (1993)

[35] D. von der Linde, K. Rzazewski, *High-order optical harmonic generation from solid surfaces*, Appl. Phys. B: Lasers Opt. **63**, 499 (1996)

[36] P. Gibbon, *High-order harmonic generation in plasmas*, IEEE Journal of Quantum Electronics **33**, 1915 (1997)

[37] K. Eidmann, J. Meyer-ter-Vehn, Th. Schlegel, S. Hüller, *Hydrodynamic simulation of subpicosecond laser interaction with solid-density matter*, Phys. Rev. E, **62**, 1202 (2000)

[38] T. Baeva, S. Gordienko, A. Pukhov, *Theory of high-order harmonic generation in relativistic laser interaction with overdense plasma*, Phys. Rev. E, **74** 046406 (2006)

[39] T. Baeva, S. Gordienko, A. Pukhov, *Relativistic plasma control for single attosecond x-ray burst generation*, Phys. Rev. E, **74** 065401 (2006)

[40] S. Gordienko, A. Pukhov, O. Shorokhov, T. Baeva, *Coherent Harmonic Focusing and the Light Extreme*,
arXiv:physics/0406019 (2004)

[41] S. Gordienko, A. Pukhov, *Scalings for ultrarelativistic laser plasmas and quasimonoenergetic electrons*, Phys. Plasmas **12**, 043109 (2005)

[42] L. D. Landau, E. M. Lifshitz, *Quantum Mechanics: Non-Relativistic Theory*, Pergamon Press, Oxford, 1984

[43] W. Kruer, *The Physics of Laser Plasma Interactions*, Westview Press, Boulder, 2003

[44] T. Baeva, *Attosecond phenomena in laser-condensed matter interaction*, Diploma thesis, 2005

[45] L. D. Landau, E. M. Lifshitz, *The Classical Theory of Fileds*, Pergamon Press, Oxford, 1984

[46] L. D. Landau, E. M. Lifshitz, *Electrodynamics of Continuous Media*, Pergamon Press, Oxford, 1984

[47] A. Pukhov, *Three-dimensional electromagnetic relativistic particle-in-cell code VLPL (Virtual Laser Plasma Lab)*, J. Plasma Physics, **61**, 425 (1999)

[48] L. D. Landau, E. M. Lifshitz, *Mechanics*, Pergamon Press, Oxford, 1984

[49] S. Gordienko, A. Pukhov, O. Shorokhov, T. Baeva, *Coherent Focusing of High Harmonics: A New Way Towards the Extreme Intensities*, Phys. Rev. Lett., **94**, 103903 (2005)

Invited Talks, Conferences and Publications

Invited seminar and colloquium presentations

"Relativistic Spikes and High Harmonic Generation at Plasma Boundaries"
at the Institute for Optics and Quantum Electronics, Jena, Germany
(invited talk, 14 December, 2007)

"High Harmonic Generation from Overdense Plasma"
Theoretical Colloquium at Technical University Darmstadt, Germany
(invited talk, 22 October, 2007)

"High Harmonic Generation from Gases and Plasma: Between Symmetry and Universality"
at Queen's University Belfast, United Kingdom
(invited talk, 11 September, 2007)

"High Harmonic Generation from Plasma: The Theory of Relativistic Spikes and its Experimental Confirmation"
ILIAS Theoretical Seminar at GSI Darmstadt, Germany
(invited talk, 17 April, 2007)

"High Harmonic Generation and Attosecond Pulses in the Relativistic Regime"
at Queen's University Belfast, United Kingdom
(invited talk, 13 December, 2006)

"Isolated Sub-attosecond Pulses from Plasma"
at the Institute for experimental physics I, Würzburg, Germany
(invited talk, 10 May, 2006)

"Relativistic Ultra-short Pulses"
at the National Research Council, Ottawa, Canada
(invited talk, 22 March 2006)

"Relativistic Plasma Control"
at Max-Plank Institute for Quantum Optics, Garching, Germany
(invited talk, 12 March, 2006)

Invited talks and oral conference presentations

February 2008: Workshop on Laser Plasmas and Magnetic Confinement, Oelde, Germany (oral presentation)

January 2008: Workshop on Physics of High Energy Density in Matter, Hirschegg, Austria (oral presentation)

December 2007: Annual Christmas Meeting of the Central Laser Facility of the Ratherford Appleton Laboratory,
Abingdon, England (oral presentation)

November 2007: Conference on High Temporal and Spectral Resolution at Short Wavelengths,
Iraklio, Crete (oral presentation)

October 2007: Conference on Theory of Short Pulse Petawatt Laser Plasma Interaction,
Darmstadt, Germany (oral presentation)

October 2007: GRK1203 Meeting,
Bad Breisig, Germany (oral presentation)

September 2007: 6th International Symposium on Ultrafast Intense Laser Science,
Tirrenia, Italy (**invited speaker**)

Juni 2007: Day of Science,
Düsseldorf, Germany (oral presentation)

Juni 2007: High Performance Computing Conference (HPC-Europa),
Bologna, Italy (oral presentation)

Juni 2007: DAMOP Conference of the American Physical Society,
Calgary, Canada (oral presentation)

March 2007: DPG Spring Conference of the AMOP Division,
Düsseldorf, Germany (oral presentation)

February 2007: Dream Beams Symposium,
Garching, Germany (**invited speaker**)

February 2007: 385. WE-Heraeus-Seminar "Laser-Particle-Acceleration",
Bad Honef, Germany (oral presentation)

January 2007: Workshop on Physics of High Energy Density in Matter,
Hirschegg, Austria (oral presentation)

November 2006: International Workshop on Atomic Physics,
Dresden, Germany (**invited speaker**)

October 2006: International Conference on the Interaction of Atoms,
Molecules and Plasmas with Intense Ultrashort Laser Pulses,
Szeged, Hungary (oral presentation)

March 2006: TR18 Meeting,
Bad Breisig, Germany (oral presentation)

January 2006: Workshop on Physics of High Energy Density in Matter,
Hirschegg, Austria (oral presentation)

October 2005: TR18 Meeting,
Wildbad Kreuth, Germany (oral presentation)

Invited scientific visits

September 2007, 1 week invited visit at the Institute for Applied Mathematics, Queen's University Belfast, Northern Ireland, UK

June-July 2006, 6 weeks invited visit at the Edinburgh Parallel Computing Centre, Scotland, UK

March 2006, 2 weeks invited visit at the National Research Council,
Ottawa, Canada

Work to be published

T. Baeva *et al*, *High harmonic generation from relativistic overdense plasma for P- and S- laser polarization* (2008)
(based on Sections 3.6.2 and 3.6.3 of this Thesis)

T. Baeva *et al*, *Relativistic invariance, universality and high harmonic generation from relativistic plasmas* (2008)
(based on Sections 2, 2.2 and 4.1.2 of this Thesis)

T. Baeva *et al*, *Electromagnetic shock waves from relativistic laser plasma* (2008)
(based on Section 4.1 of this Thesis)

T. Baeva *et al*, *Surface roughness and high harmonic generation in relativistic skin layers* (2008)
(based on Sections 4.1 and 4.4 of this Thesis)

T. Baeva *et al*, *Acceleration effects in relativistic laser-plasma interaction* (2008)
(basen on Sections 1.3.1, 3.1 and 3.4 of this Thesis)

T. Baeva, *High harmonics and ultra-short pulses from relativistic plasmas* Annual Report 2007-2008 of the Central Laser Facility (Rutherford Appleton Laboratory, UK) (2008)

Published work

T. Baeva, *Numerical Molecule Imaging*,
Science and Supercomputing in Europe (2007)
ISBN 978-88-86037-19-8

T. Baeva, *BlueGene in Femtosecond physics*,
Newsletter of the HPC-Europa consortium, invited contributor (2007)

T. Baeva, S. Gordienko, A. Pukhov, *Relativistic plasma control for single attosecond pulse generation: theory, simulations and structure of the pulse*, Laser and Particle Beams, **25**, 339 (2007)

T. Baeva, S. Gordienko, A. Pukhov, *Theory of high-order harmonic generation in relativistic laser interaction with overdense plasma*, Phys. Rev. E, **74**, 046404 (2006)

This work was selected for the November 2006 issue of Virtual Journal of Ultrafast Science http://www.vjultrafast.org

T. Baeva, S. Gordienko, A. Pukhov, *Relativistic plasma control for single attosecond x-ray burst generation*,
Phys. Rev. E, **74**, 065401 (2006)

T. Baeva, S. Gordienko, A. Pukhov, *Scalable dynamics of high energy relativistic electrons: theory, numerical simulations and experimental results*,
Astrophysics and Space Science, DOI 10.1007/s10509-006-9279-5 (2006)

S. Gordienko, T. Baeva, A. Pukhov, *Focusing of laser-generated ion beams by a plasma cylinder: Similarity theory and the thick lens formula*,
Physics of Plasmas, **13**, 063103 (2006)

S. Gordienko, A. Pukhov, O. Shorokhov, T. Baeva, *Coherent Focusing of High Harmonics: A New Way Towards the Extreme Intensities*,
Phys. Rev. Lett., **94**, 103903 (2005)

S. Gordienko, A. Pukhov, O. Shorokhov, T. Baeva, *Relativistic Doppler Effect: Universal Spectra and Zeptosecond Pulses*,
Phys. Rev. Lett., **93**, 115002 (2004)

A. Pukhov, S. Gordienko, T. Baeva, *Temporal Structure of Attosecond Pulses from Intense Laser-Atom Interactions*,
Phys. Rev. Lett., **91**, 173002 (2003)

(the results of this work were presented on the cover of Phys. Rev. Lett., 24 October, 2003)

Acknowledgments

Finally, I want to thank all the people who contributed to the successful outcome of this work.

First of all, I want to thank Prof. Dr. A. Pukhov for his interest in high harmonic generation from plasma, for his questions and remarks, which brought the investigation of the harmonic generation process to its present state.

I am especially grateful to Prof. Dr. K.-H. Spatschek, for the co-reference of the Dissertation. His interesting remarks during presentations of these results led to the development of some of most exciting parts of this work.

I want to thank Prof. Dr. K. Taylor for proof-reading the manuscript, for his enthusiasm about new physical and mathematical models and for his willingness to reference the Dissertation.

My special thanks goes to Dr. Sergey Gordienko, for his patience and willingness to teach. I owe the discussions with him a great deal of my inspiration for theoretical and mathematical physics.

I am very grateful to Prof. M. Zepf for the inspiring discussions of physics and for his eagerness to bring forward the high harmonic generation physics, and to both Prof. M. Zepf and Dr. B. Dromey for the experimental confirmation of the theory presented in the Dissertation.

I want to thank my colleagues Anupam Karmakar, Naveen Kumar, Daniel an der Brügge, Min Chen, Götz Lehmann, Dr. Andreas Wingen, Dr. Christof Karle and Vasiliy Seredov for interesting discussions, energetic working environment and readiness to help with whatever problems I ever had.

A special thanks to Mr. E. Zügge for the hardware and software support and Mrs. E. Gröters and Mrs. C. Dingle for their continuous willingness to help with any bureaucratic question that came up.

In conclusion I want to thank my parents for pointing my way in life, for their support and understanding.

Index

S-parameter, 41

Airy-function, 18, 75
Apparent reflection point, 25
  causality, 33
  definition, 30
  dynamics, 49
    perturbation theory, 49, 51
    spikes, 51, 53
  formalism, 25, 36
  relativistic invariance, 30, 69
ARP, 25

Chirped Pulse Amplification, 6, 10
Corkum model, 6, 9
CPA, 6, 10

Electromagnetic shocks, 17, 66
  harmonic coherency, 17, 72
  high harmonic spectrum, 68
  numerical simulations of, 17, 67
  shock formation, 66
Electron bursts, 15

Harmonic phase, 74
High harmonic spectrum, 18, 68, 72, 75, 77
  analytical derivation, 72, 75
  experimental observation, 21
  harmonic phase, 74
  universality, 77
High harmonics from
  gas jets, 6
  attosecond pulses, 9
  Corkum model, 6
  cut-off, 9
  quantum simulations, 9
plasma
  first observation, 10
relativistic plasma, 11, 65
  coherency, 21, 74, 79
  electromagnetic shocks, 66
  harmonic spectrum, 18, 19, 21, 68, 75, 76
  phase, 74
  physical picture of, 15, 78

Isolated pulses, 88

Laser polarization, 57, 58, 77

Oblique laser incidence, 53
  P-polarization, 57
  S-polarization, 58
  ion current, 54
  similarity parameter, 58
  transformation, 56

Phase matching condition, 15, 79
Polarization, 57, 58, 77

Relativistic Doppler effect, 11, 70
  boundary condition, 70
  conservation of energy violation, 12
  harmonic cut-off, 12
  plasma transparency, 11

pulse compression, 72
Relativistic high harmonics, 65
electromagnetic shocks, 66
harmonic phase, 74
physical mechanism of generation, 78
spectrum, 68, 72, 75, 76
universality, 77
Relativistic oscillating mirror, 70
boundary condition, 70
mirror transparency, 12, 70
pulse compression, 72
Relativistic plasma control, 88
Relativistic spikes, 14, 37, 43, 44, 48, 51, 53, 60
numerical simulations of, 60
physics of, 15
spike scaling, 51, 53
theory of, 14, 46
RPC, 88

Similarity parameter, 41
oblique incidence, 58
overdense plasma, 42
underdense plasma, 42
Sub-attosecond pulses, 84

Theory
of relativistic spikes, 14, 19, 37, 44, 46, 53
similarity, 38, 41, 42

Ultra-short pulses, 9, 10, 81
attosecond, 10
duration scaling of, 84
generation of, 82
intensity scaling of, 84
isolated, 88, 90
pulse train, 82
sub-attosecond, 10
tunable structure of, 86, 87
zeptosecond, 10

Vlasov equation, 39, 41, 55, 93
derivation of, 93, 94

Zepto-second pulses, 10, 84